

AD/A-003 731

STUDIES OF THE IGNITION AND COMBUSTION
OF BORON PARTICLES FOR AIR-AUGMENTED
ROCKET APPLICATIONS

Merrill K. King, et al

Atlantic Research Corporation

Prepared for:

Air Force Office of Scientific Research

October 1974

DISTRIBUTED BY:

NTIS

National Technical Information Service
U. S. DEPARTMENT OF COMMERCE

Qualified requestors may obtain additional copies from the Defense Documentation Center, all others should apply to the National Technical Information Service.

ACCESSION for	
NTIS	Write Section <input checked="" type="checkbox"/>
DDC	Buy Section <input type="checkbox"/>
UNANNOUNCED	<input type="checkbox"/>
JUSTIFICATION	
BY.....	
DISTRIBUTION/AVAILABILITY CODES	
Dist.	AVAIL. and/or SPECIAL
A	

Conditions of Reproduction

Reproduction, translation, publication, use and disposal in whole or in part by or for the United States Government is permitted.

V

TR-PL-10433

AFOSR SCIENTIFIC REPORT

July 1, 1971 - Dec. 31, 1973

STUDIES OF THE IGNITION AND COMBUSTION
OF BORON PARTICLES FOR
AIR-AUGMENTED ROCKET APPLICATIONS

Merrill K. King and Andrej Maček

Submitted to:

Air Force Office of Scientific Research
Contract No. F44620-71-C-0124

Submitted by:

Kinetics and Combustion Group
Applied Physics Department
Atlantic Research Corporation
5390 Cherokee Avenue
Alexandria, Virginia 22314

Date:

October 21, 1974

AIR FORCE OFFICE OF SCIENTIFIC RESEARCH (AFOSR)
RESEARCH REPORT
This report is the property of the AFOSR and is
not to be distributed outside the AFOSR (7b).
D. M. GILBERT
Technical Information Officer *iii*

UNCLASSIFIED

SECURITY CLASSIFICATION OF THIS PAGE (When Data Entered)

REPORT DOCUMENTATION PAGE		READ INSTRUCTIONS BEFORE COMPLETING FORM
1. REPORT NUMBER	2. GOVT ACCESSION NO.	3. RECIPIENT'S CATALOG NUMBER AD/A-003731
4. TITLE (and Subtitle) STUDIES OF THE IGNITION AND COMBUSTION OF BORON PARTICLES FOR AIR-AUGMENTED ROCKET APPLICATIONS		5. TYPE OF REPORT & PERIOD COVERED INTERIM 1 July 1971-31 Dec 1973
7. AUTHOR(s) MERRILL K KING ANDREJ MACEK		6. PERFORMING ORG. REPORT NUMBER TR-PL-10433
9. PERFORMING ORGANIZATION (NAME AND ADDRESS) ATLANTIC RESEARCH CORPORATION 5390 CHEROKEE AVENUE ALEXANDRIA, VIRGINIA 22314		8. CONTRACT OR GRANT NUMBER(s) F44620-71-C-0124
11. CONTROLLING OFFICE NAME AND ADDRESS AIR FORCE OFFICE OF SCIENTIFIC RESEARCH/NA 1400 WILSON BOULEVARD ARLINGTON, VIRGINIA 22209		10. PROGRAM ELEMENT, PROJECT, TASK AREA & WORK UNIT NUMBERS 681508 9711-01 61102F
14. MONITORING AGENCY NAME & ADDRESS (if different from Controlling Office)		12. REPORT DATE Oct 1974
		13. NUMBER OF PAGES 106
		15. SECURITY CLASS. (of this report) Unclassified
		15a. DECLASSIFICATION/DOWNGRADING SCHEDULE
16. DISTRIBUTION STATEMENT (of this Report) Approved for public release; distribution unlimited.		
17. DISTRIBUTION STATEMENT (of the abstract entered in Block 20, if different from Report)		
18. SUPPLEMENTARY NOTES Reproduced by NATIONAL TECHNICAL INFORMATION SERVICE U S Department of Commerce Springfield VA 22151		
19. KEY WORDS (Continue on reverse side if necessary and identify by block number) BORON DUST-CLOUD IGNITION COMBUSTION AIR-AUGMENTED ROCKETS FLAME SPEEDS		
20. ABSTRACT (Continue on reverse side if necessary and identify by block number) This report presents the results of several tasks aimed at defining the ignition and combustion characteristics of pure boron and the mostly boron condensed-phase material ejected from highly boron-loaded fuel-rich primary motor formulations. Two state-of-the-art high-boron formulations were fired under high and low pressure conditions into a tank filled with inert gas where the condensed-phase exhaust products were collected. These products were characterized physically and chemically. In addition, the ignition and combustion characteristics of these products were determined and compared to those for pure boron. The minimum		

DD FORM 1 JAN 73 1473

EDITION OF 1 NOV 65 IS OBSOLETE

UNCLASSIFIED

SECURITY CLASSIFICATION OF THIS PAGE (When Data Entered)

surroundings temperature required for ignition was essentially the same for the condensed exhaust and the pure boron, but the ignition delay time was markedly lower for the condensed exhaust, probably due to much higher surface area. Burning times for condensed exhaust particles and pure boron particles of the same size were equal within experimental error. In the size range of interest (2 to 10 micron diameter) the burning was observed to be characterized by a d^1 -law (kinetics-limited particle burning) rather than the d^2 -law (diffusion-limited burning) characteristic of larger particles. A model of boron ignition treating the inhibiting effect of a boric oxide coating has been developed. Transient differential equations describing the generation and removal of the oxide and associated thermal effects along with heat transfer between the particle and surroundings have been derived, converted to difference form and programmed for computer solution for determination of ignition limits and ignition times. Predictions for particles studied by Maček in a flat-flame burner have been compared with experimental results -- agreement is good for dry gas cases, but poor when the gas stream includes water. The program has been used to predict effects of initial oxide thickness, particle size, pressure, oxygen content, initial particle temperature, gas temperature and surroundings radiation temperature on ignition. In addition, the original differential equations have been treated by a stability analysis to determine ignition limits -- excellent agreement is found between results obtained with the stability analysis and the numerical analysis. A detailed model of boron-oxygen-nitrogen dust cloud flames including consideration of the details of boron particle ignition and the effects of oxygen depletion has been developed and used for prediction of flame speeds as functions of numerous parameters. Reasonably good agreement between measured flame speeds and those predicted by this model has been obtained. In addition, a simplified closed-form flame speed expression has been developed and the effects of the various assumptions used in its development on predicted flame speeds have been examined. The detailed and simplified models have both been used to study the effects of initial temperature, pressure, initial oxygen mole fraction, weight fraction particles, initial particle size, initial thickness of the oxide coating on the particles, radiation feedback from the post-flame zone, and Nusselt Number. Mechanisms leading to the predicted dependencies are discussed.

TABLE OF CONTENTS

	<u>Page No.</u>
I. INTRODUCTION	1
II. ROCKET PROPELLANTS AND MOTORS	3
III. PHYSICAL ANALYSIS OF CONDENSED-PHASE EXHAUST	11
IV. CHEMICAL ANALYSIS OF CONDENSED-PHASE EXHAUST	17
V. COMBUSTION OF CONDENSED PHASE EXHAUST MATERIAL	21
A. The Gas Burner	21
B. Single Particle Experiments	24
C. Particle Cloud Experiments	25
(1) Particle Sizes	27
(2) Ignition	27
(3) Burning Times	30
REFERENCES FOR SECTIONS I - V	33
VI. MODELING OF BORON PARTICLE IGNITION IN HOT GAS STREAMS (Reprinted from <u>Combustion Science and Technology</u>)	35
VII. PREDICTIONS OF LAMINAR FLAME SPEEDS IN BORON-OXYGEN-NITROGEN DUST CLOUDS (Expanded Version of Paper Presented at the 15th International Symposium on Combustion)	54

I. INTRODUCTION

Recent years have witnessed a large development of fuel-rich propellant technology to produce formulations for primary rockets in air-breathing propulsion systems. Two types of systems have been especially prominent, air augmented rockets and external-burning missiles or projectiles. In an air-augmented rocket, the incompletely combusted products of a fuel-rich primary motor formulation are mixed and burned with ram air inside a secondary chamber at a pressure equal to or less than the air inlet recovery pressure. In external burning, the fuel-rich primary motor exhaust is injected directly into the free-stream around the missile and burns at atmospheric pressure (sea level or altitude). Both types of systems primarily utilize composite solid propellants with ammonium perchlorate oxidizer: thus non-metalized formulations typically produce compounds consisting of C, H, O, N, Cl, and possibly F, while metalized systems also produce B, Al, Mg, or combinations of these metals.

An essential prerequisite of success in air-breathing applications is rapid and efficient combustion of the primary exhaust in air. It is of interest to spell out here the conditions for this combustion. In ducted propulsion the pressures in the secondary range from 15 or 20 atm down to perhaps half an atmosphere depending on the flying altitude and Mach Number, and the residence times typically are a few milliseconds. In external burning the pressures range from 1 to 0.1 atm, and the residence times are a fraction of a millisecond. Thus it is easily seen that these air-breathing systems often place stringent demands on preignition and combustion times of the primary exhaust fuel products with air.

Boron is a particularly attractive ingredient for propellants for air-breathing rocket applications due to its high heating value. Generally, it is desirable that the amount of boron in the fuel-rich propellant be maximized, subject to processability and primary motor ejection efficiency constraints. The practical upper limit of boron loading is approximately 50 to 60 percent by weight. At these loading levels, very little boron is burned

in the primary motor due to lack of sufficient oxidizer -- thus, most of the boron must be burned in particulate form with air in the secondary combustor for its heating value to be utilized. In addition, at these high loadings, primary motor flame temperatures tend to be low. These factors, combined with the low residence times available for mixing, ignition, and combustion processes in the secondary chamber have led to afterburning efficiency problems, particularly under operating conditions which result in afterburner pressures of 50 psia or less.

Substantial prior work has been reported on ignition and combustion of pure boron (1,2,3,4,5). However, at the outset of our project there remained a large uncertainty as to the nature (physical state, chemical composition) and especially as to combustion characteristics of the condensed material discharged from the primary motor, which is certainly not pure boron. The primary reaction must be expected to coat the existing particles with reaction products and/or to generate new particles. Agglomeration of particles is a definite possibility.

The objective of the present work has been to characterize the nature of the primary exhaust from fuel-rich motors containing boron, and to study its ignition and combustion characteristics, especially as compared to the known information for pure boron. Section II of the present report describes (a) the rocket-motor firing program in which the condensed exhaust (CE) from two different propellants was collected, and (b) the results of thermodynamic computations for these formulations. Sections III and IV contain the results of the physical (microscopy, density measurement) and chemical analyses of the CE. Section V deals with combustion of the CE. Finally, Sections VI and VII report the results of modeling studies describing the ignition of single boron particles in hot gas streams and propagation of flames in boron-oxygen-nitrogen dust clouds.

II. ROCKET PROPELLANTS AND MOTORS

Two propellants were studied. Both were composite ammonium perchlorate-binder formulations containing large amounts (almost 50%) of boron and a few percent of magnesium and aluminum. ARCADENE (Atlantic Research Corporation trade name) 256A is a carboxy-terminated polybutadiene formulation and ARCADENE 280 a polyester formulation. The boron used in both formulations was the Kawecki Company material with nominal average particle diameters of $3\mu\text{m}$. However, the diameters range widely from about 1 to $20\mu\text{m}$ or more. Thus both formulations are made up of the following elements: C, H, O, N, Cl, B, Mg, Al. In addition to these, the 256A formulation contains a small amount of iron, because it is catalyzed by n-butyl ferrocene.

Two motors were fired with each formulation into a large cylindrical tank (5.2 m long, 2.9 m in diameter) which was first evacuated and then filled with argon to 0.35 atm pressure prior to each run. The rocket chamber pressure and the tank pressure were measured continuously throughout each run.

Data pertaining to the four motor tests are given in Table I and Figure 1. Each propellant grain was weighed before the test; as was the residue remaining inside the motor after the test. Comparison of the third and fourth columns of Table I in which the respective weights are listed, shows that the ejection efficiency ranged from 93.8% in Run 4 to 99.4% in Run 2. During all tests, the tank pressure rose continuously from the initial to the final value. The low final value recorded in Run 2 can be ascribed to the fact that the burning time was about twice that of other runs, thus allowing more cooling and condensation during the run. As shown in Figure 1, each propellant was tested at a high and a low pressure. In three out of four runs the chamber pressure remained at a constant value over a substantial fraction of the test duration; in Run 1 it kept rising over most of the burning time, possibly due to clogging of the nozzle.

After each test the tank filled with argon was kept closed for about 1 hour so the CE would settle in a large (5.4 m^2 surface area) metal trough

TABLE I. Motor Firing Conditions

<u>Run No.</u>	<u>Propellant</u>	<u>Propellant Weight (gm)</u>	<u>Residue Weight (gm)</u>	<u>Tank Pressure (atm)</u>	
				<u>Initial</u>	<u>Final</u>
1	280 ^s	805	10.5	0.35	0.71
2	256A ^{**}	746	4.4	0.35	0.46
3	280	743	18.1	0.35	0.77
4	256A	760	47.4	0.35	0.54

* Polyester binder

** CTPB Binder

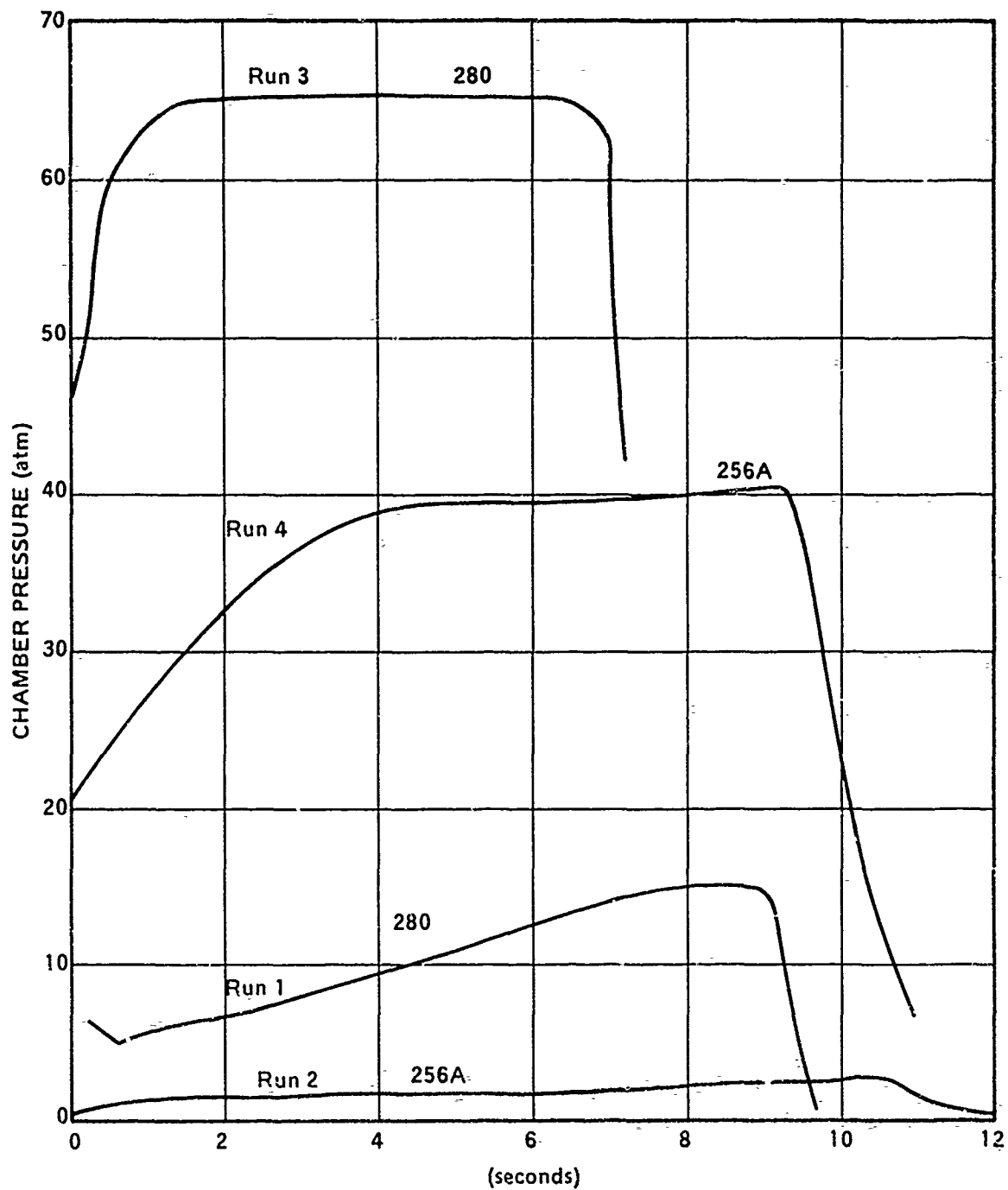


Figure 1. Motor Chamber Pressures for Two Firings with ARCADENE 256A and Two Firings with ARCADENE 280.

at the bottom of the tank. The trough was then emptied into a bottle by remote action without opening of the tank. Thus, the CE samples were not exposed to air while hot. Thereafter, ordinary precautions were observed to avoid undue exposure to air and humidity (e.g., the samples were stored in corked vials in desiccators), but no attempt was made at absolute exclusion of atmospheric oxidants.

A set of two thermodynamic equilibrium computations, "A" and "B", was made corresponding to each experimental motor run. The results are given in Table II. Chamber pressures in runs 2, 3, and 4 are the plateau pressures of Figure 1. The Run 1 chamber pressure of 10.2 atm is an average value over the duration of the run. The exhaust pressure was always taken to be 0.5 atm, corresponding to an average experimental value. Computations "A" took into account most species which can reasonably be expected to appear in the products. Computations "B" omitted B_4C and BN, two species which are very important thermodynamically, but which are sometimes suspected not to appear in reality for kinetic reasons. The species used in the computations are listed in Table III. The underlined species in Table III are arbitrarily defined as "major": they are the only ones predicted to occur in amounts exceeding 0.5 weight percent of the total formulation in any of the computer runs. However, they are not always "major"; e.g., in computations "B", Mg(g) does not appear in any appreciable amounts. The last two columns in Table II, giving percentages of condensable products, include not only liquids and solids, but also those gases which condense when cooled to 300°K, all in amounts computed in equilibrium under exhaust conditions. In other words, the exhaust equilibrium was assumed to remain frozen during mixing with argon and cooling.

The most abundant gas species is H_2 , which accounts for more than 50% of the total gas in all computations. Two other permanent gases are CO and N_2 , but the latter is absent, or virtually so, in cases which "allow" formation of BN.

TABLE II. Thermodynamic Equilibrium Computations

Run No.	Pressure (atm)		Temperature (°K)				Weight % CE	
	Chamber	Exhaust	Chamber A	Chamber B*	Exhaust A	Exhaust B*	A	B*
1	10.2	0.5	2186	2001	1872	1696	83.7	77.5
2	2.0	0.5	1888	1762	1740	1635	84.9	87.2
3	65.3	0.5	2409	2208	1858	1677	86.6	81.8
4	40.1	0.5	2071	1975	1618	1552	88.9	92.0

* B₄C and BN omitted in computations.

TABLE III. List of Species Used in Thermodynamic Computations

Gaseous:

$\underline{H_2}$, \underline{CO} , $\underline{N_2}$, $\underline{MgCl_2}$, $\underline{B_2O_2}$, \underline{HCl} , $\underline{B_2O_3}$, $\underline{B_3H_3O_3}$, \underline{Mg} , \underline{O} , $\underline{O_2}$, \underline{C} , $\underline{CO_2}$, \underline{CN} , \underline{CH} , $\underline{CH_2}$, $\underline{C_2H_4}$
 \underline{H} , \underline{OH} , $\underline{H_2O}$, \underline{N} , \underline{NO} , $\underline{NH_2}$, $\underline{NH_3}$, \underline{HCN} , \underline{B} , \underline{BH} , $\underline{BH_2}$, $\underline{BH_3}$, \underline{BO} , $\underline{BO_2}$, $\underline{B_2O}$, $\underline{B_3H_3O_6}$, \underline{BOH} ,
 $\underline{HBO_2}$, \underline{Cl} , $\underline{Cl_2}$, \underline{BCl} , $\underline{BCl_2H}$, \underline{BOCl} , \underline{Al} , \underline{AlOCl} , $\underline{Al_2O}$, \underline{AlOH} , $\underline{AlBO_2}$, \underline{AlCl} , $\underline{AlO_2}$, \underline{MgH} ,
 ∞ \underline{MgO} , \underline{MgOH} .

Liquid:

$\underline{B_2O_3}$, \underline{Fe} , \underline{B} , $\underline{B_4C}$, \underline{Al} , $\underline{Al_2O_3}$, \underline{FeO} , $\underline{MgAl_2O_4}$, \underline{MgO} .

Solid:

\underline{B} , \underline{BN} , $\underline{B_4C}$, \underline{C} , \underline{MgO} , $\underline{MgAl_2O_4}$, $\underline{Al_2O_3}$, $\underline{Fe_2O_3}$, \underline{FeO} .

The only significant liquid species under exhaust conditions is B_2O_3 . In computations "A", the amounts of B_2O_3 (l) range from 5 to 12 weight-percent of the total formulation (6 to 13% of CE). In computations "B" these amounts are substantially higher, 10 to 18% of the total (12 to 21% of CE).

The major difference between computations "A" and "B" concerns the formation of solids. When full equilibrium is assumed ("A"), most of the boron in the exhaust appears as solid B_4C , and a significant fraction as solid BN. The amount of free boron, if any, depends on the ratio of boron to carbon in the formulations: virtually all of the carbon is found in $CO(g)$ and $B_4C(s)$, so if there is excess boron left (after BN, B_4C , B_2O_3 and CO form), a substantial fraction of it will appear as B(s). ARCADENE 280 has relatively little carbon (high B/C ratio, low C/O ratio), so computations "A" on Runs 1 and 3 show some B(s), and no C(s). Computations "A" on ARCADENE 256A, which has substantially more carbon (low B/C ratio), show a small amount of C(s), but no B(s). In computations "B", the formation of boron compounds is artificially suppressed to a large extent. Thus much of the boron (range of 87 to 92% over the four runs) appears as B(s), and most of the remainder (7 to 12%) as $B_2O_3(l)$; as mentioned previously, the amount of $B_2O_3(l)$ is substantially higher in computations "B" than in "A". Carbon in computations "B" appears almost entirely as C(s) and $CO(g)$, but the abundances of these two species are very different in the two formulations: in ARCADENE 256A, more than 90% of carbon appears as C(s), and less than 10% as CO; in ARCADENE 280, only about 40% appears as C(s) and 60% as $CO(g)$. In all computations virtually all of the aluminum appears as solid $MgAl_2O_4$, which is always a major solid species (about 7% of total exhaust). Magnesium distributes itself among MgO , $MgAl_2O_4$ and $MgCl_2(g)$.

The major condensable gases predicted by the computer are $MgCl_2$, B_2O_2 , B_2O_3 , $B_3H_3O_3$, HCl, and Mg. The amount of these gases appears to be mainly a function of the exhaust temperature. Since temperatures are always higher in computations "A", these computations predict more gases than computations "B". The highest exhaust temperature is that of Run 1, computation

"A"; the condensable gases according to that computation, comprising 19% of the total exhaust, consist mostly of boron-containing species. At lower temperatures (e.g. computations "B") the equilibrium of boron-containing species shifts toward formation of substantially more $B_2O_3(l)$; the condensable gases drop to roughly 10% of the total formulation, and they consist mostly of $MgCl_2$ and HCl .

The theoretical characterization of the CE relevant to this report can be summarized as follows: (a) 11 of the boron will be found in the CE. The fraction of the CE which is boron (any form) is about 50% for either propellant, regardless of the type of computation ("A" or "B"). Quantitative data on the amounts of boron in the CE of each run, both as predicted by the thermodynamics and as determined experimentally, are detailed in Section IV. (b) Most of the boron (roughly 90% of it) is found in three solid species: B, B_4C , and BN. The question of the realistic distribution of boron among these three, i.e., the relative merits of computations "A" and "B", must be resolved by experiment. (c) The remainder of the boron is in the CE in the form of boron-oxygen-hydrogen species. While some of these are rather volatile, all will be condensed at the room temperature. (d) The remainder of the CE consists largely of $MgAl_2O_4$ and $MgCl_2$ in computations "A", and $MgAl_2O_4$, $MgCl_2$, and C(s) in computations "B".

III. PHYSICAL ANALYSIS OF THE CONDENSED EXHAUST

1. Microscopic Examination

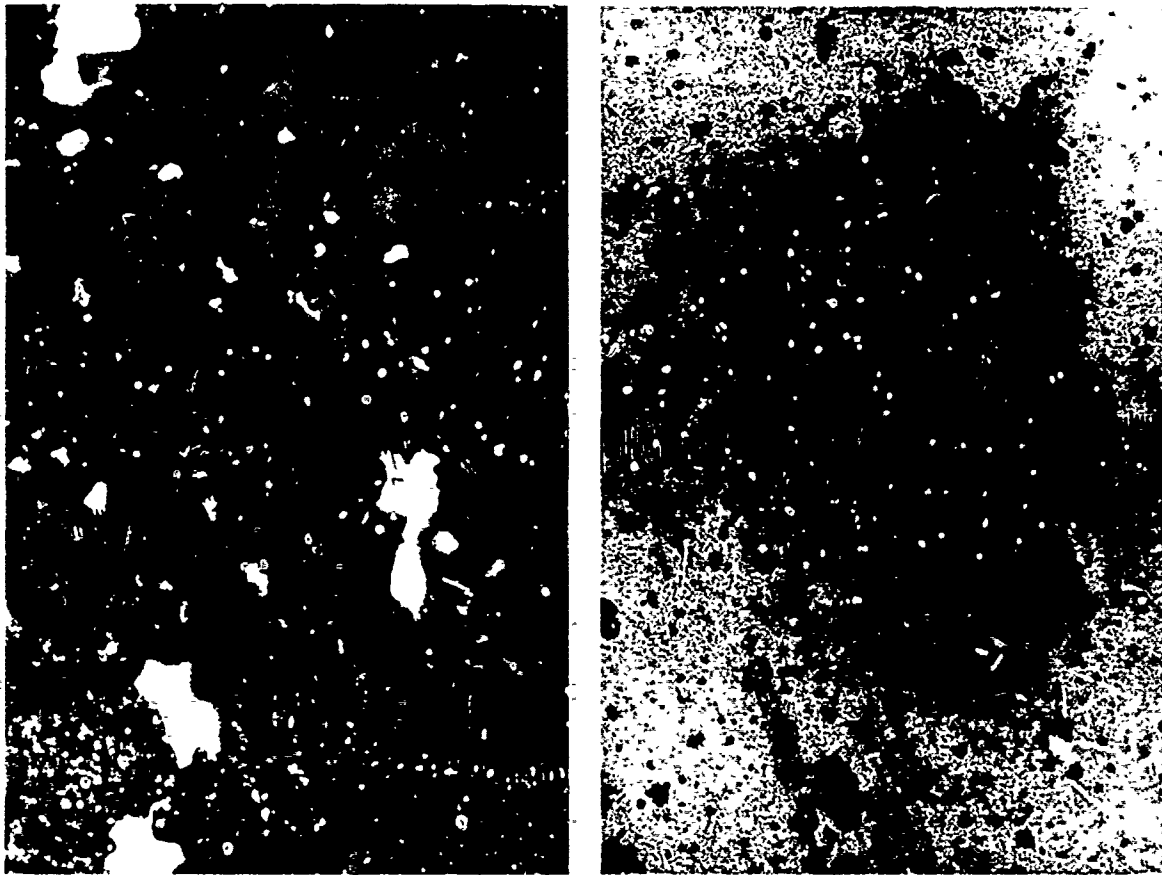
The condensed exhaust (CE), collected as described in Section II, was examined under an optical microscope with magnifications up to 500 \times . The untreated CE consists of very large, but only loosely agglomerated clusters. The tumbling of the clusters with soft (plastic) balls breaks up the mass of the CE into smaller particles. Microphotographs of CE samples (a) as collected and (b) after tumbling are shown in Figure 2. The treated material (Figure 2b) consists of particles ranging from about 3 to 50 μm in diameter. Larger particles in that range are no doubt agglomerates which could be broken up by continued tumbling. The small material ($< 10 \mu\text{m}$) may be either firm agglomerates or single particles.

Several distinctive features can be seen under the microscope. The bulk of the CE is dark and apparently amorphous, but quite a few crystals are also visible. The crystals are either white or colorless. The dark material could be carbon and carbeneous material, elemental boron, or possibly B_4C . The light material could be any and all of the following: B_2O_3 (colorless), $\text{B}_2\text{O}_3 \cdot \text{H}_2\text{O}$ (triclinic crystals, white), MgCl_2 (colorless hexagonal), $\text{MgCl}_2 \cdot \text{H}_2\text{O}$ (white), MgAl_2O_4 (colorless), and BN (white hexagonal).

2. Density Measurement

We determined the density of the CE samples by suspending them in inert liquids having several different specific gravities. The liquids were mixtures of bromoform (sp. gr. 2.89) and carbon tetrachloride (sp. gr. 1.595). The samples were found to consist of particles having different densities, mostly in the range of 1.8 to 2.1 gm/cc.

A complete set of such density measurements has been made on the CE sample collected in Run 1. Photographs of several suspensions are shown in Figures 3, 4 and 5. These photographs allow interesting conclusions to be made.



SAMPLE 104 a. AS COLLECTED (5μ PER SINGLE DIVISION)
 b. AFTER BALL-MILLING AND SIEVING (2.6μ PER DIVISION)

Fig. 2 Micrographs of Samples Collected in
Motor Test 104

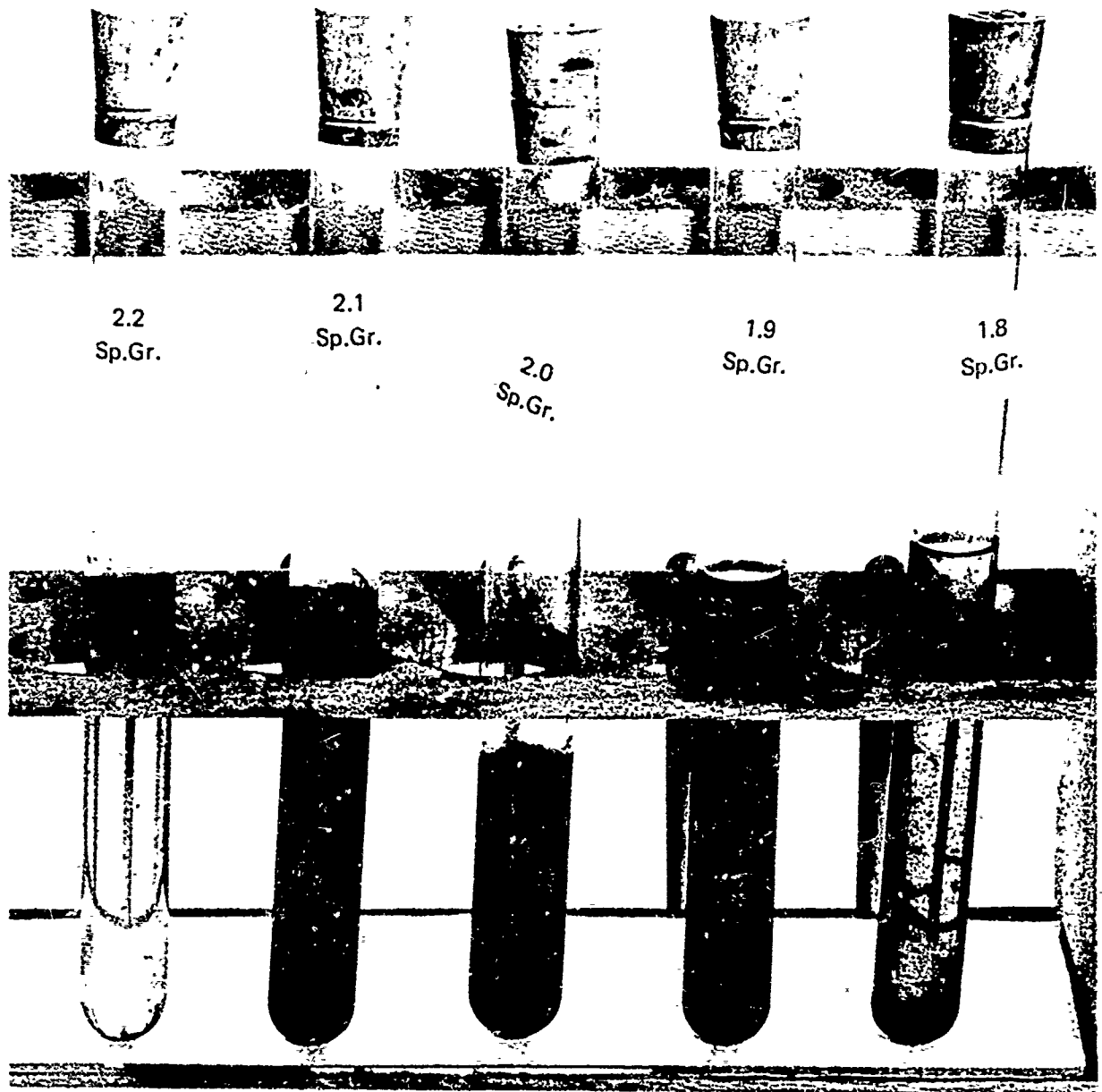


Fig. 3. CE from Run 1.

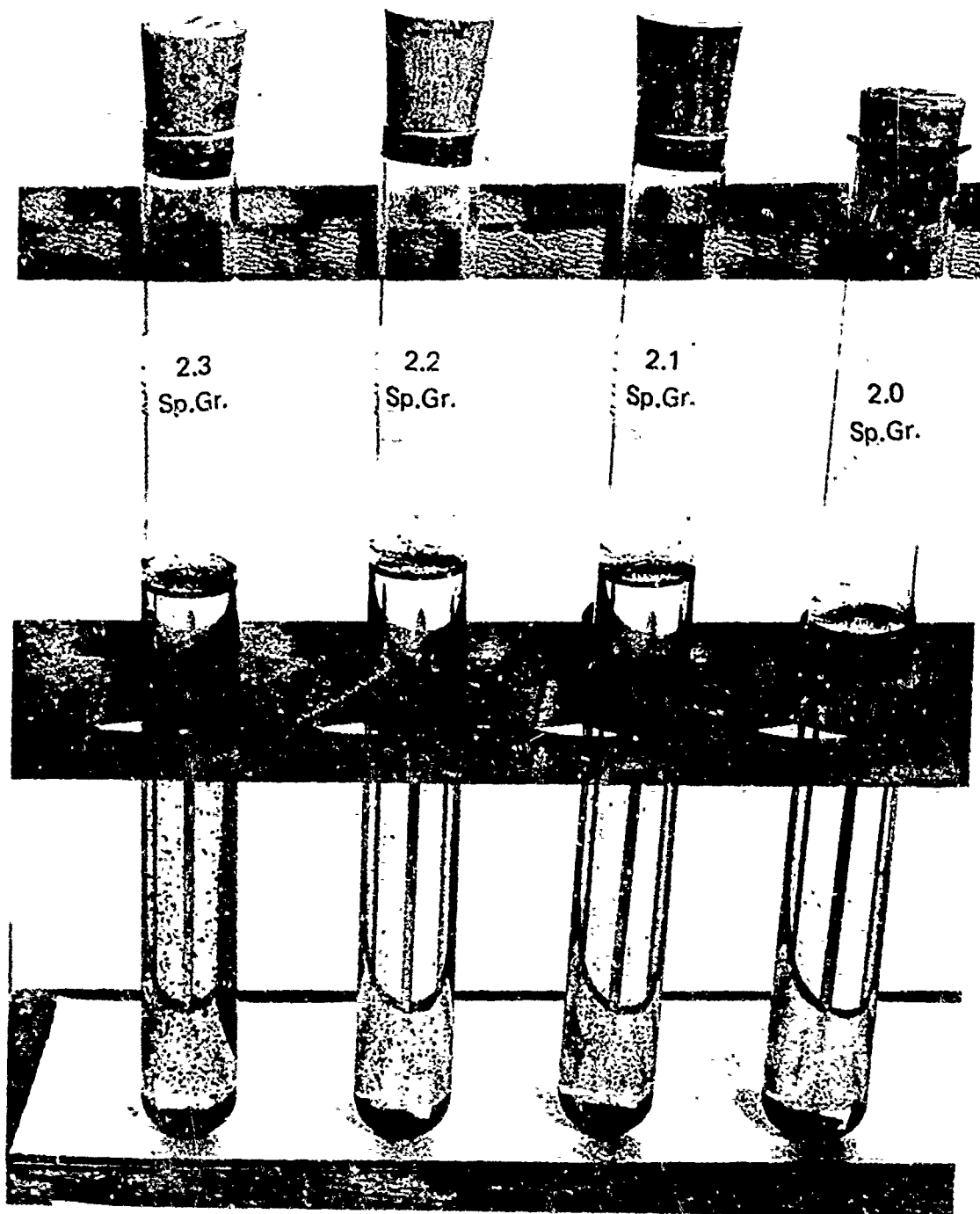


Fig. 4. CE from Run I after washing in hot alcohol.

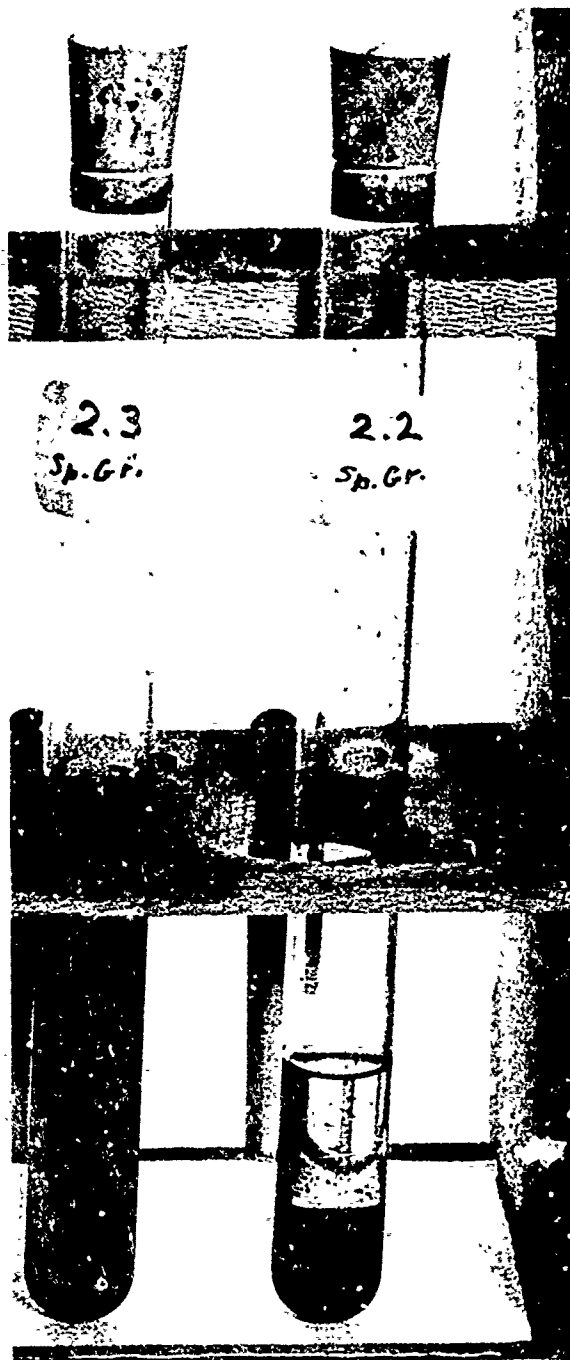


Fig. 5. Untreated boron powder.

Figure 3 shows suspensions of the CE, as collected in Run 1, in liquids having specific gravities ranging from 1.8 to 2.2. It can be seen that all particles in the sample have specific gravities lower than 2.2, and some even lower than 1.8. Most of the sample appears to be around sp. gr. 2.0.

A CE sample from Run 1 was washed in a hot mixture of methyl and ethyl alcohol, a standard procedure for removal of B_2O_3 from boron powder. Suspensions of the washed sample are shown in Figure 4. It can be clearly seen that the specific gravity of most of the washed material is higher than 2.3. It should be noted here that $MgCl_2$, a major thermodynamically predicted constituent of the CE, is also soluble in alcohol.

For the purpose of comparison, two suspensions made with the "off-the-shelf" boron powder (Kawecki Co. material used in all our propellants) are shown in Figure 5: virtually all of the powder has the specific gravity of about 2.3, i.e., distinctly higher than the unwashed CE, but perhaps slightly lower than the washed CE. The handbook value for the specific gravity of pure boron is 2.32-2.35. Thus the 2.3 value for the commercial powder is very reasonable, especially since the material is known to contain about 2% B_2O_3 , which has a lower specific gravity.

Our conclusion is that, in the CE, low-density substances coat, or are firmly attached to, solid B (and B_4C , if any). The washing removes these substances, and leaves a residue consisting largely of B (sp. gr. 2.32 - 2.35) and possibly graphite (sp. gr. 2.26), B_4C (sp. gr. 2.54), or BN (sp. gr. 2.25). The possible low-density species are: B_2O_3 (sp. gr. 1.85), $B_2O_3 \cdot 3H_2O$ (sp. gr. 1.49), and $MgCl_2 \cdot 6H_2O$ (sp. gr. 1.56); the $MgCl_2$ without any crystalline water has the specific gravity of 2.33. Since carbon is insoluble in alcohol; the fact that the washed CE contains little low-density material suggests that the untreated CE contained little or no amorphous carbon (sp. gr. 1.8 to 2.1). This has to be interpreted in the light of the thermodynamic computations: the full computation on Run 1 (Section II), including B_4C and BN in the products, predicts no solid carbon; if B_4C and BN are "suppressed," the thermodynamic computation predicts the CE to contain about 7% carbon. This comparison suggests that computations "A" may be somewhat more realistic.

IV. CHEMICAL ANALYSIS OF THE CONDENSED EXHAUST

The CE samples from all four motor runs were analyzed chemically for boron. The analysis was performed by Ledoux and Company, Teaneck, N. J. on a subcontract from Atlantic Research. The CE samples were first separated into the soluble and the insoluble portions by boiling water, and then each of the two portions was analyzed for total boron.

The results of the chemical analysis are summarized in Table IV, which lists (a) fraction of the CE which is boron (any form), (b) division of the CE into soluble and insoluble portions, and (c) fraction of the total boron in each of these portions. In each case we have listed the thermodynamically predicted values along with the experimentally determined ones. The species assumed insoluble for the purpose of comparison of the computation with the experiment are listed in Table IV. The reader should consult Table III to see which species can occur in any appreciable amounts ($> 0.5\%$ of total formulation). Inspection of Tables III and IV shows that the insoluble boron can be expected to be found in B, B_4C and BN. The soluble boron may come from a number of boron-oxygen-hydrogen species.

Before discussing the individual columns of Table IV we point out that, generally, the experimental results show somewhat larger differences from run to run than the theoretical predictions; moreover, the deviation of the theory from the experiment is not always in the same direction from run to run (e.g., always positive or always negative), but generally random. The experimental procedure consisted of three independent steps: propellant combustion (including ejection efficiency), sample collection, and chemical analysis. Since the combination of all three contributes to the final results listed in Table IV, we cannot ascertain the reasons for the random deviation in all four runs. However, the combustion of Run 4 does appear to have been faulty. Table I shows that the ejection efficiency of that run was unusually poor. Table IV shows both an exceptionally low amount of boron in the CE and an exceptionally low amount of insoluble matter in the CE; both results indicate that in Run 4, for some unknown reason, a significant fraction of

TABLE IV. Chemical Analysis of the CE (weight percent)

Run No.	Fraction of the CE which is Boron (in any form)		Insoluble Portion** (% of CE)		% B in insoluble portion		% B in soluble portion		
	Comput. A	Comput. B%	Comput. A	Comput. B%	Comput. A	Comput. B%	Comput. A	Comput. B%	
		Experim.		Experim.		Experim.		Experim.	
1	51.6	56.5	70.0	71.0	64.1	70.8	22.6	21.8	17.8
2	52.7	51.3	80.0	75.5	62.5	62.4	13.9	17.0	27.0
3	50.6	53.5	68.5	68.3	62.3	67.7	25.0	23.2	24.7
4	50.2	48.6	77.5	72.5	60.3	59.9	15.9	18.9	8.6

* B₄C and BN omitted in computations

** Species assumed insoluble: B, C, MgO, MgAl₂O₄, B₄C, BN, Fe, Mg. All others assumed soluble.

the boron had remained in the motor (the residue was not analyzed). In view of these atypical results, we shall omit Run 4 from the discussion of trends in Table IV.

In all three runs under comparison (Runs 1, 2, and 3), the measured amount of boron in the CE agrees somewhat better with computation "A" than with computation "B". The average deviations from the experiment are 12% for computations "A" and 19% for computations "B". However, it must be pointed out that the experimental data are not intermediate between the two computations, as might be expected if there were partial formation of B_4C and BN: rather, both theoretical results are low in Run 2 and high in Runs 1 and 3.

The partition of the CE into soluble and insoluble portions is predicted distinctly better by the computation "A" in Run 2, slightly better by "B" in Run 1, and about equally well in Run 3. Average deviations from the experiment: 6% for computations "A", 8% for computations "B".

The percentage of insoluble boron is predicted better by "A" in Runs 1 and 3, and equally well by "A" and "B" in Run 2. Average deviations: 12% for "A", 20% for "B".

The measured amounts of boron in the soluble portion of the CE are predicted quite well by both computations in Run 3, but very poorly in Runs 1 and 2. Computation "B" appears somewhat better of the two. Average deviations: 41% for "A", 29% for "B".

We conclude that according to both the experimental data and either one of the two computations only about 50% of the total CE is boron. Beyond that, one can see that three out of four questions which can be answered by the results of the chemical analysis - namely, the amount of boron in the CE, the fraction of the CE which is insoluble, and the amount of boron in the insoluble portion - are predicted reasonably well (order of 10%) by the full thermodynamic computation (column "A" in Table IV). Computations "B" are somewhat less successful, but it appears that they also give a rough idea of the composition of the CE. Indeed, it is possible that the assumptions

inherent in the theoretical comparisons - e. g., the freezing of the exhaust equilibrium - introduce more of an uncertainty than the difference between the two sets of computations. Only an extensive chemical analysis of several species (Mg, B₄C, C, and others) could resolve the problem of the detailed composition of the CE.

V. COMBUSTION OF THE CONDENSED EXHAUST

As described in Section III, and shown in Figure 2, the ball-milled CE consists of many small particles with sizable agglomerates interspersed. Prolonged ball-milling and sieving through a 20 μm mesh screen produced a fine powder consisting of particles having a fairly uniform size distribution with average diameters of 3 to 4 μm . By careful screening between 30 and 35 μm we also found it possible to separate coarse powder samples consisting of firm agglomerates which could be treated as single particles.

Combustion of the coarse CE samples was studied by a single-particle technique, utilizing a gas burner, which was previously developed and extensively used at Atlantic Research for combustion studies of aluminum (6, 7, 8), beryllium (9, 10) and boron (2). Since particles smaller than 10 or 20 μm in diameter are difficult to handle and observe singly, we adapted the gas-burner technique for a study of particle clouds. The newly developed technique was used to study ignition and combustion of the fine CE powder.

A. The Gas Burner

The gas-burner used for both the work with single particles, 30 to 40 μm in diameter, and clouds of fine particles, 3 to 4 μm in diameter, is shown in Figure 6. In the single-particle work, the powder is introduced directly into the flotation chamber; the lower chamber is not used. This apparatus was described in detail in Ref. 6. The particles are entrained through the hypodermic needle by an inert carrier gas, usually helium, and thus introduced rapidly into the stream of a burner gas having known composition and temperature. The linear velocity of the burner gas is of the order of 1 cm/msec. The effect of the inert gas on combustion of particles can be neglected, because the hypodermic tube is only 0.25 mm in diameter, and ignition of particles takes place several centimeters above the burner plate.

The modification of the burner to allow combustion studies of clouds consisting of small particles has been accomplished by (a) the addition of the lower chamber, and (b) enlargement of the hypodermic tube to 0.6 mm

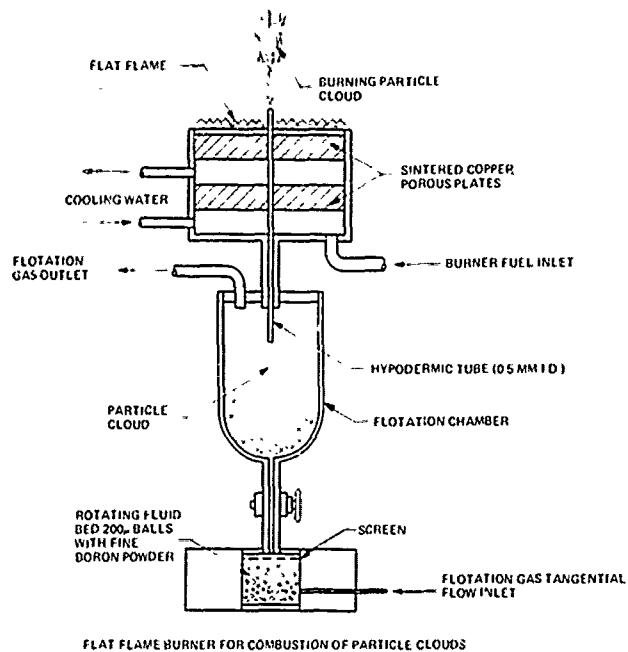


Figure 6. Flat-Flame Gas Burner for Combustion of Particle Clouds

in diameter. The purpose of the lower chamber is to break up particle clusters, or to prevent them from forming in the first place. This is done by the introduction of a high-velocity tangential jet of the carrier gas which stirs up the powder and the plastic balls with which the chamber is packed. In this way a steady stream of powder can be introduced into burner gases for prolonged periods of time. Our experiments usually lasted 5 to 15 minutes.

One disadvantage of the continuous cloud combustion experiments is that the effect of the carrier gas on ignition of particles cannot be neglected. This is so primarily because the preignition delays of small particles are very short. As will be described later in this report, the CE particles ignite when their temperature approaches 2000°K. Heat transfer estimates show that heatup times from room temperature to 2000°K of 3.5 μ m diameter particles, injected into gases having temperatures of 2200 to 2500°K, are only of the order of 10 to 100 μ sec. The laminar diffusion mixing time for a 6 mm diameter jet will be of the order of 0.5 msec. Thus, the preignition delays and the carrier-gas mixing times overlap, so a quantitative study of ignition delays would require detailed heat transfer and mixing calculations. Our work did not include such calculations. On the other hand, studies of post-ignition burning times are not seriously affected by the carrier gas mixing process, because the temperature of the gas adjacent to the particle must approach the burner-gas temperature (i.e., the mixing must be nearly completed) before ignition. Moreover, in the actual experiments described in Section V-C, the carrier gas was air, and the mole fraction of oxygen in the burner gases was $X = 0.2$ in most experiments. Thus, the mole fractions of O_2 , the most important oxidant, were matched in the two gases. Since the carrier air was initially cold, the effective gas temperature during combustion was not known accurately (it was probably a little below the gas-burner temperature), but the gas temperature is not a dominant parameter during self-sustained combustion; the mole fraction of the oxidant is. Thus, the experiment is well controlled as far as post-ignition processes are concerned.

B. Single-Particle Experiments

The single-particle technique has been used for a study of both the ignition and the subsequent combustion of a 30-40 μm CE sample collected in Run 4. The gas burner was run on propane-oxygen-nitrogen mixtures. The burner gases consisted of 1.4 - 20% O_2 , most observations having been made with about 20% O_2 , 15 - 20% H_2O , and 10 - 12% CO_2 ; the remainder was mostly N_2 . Gas temperatures were varied from 1850 to 2300°K. Velocities of burner gases were about 1000 cm/sec, and those of the carrier (helium) about 100 cm/sec.

Quantitative ignition and combustion parameters of neat boron powder in the 30 to 40 μm range are well known from our previously published work (2). Since it is of obvious interest to compare the combustion characteristics of the CE to those of boron, we shall now briefly state the relevant results of Ref. 2. The entire history of the boron particles ($\bar{d} = 35 \mu\text{m}$) in the burner gases (2240°K, 19% O_2 , 16% H_2O) can be divided into three phases: a dark pre-ignition period (ca. 8 msec), followed by a peculiar two stage combustion, the durations of the two periods being $t_1 = 4 \text{ msec}$ and $t_2 = 11 \text{ msec}$. The first combustion stage begins when the particle temperature is about 1850°K. The first stage is generally believed to correspond to slow combustion, impeded by a layer of liquid B_2O_3 . Most of the mass of boron is consumed during the rapid second stage, controlled by the gas-phase diffusion of oxidants toward the particle; thus t_2 approximates the total diffusion-combustion time of the particle, $t_2 \sim t_p$. The minimum temperature of the burner gases necessary for ignition of particles was found to be $1880 \pm 20^\circ\text{K}$.

The CE agglomerates, $30 \mu\text{m} < d < 40 \mu\text{m}$, were found to burn as single particles: there is no separation of particle trajectories. Thus, we can make a quantitative comparison of the CE combustion to combustion of boron. When the CE, $30 \mu\text{m} < d < 40 \mu\text{m}$, is burned in the same burner gases as the 35 μm boron ($T_g = 2240^\circ\text{K}$, 19% O_2 , 16% H_2O - see previous paragraph), the following differences are observed:

1. The CE "particles" give well-defined burning times, but there is no sign of two-stage combustion.
2. The average burning time of the CE is $t_b = 10 \pm 1.5$ msec.
3. The CE ignites substantially lower in the burner gases than boron: we estimate that the preignition delay of the CE is 30 to 50% lower than for boron particles.

In addition to the tests at constant gas temperature and constant mole fraction of O_2 , we ran two series of experiments in which these two parameters were varied. Variation of temperature at constant mole fraction of O_2 (ca. 0.2) showed that the minimum gas temperature necessary for ignition of the CE is $1850 \pm 25^\circ K$. Variation of O_2 content at the approximately constant gas temperature of 2200 to 2300°K shows that the CE continues to burn, although very slowly, even at the lowest mole fraction of O_2 which we tried, 0.014.

Since the burning time of a particle is a strong function of its diameter, and since we have no accurate value for the average diameter of the CE, the two values, $t_b = 10$ msec for the CE and $t_b \sim t_2 = 11$ msec for boron, must be considered the same within the experimental error.

C. Cloud Combustion Experiments


The cloud technique for combustion of small particles, described in Section V-A, yields average preignition delays t_i and burning times, t_b . A cloud of burning CE particles (Run 1) is shown in Figure 7. Inspection of this photograph will show that both t_i and t_b are approximate, because in a burning cloud one cannot define clear points of onset and cessation of combustion. Furthermore, since the preignition delay necessarily overlaps the carrier-gas mixing time (see Section V-A for discussion), one cannot obtain cloud ignition temperatures from measured preignition delays as in single-particle work; one can only determine relative ignitabilities of two clouds by comparing the preignition distances in two replicate experiments.

Two CE samples, from Runs 1 and 4, have been studied by this technique. The results obtained with these two samples are indistinguishable



Fig. 7. Combustion of a Cl particle cloud.

$T = 2070^{\circ}\text{F}$, $X(\text{O}_2) = 0.2$, $X(\text{H}_2\text{O}) = 0.18$

Reproduced from
best available copy. 

from each other. In the subsequent sections the "CE sample" means either Run 1, or Run 4, or both.

1. Particle Sizes

The CE samples used in the cloud experiments consisted of the material which had passed through a 20 μm mesh screen. However, since the gas burner operates in such a way that the material is subjected to prolonged swirling with plastic balls (see Section V-A and Fig. 6), there is no assurance that the particle size distribution injected into the burner gases is the same as in the original (sieved) sample. We therefore sampled the unburned material after injection into the burner gases, i.e., at a point between the injection orifice but below the point of ignition. Microscopic examination of the sampled material revealed that the particle diameters were in the range between 2 and 7 μm . The average diameter was about 3.5 μm .

In addition to the CE, two other samples were studied by the cloud-combustion technique for the purpose of comparison: an amorphous boron sample, supplied by U. S. Borax, Inc., stated to be 98% pure, and the material supplied by Kawecki, Inc. The Borax powder particle diameters are in the narrow range of $1.0 \pm 0.2 \mu\text{m}$. The Kawecki powder has a wide distribution of particle diameters, ca. 1 to 20 μm , with the number average of 3 μm . The Kawecki boron is used both in ARCADENE 256A and 280 propellants.

2. Ignition

A technique for direct measurement of minimum gas temperatures necessary for ignition of particles had been developed previously in connection with our single-particle work (2): a stream of particles is continuously injected into burner gases, the temperature of which is gradually decreased until the particles cease to ignite. This technique has now been successfully applied in the cloud-combustion work. The mole fraction of O_2 in these ignition-limit experiments was kept about 0.2.

The limiting temperature was found to be the same, within the experimental error, for the Borax sample and for the CE: $1980 \pm 20^\circ\text{K}$. It will be noted that this is 100 - 150° higher than the analogous temperature

limit for 30 - 40 μm particles of either the CE or crystalline boron (Section V-B of this report and Ref. 2).

Measurements of the minimum gas temperatures necessary for ignition of powders, which we shall refer to as "temperature limits" from now on, have resulted in two conclusions: (a) temperature limits for clouds of small ($< 10 \mu\text{m}$) particles are 100 to 150°K higher than for large (30 to 40 μm) particles; (b) regardless of the particle size, temperature limits are the same for the CE and for boron.

We shall first discuss the second conclusion: similarity of the temperature limits. This result is surprising for two reasons. First, as discussed in Section IV, only about half of the CE is boron. The remainder consists of substances which have different ignition temperatures. Referring to Tables II through IV, we can see that ignition temperatures of some expected ingredients will be higher than those of boron (B_4C , BN, Al), while others will be lower (Mg, MgCl_2 , Fe, C). One would expect a priori that ignition of any appreciable fraction of the CE would lead to ignition of the entire sample. The experimentally determined ignition temperature of the CE perhaps suggests that the amounts of ignitable ingredients are relatively small. We have no chemical analysis of the CE ingredients other than boron, nor do we know the critical degree of admixture of ignitable materials required to lower the ignition temperature of samples below that of boron.

The measured ignition temperature of the CE also appears surprising at the first glance, because the observed preignition delays are substantially lower than for boron. This result, however, can be rationalized. First, we point out that the density of the CE is lower than that of boron (Section III). Now the heating rate of a particle is inversely proportional to its density:

$$\frac{dT_p}{dt} = \frac{6}{\rho_p C_p d} \left[\frac{k_g \text{Nu}}{d} (T_g - T_p) - \sigma \epsilon T_p^4 \right],$$

where ρ is density, C heat capacity, and k thermal conductivity; the subscripts p and g refer to particle and gas respectively. This means that the heat-up time of a particle to any specified temperature will be directly proportional to its density. Since the measured densities of the CE are 10 to 20% lower than that of boron, the heat-up times will be lower by the same factor.

In addition to the density effect, there may be a more subtle difference in the pre-ignition processes between the CE and boron. The CE particles are almost certainly agglomerates, so they are apt to have much larger surface areas than crystalline boron, which was studied in Ref. 2. Since during the pre-ignition stage the rate process will usually not be controlled by gas-phase diffusion toward the particle, but rather by the global surface kinetics - including the processes of diffusion across a surface layer, vaporization, and chemical reaction (11, 12) - the pre-ignition rate will be proportional to the effective surface area. The large surface area of the CE may be expected to have two observable effects: (a) the ignition "runaway" temperature, and therefore the pre-ignition delay will be decreased; and (b) the duration of the first combustion stage (t_1 observed in the case of boron) will also be decreased. As described earlier in this section, a substantial decrease in the pre-ignition delay of the CE as compared to boron was indeed observed. Concerning the second expected effect, decrease in t_1 , we have observed no first stage at all in the case of the CE. Since a decrease in t_1 by a factor of about 4 would suffice to make the first stage elude the observation, a large increase of the effective surface may account for the effect; however, this is a matter of conjecture.

We now turn briefly to the other quantitative conclusion regarding the ignition, namely that temperature limits of clouds consisting of small particles are higher than for large single particles. A detailed theoretical analysis of the boron ignition (11, 12, 14) shows that the process is complex involving problems of heat transfer, gas-phase and surface-layer diffusion, and vaporization. Examination of Figure 17 in Section VI (a reprint of Reference 12) indicates that 2 micron particles are predicted to

have a minimum required surroundings temperature for ignition approximately 90°K higher than that predicted for 30 micron particles, consistent with the experimental observations. (This is not conclusive, however, since the predictions are in both cases for single particles and the cloud effect on minimum required surroundings temperature for ignition is not well-defined.)

3. Burning Times

The cloud combustion technique has been used for burning time measurements of the CE, of the Borax boron, and of the Kawecki boron. The burning time t_b was taken to be equal to the length of the burning cloud (see Fig. 7), divided by the linear velocity of the burner gases. Since the luminosity of the cloud both develops and fades out gradually, an approximate visual judgement concerning the length of combustion must be made. The velocity of the burner gases can be calculated from known (metered) input gas flow and known flame temperature; it can also be obtained by measurement of single-particle velocities. The calculated and the measured values usually agree within about 25%. We estimate that the combined uncertainties of the cloud length and particle velocity may conceivably lead to an error in determination of t_b of up to a factor of two, but most t_b values are probably better than that.

The average results of three cloud-combustion measurements are shown in Figure 8. The burner gas properties in all three experiments were: $T = 2240^\circ\text{K}$, $X(\text{O}_2) = 0.19$, $X(\text{H}_2\text{O}) = 0.16$. A single point for the t_b of a spherical boron particle, $d = 37 \mu\text{m}$, is given in the same plot. The single-particle point is a small extrapolation of an accurate measurement (see Table VI of Ref. 5) in a somewhat different burner gas: $T = 2280^\circ\text{K}$, $X(\text{O}_2) = 0.23$, $X(\text{H}_2\text{O}) = 0$. Even with the extrapolation, the values of both t_b and of d are no doubt much more accurate for the single-particle point than for the cloud measurements. In view of the uncertainties in the cloud measurements, one should be careful about assigning a specific numerical value to the slope n in Figure 8. However, an inspection of the figure shows that even if the cloud data are in error by a factor of 2, n will still be closer to unity than to a value of 2, predicted by single-particle diffusion theories (13, 14).

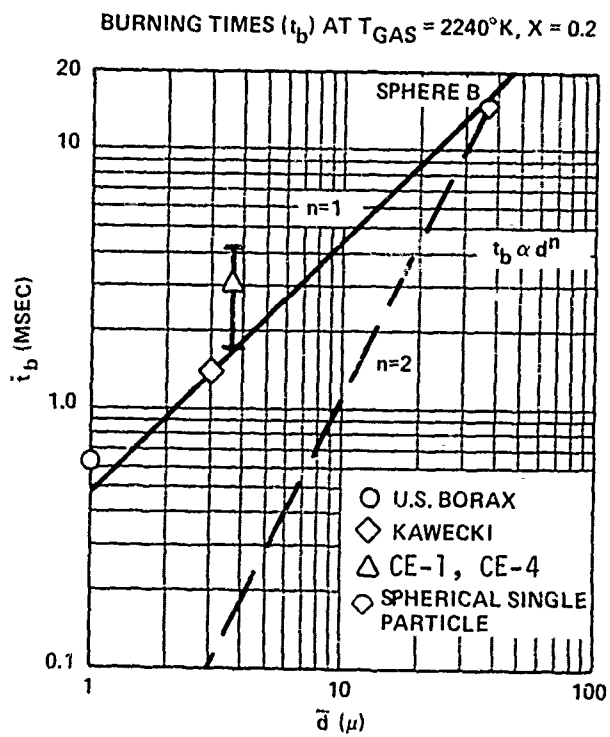


Fig. 8. Burning Times (t_b) of Various Particles

In addition to experiments run with burner gases having a constant relatively high mole fraction of oxygen, $X(O_2) = 0.2$, cloud experiments were made with decreasing values of $X(O_2)$ both with the CE and with the Borax boron powder. Gas temperatures in all the tests were kept at about 2300°K. Only visual observations were made. It was found that both powders burned about equally vigorously down to $X(O_2) = 0.14$. The combustion brightness decreased rather sharply between $X(O_2) = 0.14$ and 0.12, and then very gradually down to about $X(O_2) = 0.05$ with both powders. At very low mole fractions of oxygen, 0.015 to 0.05, the CE powder burned very weakly, and the boron powder hardly at all.

The single-particle experiments indicate that the burning times t_b of the CE are about the same as for boron. This appears a priori reasonable, because one would expect the limiting process to be the gas-phase diffusion of oxidants regardless of the chemical composition. Higher volatility of some expected CE ingredients should accelerate the burning rate of particles. Thus if the CE is rich in species such as Mg, $MgCl_2$, and Fe, one should expect it to burn somewhat faster than boron. On the other hand, if it contains large amounts of B_4C (and possibly BN), it may burn more slowly: B_4C is known to burn more slowly than boron (15), and BN has been observed to ignite only with difficulty. In either case, the change in t_b of boron caused by adulteration is probably not sufficient to be clearly demonstrated by our experiments.

REFERENCES FOR SECTIONS I - V

1. Talley, C.P., and Henderson, U.V., "Combustion of Elemental Boron," Proceedings of the 4th Meeting of the JANNAF-ARPA-NASA Thermochemical Panel, p. 107 (1961).
2. Maček, A., and Semple, J., "Combustion of Boron Particles At Atmospheric Pressure," Combustion Science and Technology, 1, pp. 181-191 (1969).
3. Uda, R.T., "A Shock-Tube Study of the Ignition Limit of Boron Particles," GA/ME Thesis, Air Force Institute of Technology, Wright-Patterson Air Force Base, Dayton, Ohio (1968).
4. Maček, A., and Semple, J., "Combustion of Boron Particles At Elevated Pressures," 13th Symposium (International) on Combustion, The Combustion Institute, Pittsburgh, Pa., pp. 859-868 (1971).
5. Maček, A., "Combustion of Boron Particles: Experiment and Theory," 14th Symposium (International) on Combustion, The Combustion Institute, Pittsburgh, Pa., pp. 1401-1411 (1973).
6. Friedman, R., and Maček, A., "Ignition and Combustion of Aluminum Particles in Hot Ambient Gases," Combustion and Flame, 6, 1, pp. 9-19 (1961).
7. Friedman, R., and Maček, A., "Combustion Studies of Single Aluminum Particles," 9th Symposium (International) on Combustion, Academic Press, N. Y., pp. 703-712 (1963).
8. Friedman, R., Maček, A., and Semple, J., in Heterogeneous Combustion, Academic Press, N. Y., p. 3 (1964).
9. Maček, A., "Fundamentals of Combustion of Single Aluminum and Beryllium Particles," 11th Symposium (International) on Combustion, The Combustion Institute, Pittsburgh, Pa., pp. 203-217, (1967).
10. Maček, A. and Semple, J., "Experimental Burning Rates and Combustion Mechanisms of Single Beryllium Particles," 12th Symposium (International) on Combustion, The Combustion Institute, Pittsburgh, Pa. pp. 71-81 (1969).
11. King, M.K., "Boron Ignition and Combustion in Air-Augmented Rocket After-Burners," Comb. Science and Technology, 5, pp. 155-64 (1972).
12. King, M.K., "Boron Particle Ignition in Hot Gas Streams," Comb. Science and Technology, 8, 6, p. 255 (1974).
13. Prentice, J.L., et al., Metal Particle Combustion Progress Report, Naval Weapons Center Report TP4435, Appendix A, p. 106, (1968).

14. Mohan, G., and Williams, F., "Ignition and Combustion of Boron in O₂/Inert Atmospheres," AIAAJ, 10, 6, pp. 776-83, (1972).

VI. MODELING OF BORON PARTICLE IGNITION IN HOT GAS STREAMS (Reprinted from Combustion Science and Technology)

Combustion Science and Technology
1974, Vol. 8, pp. 255-273

© Gordon and Breach, Science Publishers Ltd.
Printed in The United Kingdom

Boron Particle Ignition in Hot Gas Streams

MERILL K. KING

Atlantic Research Corporation, Alexandria, Virginia

Abstract—A model of boron ignition treating the inhibiting effect of a boric oxide coating has been developed. Transient differential equations describing the generation and removal of the oxide and associated thermal effects along with heat transfer between the particle and surroundings have been derived, converted to difference form and programmed for computer solution for determination of ignition limits and ignition times. Predictions for particles studied by Macek in a flat-flame burner have been compared with experimental results—agreement is good for dry gas cases, but poor when the gas stream includes water. The program has been used to predict effects of initial oxide thickness, particle size, pressure, oxygen content, initial particle temperature, gas temperature and surroundings radiation temperature on ignition. In addition, the original differential equations have been treated by a stability analysis to determine ignition limits—excellent agreement is found between results obtained with the stability analysis and the numerical analysis.

NOMENCLATURE

$A, B, C, D,$	constants in stability analysis	$P_{B_2O_3, \infty}$	boric oxide partial pressure in free-stream (atm)
E, F	dependent only on initial particle size and such boundary conditions as pressure, oxygen mole fraction, and ambient temperature	Q_{RX}	heat release of $B(s) + \frac{3}{2}O_2 \rightarrow \frac{1}{2}B_2O_3(l)$ (cal/gm-mol)
c_{PB1}	liquid boron heat capacity (cal/gm °K)	Q_{RX2}	heat release of $B(l) + \frac{3}{2}O_2 \rightarrow \frac{1}{2}B_2O_3(l)$ (cal/gm-mol)
c_{PBS}	solid boron heat capacity (cal/gm °K)	R	gas law constant, 82.06 atm-cm ³ /gm-mol °K
$c_{PB_2O_3}$	liquid boron oxide heat capacity (cal/gm °K)	R'	gas law constant, $8.316 \cdot 10^{-10}$ erg/gm-mol °K
f	fraction of boron in the liquid phase	R_B	molar rate of boron consumption (gm-mol/sec)
h	gas-particle heat transfer coefficient (cal/cm ² sec °K)	R_E	molar evaporation rate of boric oxide (gm-mol/sec)
k	mass transfer coefficient for transport of boric oxide gas from particle to free-stream (gm-mol/cm ² atm sec)	R_{II}	molar rate of removal of B_2O_3 by water reaction (gm-mol/sec)
M, N, S, U	constants defined by equations (20-23) fixed by A, B, C, D, E, F, T_0 and \bar{X}	r_p	boron particle radius (cm)
$(MW)_B$	boron atomic weight (gm/gm-mol)	RGEN	mass rate of generation of boric oxide liquid (gm/sec)
$(MW)_{B_2O_3}$	boric oxide molecular weight (gm/gm-mol)	REVAP	mass rate of evaporation of boric oxide (gm/sec)
Nu	Nusselt Number	T_∞	free stream gas temperature (°K)
P	total pressure (atm)	T_{CL}	particle center temperature (°K)
P_{O_2}	oxygen partial pressure in free stream (atm)	T_p	particle temperature (°K)
$P_{B_2O_3, surf}$	boric oxide partial pressure adjacent to particle surface (atm)	T_{RAD}	surroundings radiation temperature (°K)
$P_{B_2O_3}^*$	boric oxide vapor pressure (atm)	T_S	particle surface temperature (°K)
$P_{H_2O, \infty}$	water gas partial pressure in free stream (atm)	V_j	molecular volume of species j (cm ³)
$P_{H_2O, surf}$	water gas partial pressure adjacent to particle surface (atm)	X	oxide layer thickness (cm)
$P_{HBO_2, surf}$	HBO ₂ partial pressure adjacent to particle surface (atm)	$D_{B_2O_3, N_2}$	diffusivity of gaseous boric oxide in nitrogen (cm ² /sec)
		D_{HBO_2, N_2}	diffusivity of HBO ₂ in nitrogen (cm ² /sec)
		D_{H_2O, N_2}	diffusivity of water gas in nitrogen (cm ² /sec)

ΔH_{II}	heat absorbed by reaction of H_2O with $B_2O_3(l)$ (cal·gm-mol)
ΔH_m	heat of fusion of boron (cal·gm)
$\Delta H_{v, \Delta T}$	heat of vaporization of $B_2O_3(l)$ (cal·gm-mol)
z	evaporation coefficient of boric oxide liquid
α_{II}	surroundings absorptivity
α_t	thermal diffusivity of boron (cm^2/sec)
σ	Stefan-Boltzmann constant, $1.354 \cdot 10^{-12}$ cal/ cm^2 sec K^4
ϵ	particle emissivity
ν	Hertz-Knudsen impingement factor ($gm\text{-}mol/cm^2$ atm sec)
θ	time (sec)
ρ_B	boron density (gm/cm^3)
$\rho_{B_2O_3}$	boric oxide density (gm/cm^3)

Superscripts

Overscore (\bar{T}, \bar{X}) indicates quasi-steady-state value in stability analysis

Prime (T', X') indicates perturbation value in stability analysis

Subscript

0 indicates initial value

INTRODUCTION AND BACKGROUND

Recently, King (1972) published a model for the ignition of single boron particles in hot oxygen-containing gas streams. This model was used to predict ignition times observed by Macek (1969) in flat-flame burner boron particle ignition studies and to predict conditions required for ignition of boron particles in air-augmented rocket afterburners. Macek (1969) observed in his flat-flame burner studies that the combustion of boron occurs in two successive stages. After heat up to about 1800–2000 K., the particle becomes luminous, glows for a short period of time, fades out, and finally re-ignites to burn completely in a second stage which is much brighter and longer than the first stage. This author interprets the first stage as an ignition stage during which the boron particle is coated by a molten boric oxide layer through which oxygen must diffuse to react with the boron to provide reaction heat for vaporization of the oxide layer. Before the second stage of full-fledged combustion can occur, the oxide layer must be completely removed from the boron particle.

The processes occurring during the ignition of an initially oxide-coated boron particle in a hot-gas stream are complex. First, there is a heat-up stage during which the comparatively cold boron particle

is heated solely by convective and/or radiative flux(es) from hotter surroundings. At sufficiently high particle temperature (approximately 1800 K.) non-negligible self-heating of the particle by exothermic oxidation begins to be superimposed on the convective and radiative fluxes. Since the particle is initially coated with an oxide layer, the oxygen for this reaction must diffuse through the liquid oxide layer. As the oxidation of the boron core occurs, of course, it makes the oxide layer thicker, increasing diffusional resistance. At the same time, as long as the particle temperature continues to rise, the viscosity of the oxide decreases and consequently the diffusivity of oxygen in the oxide increases. In addition, boron oxide simultaneously evaporates and diffuses away from the layer at a rate which depends on the particle temperature, tending to thin the layer. However, this evaporation is an endothermic process which tends to cool (or at least lower the rate of heating) the particle. Once the particle temperature rises above the surroundings temperature the convective and radiative heat fluxes turn negative and begin to cool the particle. As long as the sum of the self-heating term and convective-radiative heating term remains greater than the product of the oxide vaporization rate and heat of vaporization, the particle temperature will continue to rise. If this situation persists to the point where the remaining oxide layer is sufficiently thin, a temperature runaway will occur, the particle will finish cleansing itself of oxide, and full-fledged combustion will occur. If, on the other hand, the sum of the self-heating and convective-radiative terms drops below the vaporization heat demand before the surface is cleaned, the particle will not ignite.

In King's (1972) original model, it was assumed that oxide production is controlled by diffusion of oxygen through the liquid oxide film. Henry's Law, the Wilke correlation for diffusivity of a gas through a liquid as a function of viscosity, and an Arrhenius viscosity-temperature law were used to derive a two-constant expression for the oxygen delivery rate to the boron core, the two constants being evaluated from Talley and Henderson (1961) data for the oxidation of boron rods. It was assumed that the removal of oxide from the surface was evaporation-rate-controlled, with an activation energy equal to the oxide heat of evaporation and a pre-exponential factor determined again from Talley and Henderson data. Three nonlinear unsteady-state differential equations in boron mass, oxide mass, and temperature resulting from

application of mass and enthalpy balances were integrated numerically for given boundary conditions and initial conditions to determine whether or not a given particle would ignite and, if so, how long the ignition time would be (both important factors in determining whether a boron particle will release its heat in a finite-residence-time afterburner).

The original model of King (1972) has subsequently been revised to eliminate several shortcomings. Details of the modified model development and results predicted with it are presented in the subsequent sections. Briefly, the changes are:

1) In the original model, the heat of fusion of the boron, which must be supplied when the particle reaches the boron melting point of 2450°K, was not considered—it is included in a modified treatment of the enthalpy balance in the new model.

2) It was assumed in the original model that the liquid boric oxide removal rate was limited by evaporation kinetics, with Talley and Henderson data being used to obtain a pre-exponential factor (and thus an evaporation coefficient of approximately 0.006). This assumption has been questioned by Mohan and Williams (1972) in another boron ignition model (discussed later) in which they assume the oxide removal rate to be limited by diffusion of the oxide gas away from the particle rather than by vaporization kinetics. A dimensionless group, k/zr , may be examined to determine the controlling process. If this parameter is near unity the resistances of the evaporation and diffusion steps are nearly equal and neither resistance may be neglected, while if it is much larger than unity, the process is essentially evaporation rate controlled and if it is much less than unity, the process is essentially diffusion controlled. Substitution of expressions from Bird, Stewart, and Lightfoot (1960) for k and r and use of an average gas temperature adjacent to the particle of approximately 2000°K leads to:

$$\frac{k}{zr} = \frac{1.85 \cdot 10^{-4}}{zPr_p} \quad (1)$$

where z is the boric oxide evaporation coefficient, r_p is the particle radius in centimeters, and P is the pressure in atmospheres. Parametric studies leading to best fit of the data of Maček (1969) as discussed later indicate that z should be approximately 0.04—this value is consistent with a value for boric oxide of 0.03 ± 0.01 measured by

Blackburn (1965). (The Blackburn value was brought to this author's attention subsequent to determination of the best fit value of 0.04.) Substitution of this value into equation (1) yields $k/zr = 46.2/Pr_p$, where the particle radius is now expressed in microns. In Maček's experiments, the particle radii were 17.5 to 22 microns and the pressure was one atmosphere, yielding $k/zr \sim 2$. Under typical afterburner conditions examined, the particle radii ranged from 1 to 10 microns and pressure ranged from 1 to 20 atmospheres, yielding k/zr values of approximately 0.2 to 5. Accordingly, in the revised model no limiting assumption is made regarding evaporation kinetics or oxide gas diffusion control for the oxide removal step—rather, these processes are considered as series resistances.

3) Water appears to have more beneficial effect on boron particle ignition than would be predicted by assuming that it diffuses through the oxide layer to react with the boron core in the same manner as oxygen. Accordingly, the model has been modified to treat H₂O vapor as reacting by a diffusion-limited reaction with the boric oxide [H2O + B2O3(l) -> 2HBO2] to aid in removal of the oxide layer.

Mohan and Williams (1972) have developed similar (though not identical) equations for the generation and removal of a boron oxide layer on a boron particle and the consequent variation in particle temperature with time. However, rather than numerically integrate the resulting equations to determine whether or not a particle ignites and, if so, how long the ignition time is, they have taken a different approach to predict whether or not the particle will ignite for a given set of boundary conditions (with no information regarding the time involved). In this technique, they convert the boron and boric oxide mass balance equations into an equation for the derivative of oxide thickness with time and use the enthalpy balance to develop an equation for the derivative of particle temperature with respect to time. They then set the derivatives equal to zero and solve the resulting algebraic equations for quasi-steady-state values of oxide thickness and particle temperature for the given boundary conditions (particle size, surroundings temperature, etc.). They next examine these points for stability using a linearization technique around the quasi-steady-state values. As part of the current work, this author has applied Mohan and Williams' technique to his equations for the basic processes occurring during the boron particle ignition. The basic differences between the

stability analyses carried out by this author and by Mohan and Williams are:

1) Mohan and Williams treat a planar geometry whereas this author treats a spherical geometry.

2) Mohan and Williams assume that the removal of boric oxide from the particle surface is gas-diffusion-controlled whereas this author treats both evaporation kinetics and gas-diffusion resistances in series.

3) Mohan and Williams neglect heat loss from the oxide layer into the boron itself whereas this author does not.

Results obtained using the stability analysis technique and using the numerical integration treatment of the same basic equations are compared and discussed in a later section.

MODEL DEVELOPMENT

The boron ignition model employed is depicted in Figure 1. It is a transient model treating particle temperature, boron mass, and oxide mass (and, consequently, oxide thickness) as time-dependent parameters. Boric oxide is generated, boron is consumed, and heat is released by reaction of oxygen which diffuses across the oxide layer with boron at the boron-boric oxide interface. This

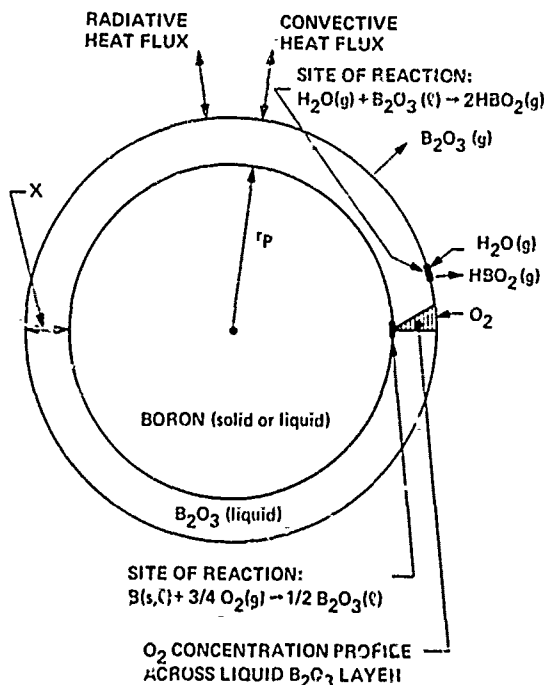


FIG. 1. Boron particle ignition model processes.

oxide generation is assumed to be controlled by the diffusion of the oxygen through the liquid oxide layer. (Sample calculations indicate that in excess of 95 percent of the resistance of transport of oxygen from the gas free-stream to the boron-boric oxide interface is in the liquid layer.) It is also assumed that the heat released by this reaction (and in fact any heat gained or lost by the particle) is distributed rapidly throughout the particle—that is, it is assumed that the particle is isothermal at any given time. An expression may be easily derived for the difference between particle surface and center temperature as a function of the rate of change of surface temperature:

$$T_S - T_{CL} = \frac{(dT_S/dt)r_p^2}{6\alpha_s} \quad (2)$$

Numerical calculations indicate that for boron particles being ignited by hot gas streams, except in the later stages of thermal-runaway, for particles of 10 micron radius, $dT_S/dt \leq 5 \cdot 10^3$ K second. At 2000 K, the thermal diffusivity of boron is approximately $5 \cdot 10^{-3}$ cm² sec. Substitution of these values into equation (2) yield a rather negligible temperature differential from surface to center of 17 K. Similar calculations for other particle sizes yield the same results since the maximum dT_S/dt value is essentially inversely proportional to the square of the particle radius. It should be noted however that this assumption of an isothermal particle is totally untenable for heat fluxes associated with laser-ignition and the model therefore cannot be used for laser-ignition studies.

While oxygen is diffusing in through the liquid oxide layer to convert boron to boric oxide and release heat, boric oxide is simultaneously vaporizing at the outer surface and diffusing out to the free-stream. As previously mentioned, both the finite kinetics of vaporization and the diffusion process are considered as series resistances controlling this type of oxide removal. In addition, in cases where the hot gas stream contains water gas, this H₂O is assumed to remove oxide from the outer surface by a diffusion-limited reaction: $H_2O(g) + B_2O_3(l) \rightarrow 2HBO_2(g)$. The model is limited to treatment of low H₂O concentrations (less than 10 to 20 percent) through use of the lean-gas approximation in treatment of the H₂O and HBO₂ diffusion. Finally, heat is added to or removed from the particle by convection and radiation.

The careful observer may note in examining

some of the figures presented herein and considering the vapor pressure versus temperature relationship of boric oxide that in some cases the vapor pressure of the oxide exceeds the total pressure and that boiling should thus be considered. However, at the times that such situations occur the oxide layer is only on the order of 100 Angstroms thick and it is not clear to this author that the phenomenon of generation of unlimited surface area for vaporization associated with boiling will occur. Accordingly, the phenomenon of boiling is not considered and the surface area available for transport of the boric oxide from liquid to gas phase is assumed to remain equal to the particle geometrical surface area. For all cases studied, the calculated partial pressure of boric oxide gas at the surface does not exceed approximately 10 to 20 percent of the total pressure until well into thermal runaway since, due to the low evaporation coefficient of the boric oxide, the pressure of oxide at the surface remains considerably less than the equilibrium vapor pressure. (See equation (3).) The dark period observed by Maček (1969) between the first bright period and the subsequent very-bright period in the history of an igniting boron particle in his flat-flame burner is probably due to the superheated oxide finally flashing off during some part of the thermal runaway, temporarily blocking the inflow of oxygen to the particle and causing a temporary temperature drop—this part of the overall history is not included in the model.

With the above assumptions and limitations, the following three equations (boron mass balance, oxide mass balance, enthalpy balance) may be written (note that three different enthalpy balances must be employed depending on whether the particle temperature is less than, equal to, or greater than the melting point of boron, 2450 °K):

$$\frac{dr_p}{dt} = -\frac{R_B(MW)_B}{4\pi r_p^2 \rho_B} \quad (3)$$

$$\frac{dX}{dt} = \frac{(R_B/2 - R_E - R_H)(MW)_{B_2O_3}}{4\pi r_p^2 \rho_{B_2O_3}} \quad (4)$$

$$\frac{dT_p}{dt} =$$

$$\left\{ \frac{R_B(Q_{RX}) - R_E(\Delta H_{VAP}) - R_H \Delta H_H}{+ 4\pi(r_p + X)^2 \times [h(T_g - T_p) + \sigma \epsilon_{LE}(T_{RAD}^4 - T_p^4)]} \right\} \quad (5a)$$

$$(\rho_B c_{PB} + 4\pi r_p^2 X \rho_{B_2O_3} c_{PB_2O_3})$$

$$(T_p < 2450 \text{ °K}, f = 0)$$

$$\frac{df}{dt} =$$

$$\left\{ \frac{R_B(Q_{RX}) - R_E(\Delta H_{VAP}) - R_H \Delta H_H}{+ 4\pi(r_p + X)^2 \times [h(T_g - T_p) + \sigma \epsilon_{LE}(T_{RAD}^4 - T_p^4)]} \right\} \quad (5b)$$

$$(\rho_B c_{PB})$$

$$(T_p = 2450 \text{ °K}, 0 \leq f \leq 1)$$

$$\frac{dT_p}{dt} =$$

$$\left\{ \frac{R_B(Q_{RX}) - R_E(\Delta H_{VAP}) - R_H \Delta H_H}{+ 4\pi(r_p + X)^2 \times [h(T_g - T_p) + \sigma \epsilon_{LE}(T_{RAD}^4 - T_p^4)]} \right\} \quad (5c)$$

$$(\rho_B c_{PB} + 4\pi r_p^2 X \rho_{B_2O_3} c_{PB_2O_3})$$

$$(T_p > 2450 \text{ °K}, f = 1)$$

Equation 5a expresses the rate of change of particle temperature for temperatures below the melting point of boron (2450 °K) with df/dt being zero during this period. Equation (5b) expresses the rate of change of fraction of the boron melted at the boron melting point, dT_p/dt being zero until f reaches unity. Finally, equation (5c) expresses the rate of change of particle temperature for temperatures in excess of 2450 °K, f being unity and df/dt being zero in this region.

R_B is the molar consumption rate of boron, R_E is the molar rate of vaporization of boron oxide, and R_H is the molar rate of removal of boric oxide by the reaction $H_2O + B_2O_3(l) \rightarrow 2HBO_2$. (See Nomenclature for definition of other symbols).

Talley and Henderson (1961) data were used in evaluation of the molar consumption rate of boron (as limited by diffusion across the liquid B_2O_3 layer). With the use of Henry's Law, the Wilke correlation for diffusivity of a gas through a liquid as a function of viscosity, and an Arrhenius viscosity-temperature law, the following equation form may be derived for R_B :

$$R_B = \frac{4\pi(r_p + X)^2 K_1 e^{-K_2/T_p} (P_{O_2})^{1/2}}{X} \quad (6)$$

Talley and Henderson measured the oxide layer thicknesses at two temperatures in their experiments conducted with boron rods at one atmosphere oxygen pressure. In addition, they reported the boron consumption rate per unit sample area for these two test conditions. These data permit evaluation of the constants K_1 and K_2 in equation

(6). The resulting expression for the molar consumption rate of boron is:

$$R_B = \frac{64.8(10^{-8})(r_p + X)^2 T_p e^{-22,600/T_p} (P_{O_2})}{X} \quad (7)$$

In the development of an expression for R_E (the molar rate of evaporation of boric oxide from the particle surface) both the kinetic limitations on evaporation rate and the diffusional limitations on transport of boric oxide gas from adjacent to the particle out to the free-stream were considered as series resistances—thus,

$$\frac{R_E}{4\pi(r_p + X)^2} = zr(P_{B_2O_3}^{\circ} - P_{B_2O_3, \text{surface}}) \\ = k(P_{B_2O_3, \text{surface}} - P_{B_2O_3, \infty}) \quad (8)$$

In this study, it was assumed that the partial pressure of boric oxide in the free-stream (far from the particle) was zero. Thus, thru manipulation of the two equalities in equation (8), the expression for R_E may be rewritten as:

$$R_E = 4\pi(r_p + X)^2 zr P_{B_2O_3}^{\circ} / (1 + zr/k) \quad (8a)$$

Following substitution of expressions for the Hertz-Knudsen impingement factor r , the boric oxide vapor pressure ($P_{B_2O_3}^{\circ}$), and k (equations (9), (10), and (11)) into (8a), we arrive at equation (12) as a final expression for R_E :

$$r = \frac{1}{4RT_p} \sqrt{\frac{8R'T_p}{\pi(MW)_{B_2O_3}}} \\ = 5.30T_p^{-1/2} \text{ mol/cm}^2 \text{ atm sec} \quad (9)$$

$$P_{B_2O_3}^{\circ} = 1.51 \cdot 10^8 e^{-11,000/T_p} \quad (10)$$

$$k = \frac{D_{H_2O, N_2}(\text{Nu})}{2RT(r_p + X)} = \frac{1.18(10^{-7})T_p^{1/2}(\text{Nu})}{P(r_p + X)} \quad (11)$$

$$R_E = \frac{1.005 \cdot 10^{10} (r_p + X)^2 z e^{-11,000/T_p}}{T_p^{1/2} [1 + (4.50(10^7) z P(r_p + X) / T_p (\text{Nu}))]} \quad (12)$$

Regarding the action of water vapor in the ignition of boron particles, it is assumed that the water gas reacts in a diffusion-limited endothermic reaction, $H_2O(g) + B_2O_3(l) \rightarrow 2HBO_2(g)$ at the outer surface of the oxide layer, removing oxide and absorbing heat. Thus, the molar rate of removal of oxide by this process, R_H , may be

expressed as:

$$\frac{R_H}{4\pi(r_p + X)^2} \\ = \frac{D_{H_2O, N_2}(\text{Nu})}{2(r_p + X)RT_p} (P_{H_2O, \infty} - P_{H_2O, \text{surface}}) \\ = \frac{D_{HBO_2, N_2}(\text{Nu})}{4(r_p + X)RT_p} (P_{HBO_2, \text{surface}}) \quad (13)$$

(assuming that the partial pressure of HBO_2 in the free-stream is negligibly small).

A relationship between the partial pressures of H_2O and HBO_2 at the surface provided by thermodynamics permits elimination of these quantities from the two equalities of equation (13) to yield with use of equation (7) (Gilliland (1934)) for the diffusivities, equation (15) for R_H :

$$D_{H_2O, N_2} = 4.3 \cdot 10^{-3} \frac{T_p^{3/2}}{P(1 + V_{N_2}^{1/3})} \\ \times \sqrt{\frac{1}{(MW)_H} + \frac{1}{(MW)_{N_2}}} \quad (14) \\ R_H = (9.15 \cdot 10^{-7} / P)(\text{Nu})(r_p + X)T_p^{1/2} \\ \times \exp \left[18.1 \left(1 - \frac{2100}{T_p} \right) \right] \times \left[-0.15 \right. \\ \left. + \sqrt{0.0225 + P_{H_2O, \infty} \exp \left[-18.1 \left(1 - \frac{2100}{T_p} \right) \right]} \right] \quad (15)$$

The following values were used for other parameters appearing in equations (3-5), (7), (12), and (15):

$$\begin{aligned} MW_B &= 10.82 \\ \rho_B &= 2.33 \text{ gm/cm}^3 \\ MW_{B_2O_3} &= 69.64 \\ \rho_{B_2O_3} &= 1.85 \text{ gm/cm}^3 \\ Q_{RX} &= 146,000 \text{ cal/mole} \\ \Delta H_{VAP} &= 90,000 \text{ cal/mole} \\ \Delta H_H &= 75,000 \text{ cal/mole} \\ h &= 0.347 \cdot 10^{-6} (\text{Nu}) T_p^{0.5} / (r_p + X) \\ &\quad \text{cal/cm}^2 \text{ sec } ^\circ\text{K} \\ \epsilon &= 0.8 \\ \alpha_R &= 1.0 \\ C_{PBS} &= 0.507 + 7.0 \cdot 10^{-5} T_p, \text{ cal/gm } ^\circ\text{K} \\ C_{PB_2O_3} &= 0.438 \text{ cal/gm } ^\circ\text{K} \\ \Delta H_M &= 498 \text{ cal/gm} \\ C_{PBH} &= 0.675 \text{ cal/gm } ^\circ\text{K} \\ Q_{RN_2} &= 151,000 \text{ cal/mole} \end{aligned}$$

For all of the cases considered to date in this study the Nusselt Number was set equal to 2. That is, it was assumed that the particle is essentially stationary with respect to the surrounding gases. This is obviously not the case for a particle released into a high-velocity gas stream for times very shortly after such release. For treatment of such a situation, the model may be simply modified by addition of a velocity-lag equation and suitable Nusselt Number versus Reynolds' Number relationships. For cases of practical interest, by the time the particle is sufficiently hot for the reaction heat release terms in equation (5) to be significant, the particle velocity has equilibrated sufficiently with the gas velocity to yield a Nusselt Number of approximately 2. This analysis is meant to deal only with the ignition period (defined as the period from initiation of first particle glow to initiation of the second stage of combustion), the preceding heatup time having been treated in the study by Maček (1969). As mentioned earlier, the evaporation coefficient, z , was varied parametrically in the early phases of this study, a value finally being chosen (0.04) which gave good agreement between prediction and Maček's experimental data.

The above set of equations [(3-5), (7), (12), (15)] was converted to difference form and programmed for numerical solution on the computer. The following quantities were supplied as input parameters: pressure, free-stream oxygen partial pressure, free-stream water partial pressure, ambient temperature, radiation temperature of the surroundings, initial oxide layer thickness, initial particle radius, and initial particle temperature. Outputs included particle radius, oxide thickness, particle temperature, oxide mass, boron mass, oxide generation rate, oxide evaporation rate, and rate of removal of oxide by water vapor, all as functions of time. These calculations were performed for sufficient time to permit conclusion that for a given set of input conditions particle ignition would not occur, or if it did occur, to quantitate the ignition delay time.

As a second approach to calculating ignition limits (minimum required ambient temperature for ignition) the stability analysis technique used by Williams (1972) on a somewhat different set of equations describing the various processes occurring during boron ignition was applied to the above equations. Numerical calculations indicated that the total boron plus oxide mass changed only very slightly during the ignition process for particle sizes of interest and that the stability analysis in

all cases of practical interest should be applied at particle temperatures well below 2450 K (boron melting point). Accordingly, equation (5a) was used (rather than (5b) or (5c)) in this analysis, and equation 3 was not used, r_p and $(r_p + X)$ being set equal to their initial values. In addition, use of this analysis was limited to no-water cases, eliminating the need for equation (15). Finally, the variation of $zr_p k$ with particle temperature was neglected as a second order effect. With these approximations, equations (4), (5a), (7), and (12) may be reduced to:

$$\frac{dT_p}{d\theta} = \frac{AT_p e^{-22,600/T_p}}{X} - \frac{Be^{-41,000/T_p}}{T_p^{1.2}} + C(T_\infty - T_p) + D(T_{RAD}^4 - T_p^4) \quad (16)$$

$$\frac{dX}{d\theta} = \frac{ET_p e^{22,600/T_p}}{X} - \frac{Fe^{-41,000/T_p}}{T_p^{1.2}} \quad (17)$$

where A , B , C , D , E , and F are functions only of the boundary conditions (pressure, oxygen partial pressure, ambient temperature) and the initial particle size, independent of T_p and X :

$$\begin{aligned} A &= f_1 \text{ (Initial Particle Size, } P_{O_2}) \\ B &= f_2 \text{ (Initial Particle Size, } P) \\ C &= f_3 \text{ (Initial Particle Size, } T_\infty) \\ D &= f_4 \text{ (Initial Particle Size)} \\ E &= f_5 (P_{O_2}) \\ F &= f_6 \text{ (Initial Particle Size, } P) \end{aligned}$$

For a given set of values of boundary conditions and a given particle size, equations (16) and (17) may be set equal to zero and solved for quasi-steady values of particle temperature (\bar{T}_p) and oxide thickness (\bar{X}). The stability of this solution can then be investigated by linearization about this quasi-steady-state. Such linearization results in:

$$\frac{dT_p'}{d\theta} = -MX' + NT_p' \quad (18)$$

$$\frac{dX'}{d\theta} = -SX' + UT_p' \quad (19)$$

where:

$$\begin{aligned} M &= A\bar{T}_p e^{-22,600/\bar{T}_p} / \bar{X}^2 \quad (20) \\ N &= \frac{Ae^{-22,600/\bar{T}_p}}{\bar{X}} \left(1 + \frac{22,600}{\bar{T}_p} \right) \\ &+ \frac{Be^{-41,000/\bar{T}_p}}{\bar{T}_p^{1.2}} \left(\frac{1}{2\bar{T}_p} - \frac{44,000}{\bar{T}_p^2} \right) - C - 4D\bar{T}_p^3 \quad (21) \end{aligned}$$

$$S = E\bar{T}_p e^{-22,600/T_p} \bar{X}^2 \quad (22)$$

$$L = \frac{E e^{-22,600/T_p}}{\bar{X}} \left(1 + \frac{22,600}{T_p} \right) + \frac{F e^{-11,000/T_p}}{T_p^{1.2}} \left(\frac{1}{2T_p} - \frac{44,000}{T_p^2} \right) \quad (23)$$

Differentiation of equation (18) and subsequent substitution of equation (19) yields:

$$\frac{d^2 T_p}{d\theta^2} + (S - N) \frac{dT_p}{d\theta} + (UM - SN) T_p = 0 \quad (24)$$

for which the general solution is:

$$T_p = k_1 e^{m_1 \theta} + k_2 e^{m_2 \theta}$$

$$m_{1,2} = \frac{-(S - N) \pm \sqrt{(S - N)^2 - 4(UM - NS)}}{2} \quad (25)$$

Examination of this solution indicates that for stability, both roots (m_1 and m_2) must be negative, which in turn requires that:

$$S > N \quad (26)$$

$$UM > NS \quad (27)$$

Numerical substitution indicates that if the second inequality is satisfied, then the first one is also satisfied—thus, for $UM > NS$ the solution is stable and the particle does not ignite, while for $UM < NS$ the solution is unstable and the particle ignites. Algebraic manipulation shows that the inequality required for stability (27) reduces to:

$$\left(\frac{0.5}{\bar{T}_p} - \frac{44,000}{\bar{T}_p^2} \right) [C(\bar{T}_p - T_\infty) + D(\bar{T}_p^4 - T_{RAD}^4)] + C + 4D\bar{T}_p^3 > 0 \quad (28)$$

Equations (16), (17), and (28) are used in the following manner to examine ignition limits for ignition of boron particles in a hot gas stream. First, the surroundings radiation temperature, the gas stream temperature, pressure, and oxygen partial pressure are chosen. Equation 16 is then set equal to zero and solved for the quasi-steady-state temperature values for various particle sizes. In this manner, curves of \bar{T}_p versus particle radius are generated for various ambient (gas stream) temperatures (as shown in Figure 16 for $P = 1$ atmosphere, $P_{O_2} = 0.2$ atmosphere, $T_{RAD} = 300$ K). Equation 17 (set equal to zero) is then used to

solve for the corresponding \bar{X} values. Equation (28) is finally used to determine the unstable and stable portions of each T_p curve—the dotted line in Figure 16 indicates the boundary between the stable and unstable solutions (ignition versus no ignition). Results and interpretation of this analysis are presented in the next section.

RESULTS AND DISCUSSION

In Figure 2, plots of particle temperature, oxide layer thickness, fraction boron melted, oxide mass generation rate, and oxide mass evaporation rate versus time are presented for a typical case in which the numerical analysis predicts particle ignition. The particle treated is 20 microns in diameter with an initial oxide layer thickness of 0.1 micron and an initial temperature of 1800 K. The pressure is 5 atmospheres, the oxygen mole fraction is 0.2, and the ambient temperature and surroundings radiation temperatures are both 2100 K. As may be seen, once the particle temperature exceeds approximately 2000 K, the oxide evaporation rate rises above the oxide generation rate, resulting in thinning of the oxide layer. Particle temperature continues to increase as the oxide layer thins until the boron melting point is reached. At this point the oxide thickness and temperature remain constant while the boron melts (this process requiring approximately 15 percent of the total ignition time). After the boron has melted, the particle temperature resumes its rise and the oxide layer thins enough that the self-heating term (limited by oxygen diffusion through the oxide layer) becomes so large as to cause a thermal runaway. At this point, the super heated oxide probably flashes off of the particle, temporarily interrupting the influx of oxygen and resulting in the dark period observed by Mažek (1969)—this process, as mentioned earlier, is not included in the model.

In Figure 3, similar results are presented for a case identical except for reduction of the ambient temperature and effective surroundings radiation temperature by 100 K to 2000 K. The initial stages of the process are quite similar however, heat losses to the surroundings when the particle temperature rises above the 2000 K ambient temperature are sufficient to retard the evaporation rate sufficiently that it drops back to the generation rate with the result that the oxide layer ceases thinning. In this case (referred to as a degenerate ignition case) a stable quasi-steady-state is reached,

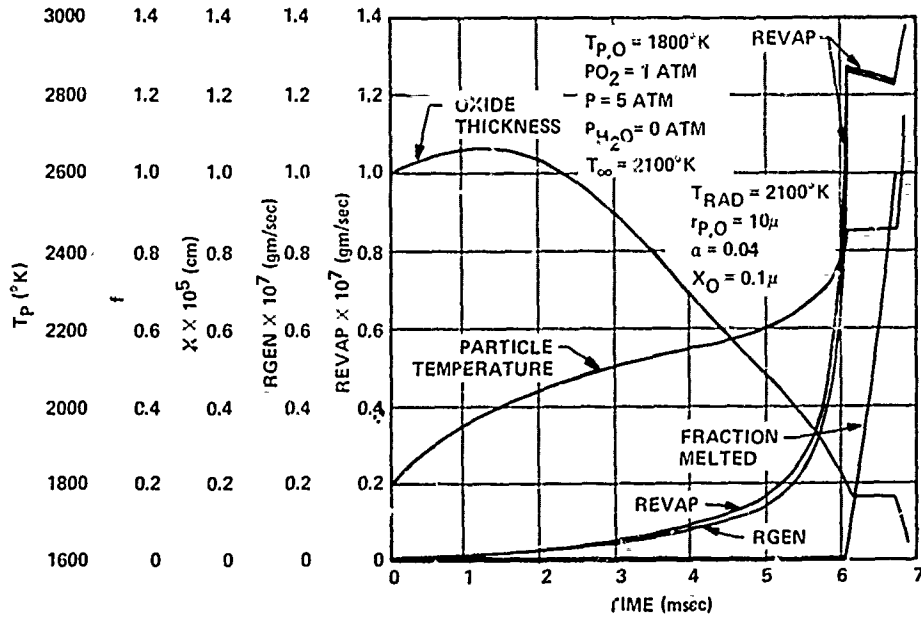


FIG. 2. Predicted time dependence of important variables for particle which ignites.

the temperature levels out to a steady value, and ignition does not occur.

Figure 4 presents results for a third similar case, this time with a further 100°K reduction in ambient and radiation temperature to 1900°K. In this case, the oxide evaporation rate never does exceed the

generation rate and the oxide layer continuously thickens, no ignition occurring.

Maček (1969) studied the ignition and combustion of 35 and 44 micron diameter boron particles in a flat-flame burner. The partial pressure of oxygen in the burner flame was approximately 0.25 for most

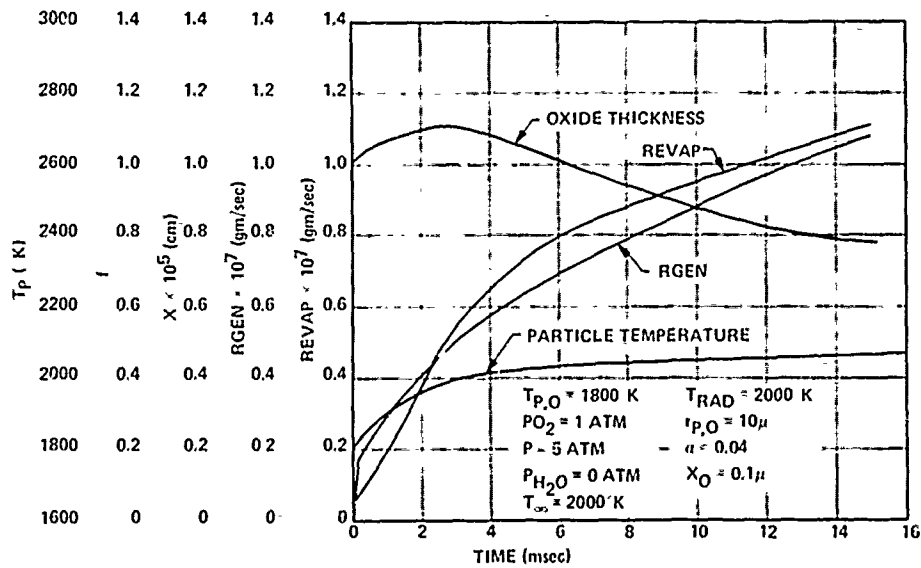


FIG. 3. Predicted time dependence of important variables for degenerate ignition case.

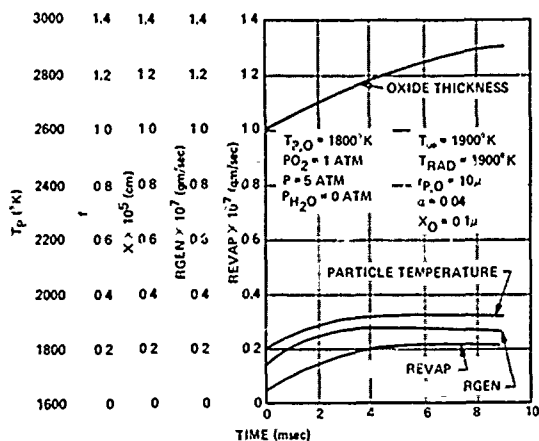


FIG. 4. Predicted time dependence of important variables for particle which does not ignite.

of the tests, with a total pressure of one atmosphere. Water gas was present in several of the tests. Single boron particles were injected into the flat-flame burner product stream and their history was observed with time-resolved photography. The particles were observed to glow briefly, die out for a short time, and finally glow brightly (full combustion) until consumed. Heat and momentum transfer calculations indicated that the first glow occurred at 1900 °K, a temperature which the model indicates would be reached with negligible contribution from the boron-oxygen reaction. Ignition time was measured as the time between the appearance of this first glow and the appearance of full combustion.

These experimental results were used to check the ignition model. Since the initial oxide thickness on the particles was unknown, calculations were performed with initial thicknesses of 0.02 to 0.10 microns (a range likely to encompass the actual initial thickness)—variation over this factor of 5 resulted in only about 20% variation in the predicted ignition time. Predicted and experimental results for a series of tests in which no water was present and the oxygen mole fraction in the burner product gases was approximately 0.25 are presented in Figure 5, in the form of ignition time versus ambient gas temperature for each of the two particle sizes (17.5 and 22 micron radius) for several assumed values of the boric oxide evaporation coefficient (α). As may be seen, use of $\alpha = 0.04$ gives quite good agreement between experimental data and prediction. Accordingly, a value of 0.04 was used for α in all further studies.

Another test of the model is its capability to predict the minimum ambient temperature required for ignition of the particles, a value also measured by Maček (1969). For a dry gas stream at one atmosphere with an oxygen partial pressure of approximately 0.25 atmospheres, Maček found the minimum gas temperature required for ignition to be 1960–1990 °K when the diluent used was nitrogen and 1930 °K when the diluent was argon. This compares extremely well with the model which predicts a minimum ignition temperature under these conditions of 1950–2000 °K. (The range of temperatures given, rather than a precise value, results from the fact that between 1950 °K and 2060 °K, the model predicts ignition, but with ignition times of greater than 30 milliseconds, the maximum particle residence time in Maček's apparatus.)

As indicated in the model-development section, an attempt was made to incorporate the effects of water gas on boron particle ignition into this model. In Table I, predicted and observed ignition times for exact test conditions employed by Maček are presented for all of his tests, including those with water gas in the flat-flame burner product stream. As may be seen, based on limited evidence, it appears that the model underpredicts the effect of oxygen partial pressure on ignition time relative to the effect of ambient temperature. More important, the model grossly overpredicts the effect of water vapor on the ignition time. Moreover, with a water mole fraction of approximately 0.15–0.20, Maček observes a minimum ambient

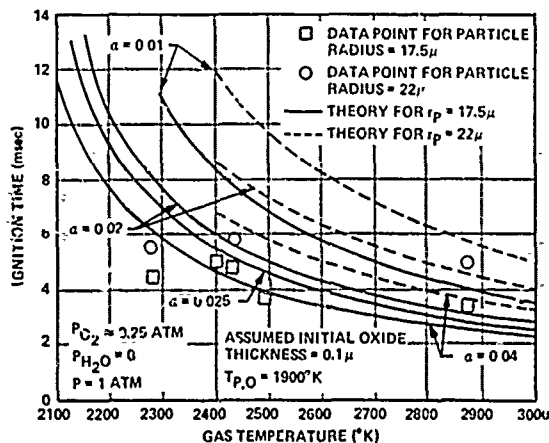


FIG. 5. Predicted and observed ignition times for boron particles studied experimentally by Maček (1969).

TABLE I. COMPARISON OF MEASURED AND PREDICTED IGNITION TIMES FOR EXACT CONDITIONS USED BY MACEK (1969) IN FLAT-FLAME BURNER BORON PARTICLE IGNITION STUDIES.

$P_{\text{TOTAL}} = 1 \text{ ATM}$

$\alpha = 0.04$

$T_{\text{RADIATION}} = 300^\circ\text{K}$

ASSUMED INITIAL OXIDE THICKNESS = 0.1μ

P_{O_2} (atm)	$P_{\text{H}_2\text{O}}$ (atm)	T_∞ ($^\circ\text{K}$)	IGNITION TIME (msec)	
			PREDICTED	OBSERVED
a. PARTICLE RADIUS = 17.2μ				
0.23	0	2280	5.26	4.4
0.20	0	2430	3.85	4.8
0.23	0	2870	2.24	3.4
0.20	0	2400	4.09	5.0
0.08	0	2510	2.82	*
0.28	0	2490	3.50	3.6
0.37	0	2450	3.72	2.1
0.19	0.16	2240	1.49	4.0
0.21	0.16	2330	1.76	3.5
0.19	0.19	2430	1.20	3.8
0.20	0.21	2640	1.00	2.6
b. PARTICLE RADIUS = 22.1μ				
0.23	0	2280	7.99	5.5
0.20	0	2430	5.83	5.7
0.23	0	2870	3.40	5.0
0.37	0	2450	5.61	3.3
0.19	0.16	2240	2.30	7.2
0.21	0.16	2330	2.76	5.8
0.19	0.19	2430	1.88	6.1
0.20	0.21	2640	1.55	5.6

*IGNITED, BUT IGNITION TIME NOT MEASURED

temperature required for ignition of 1870-1890 $^\circ\text{K}$.; the model predicts ignition with this amount of water vapor at as low as 1600 $^\circ\text{K}$ (the lowest ambient temperature tested in the program). Thus, it appears that the attempt to model the effect of water vapor on boron particle ignition by assuming a diffusion-limited reaction, $\text{H}_2\text{O}(\text{g}) + \text{B}_2\text{O}_3(\text{l}) \rightarrow 2\text{HBO}_2$, removing oxide from the surface

was unsuccessful. A possible explanation is that such a reaction (which is quite endothermic) is in actuality kinetics-limited. However, this author is unaware of any data on the kinetics of this reaction. Therefore, the attempt to model the effect of water vapor on boron particle ignition has been discontinued (at least for the time being) and the remainder of the work conducted in this study is

limited to ignition of boron particles in dry gas streams.

The model of boron ignition developed in this study (minus considerations of the effects of water vapor) involves seven independent variables, values of which must be input to the resulting numerical computer program for prediction of particle ignition time. These parameters are: initial oxide thickness, initial particle temperature, initial particle size, ambient temperature (surroundings gas temperature), effective surroundings radiation temperature, pressure, and oxygen mole fraction (or partial pressure). As part of this study, each of the above independent parameters (except initial particle temperature) has been systematically varied to determine its effect on whether the particle will ignite and, if so, what the ignition time will be. Results of these parametric studies are presented in Figures 6-15 and Table II.

In Figure 6, the effect of assumed initial oxide thickness over a five-fold variation on ignition time is presented. As may be seen, the smaller particle ignition times are more sensitive to assumed initial oxide thickness. With a one micron radius particle, increasing the assumed initial oxide thickness from 0.02 microns to 0.10 microns approximately doubles the predicted ignition time, while for 15 micron radius particles, similar variation in assumed initial thickness changes predicted ignition time only 20 to 25%.

The effects of pressure and oxygen mole fraction in the gas free-stream on minimum gas temperature required for particle ignition are shown in Figures 7 and 8. These calculations were all performed for

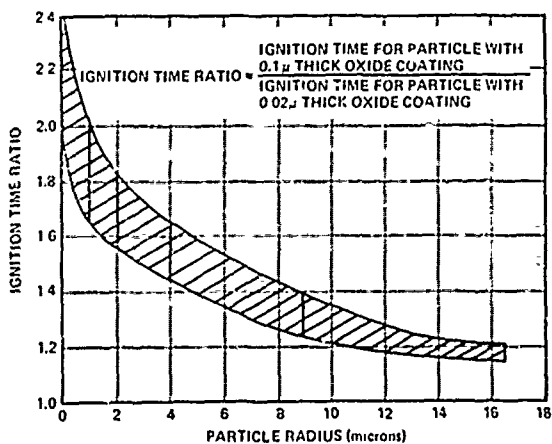


FIG. 6. Effect of assumed initial oxide thickness on predicted ignition time.

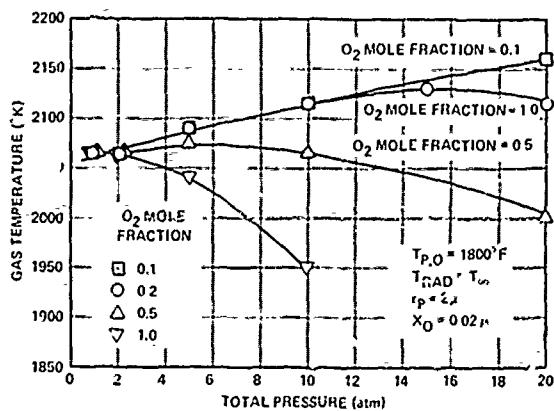


FIG. 7. Minimum gas temperature required for ignition versus total pressure for various oxygen mole fractions.

particles of 2 micron radius with an initial temperature of 1800 °K and an initial thickness of 0.02 microns. Similar trends were noted with other particle sizes and initial oxide thicknesses. As shown in Figure 7, increased total pressure raises the gas temperature required for ignition at low oxygen mole fractions, but lowers the required gas temperature at high oxygen mole fractions. When the data are cross-plotted as shown in Figure 8, it is seen that the gas temperature required for ignition is independent of oxygen mole fraction at one and two atmospheres total pressure, but shows increasing dependence on oxygen mole fraction at higher total pressure, required temperature decreasing with increasing

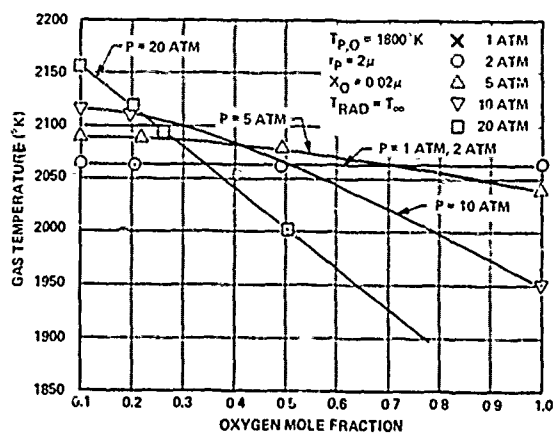


FIG. 8. Minimum gas temperature required for ignition versus oxygen mole fraction for various total pressures.

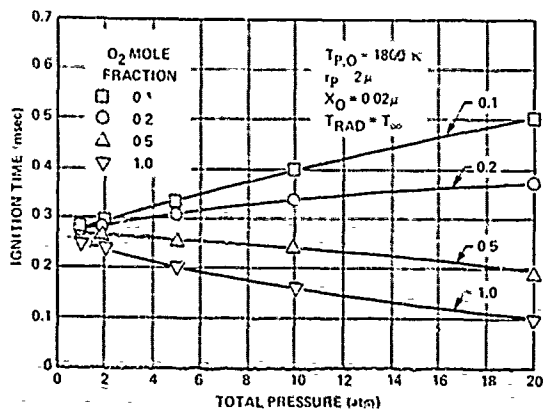


FIG. 9. Ignition time versus total pressure for various oxygen mole fractions at $T_{\infty} = 2200$ K.

oxygen mole fraction. These fairly complex dependencies result from interaction of the effect of oxygen partial pressure on the oxide generation rate and the effect of total pressure on the oxide removal rate (increased total pressure leading to increased resistance to diffusion of B_2O_3 gas away from the particle). Similar effects on the ignition time at a fixed gas temperature as functions of total pressure and oxygen mole fraction are shown in Figures 9 and 10. At low oxidizer mole fractions, ignition time increases with increasing total pressure while at high oxidizer mole fractions, the pressure dependency is reversed. Similarly, at one atmosphere total pressure, ignition time is predicted to be independent of oxygen mole fraction while at higher total pressures, ignition time decreases with increased oxygen mole fraction, the sensitivity

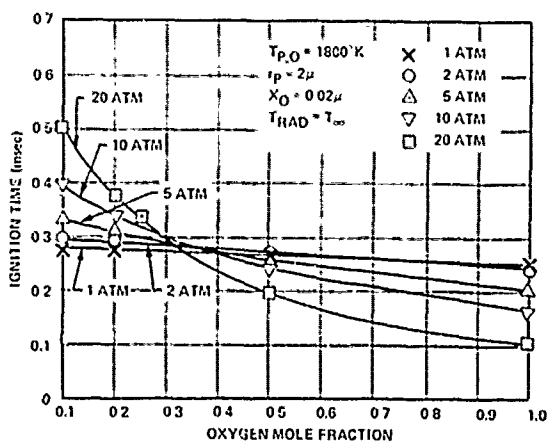


FIG. 10. Ignition time versus oxygen mole fraction for various total pressures at $T_{\infty} = 2200$ K.

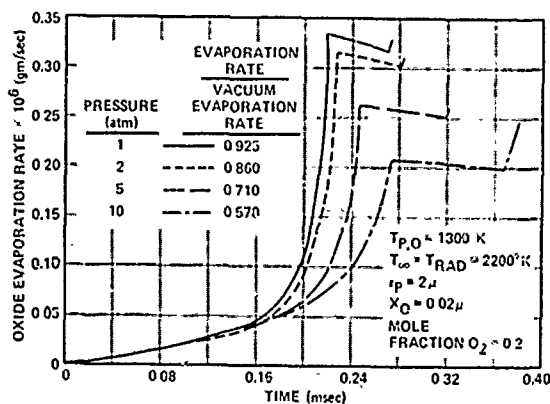


FIG. 11. Oxide evaporation rate versus time at various total pressures at fixed oxygen mole fraction.

increasing continuously with increased total pressure.

The cause of the increase in ignition time with increasing total pressure at fixed oxygen mole fraction for low oxygen mole fraction (0.1, 0.2) is shown in Figures 11 and 12, where the oxide removal rate and particle temperature are plotted against time. As indicated on the figures, the ratio of oxide evaporation rate to the evaporation rate that would be observed in vacuo decreases with increased pressure, since the diffusional resistance to oxide gas removal from the vicinity of the particle increases. Since, for fixed oxygen mole fraction, the oxygen partial pressure increases with increased total pressure, early in the process the rate of diffusion of oxygen through the oxide layer for reaction with the boron to release heat increases with increased total pressure, leading to a faster

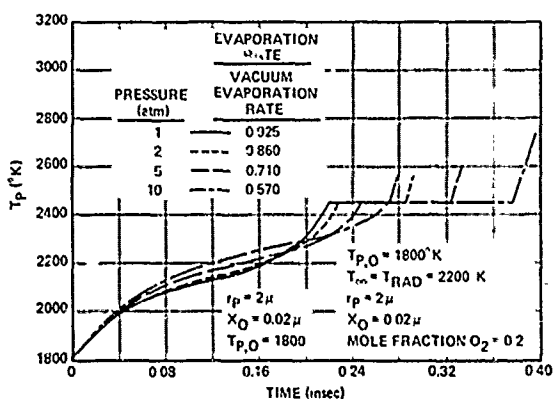


FIG. 12. Particle temperature versus time at various total pressures at fixed oxygen mole fraction.

temperature rise as shown in Figure 12. However, the increased total pressure also decreases the oxide removal rate at any given temperature with the net result that the removal rate increases only very little with increased pressure during the early stages, less than the generation rate increase. As a result, the oxide layer thickness versus time is higher in the higher total pressure cases, eventually causing a decrease in heat release rate despite the higher oxygen partial pressure so that the temperature versus time curves cross in Figure 12, temperature rising more quickly with time in the low total pressure case than in the high total pressure case. This, combined with the higher diffusional resistance to evaporation in the high pressure case causes the oxide removal rate to lag well behind that in the low pressure case in the later stages. The net result is an increase in ignition time with increased total pressure at fixed oxygen mole fraction, ambient temperature, etc. At higher mole fractions of oxygen on the other hand (0.5 and 1.0) the increased retardation of oxide removal rate associated with increased total pressure is overshadowed by the increased heat release rate associated with the higher oxygen partial pressure, resulting in decreased ignition time with increased total pressure at fixed oxygen mole fraction, ambient temperature, etc.

The effect of particle radius on minimum ambient temperature required for ignition was also studied. Results, presented in Figure 13, indicate a decrease in minimum required gas temperature with increasing particle size for particles in the 1 to 10 micron radius size range. (The upper end of each bar indicates the lowest temperature examined which resulted in ignition while the lower end indicates the highest temperature investigated

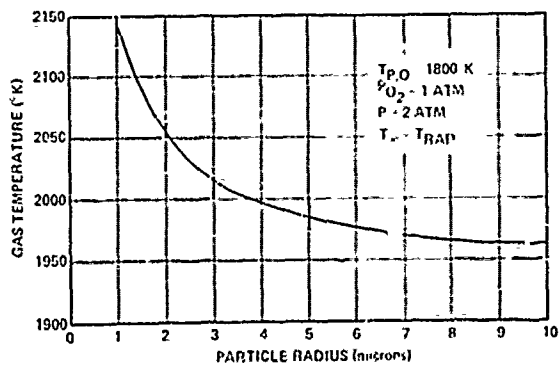


FIG. 13. Effect of particle radius on minimum ambient temperature required for ignition.

which did not result in ignition). The dependency noted with these small particle sizes (1 to 10 microns) is associated with the oxide removal rate being mainly evaporation kinetics limited ($k_{ev} \gg 1$) for the smaller sizes.

In Figure 14, predictions of ignition time versus particle radius for particles which are predicted to ignite are presented for several gas temperatures ranging from 2050 °K to 2200 °K. For the higher temperatures, the ignition time increases monotonically with increasing particle radius due to the increase in particle mass to surface area ratio with increasing radius. At the lower surroundings temperatures, however, predicted ignition time decreases with increasing particle radius at the lower sizes and then increases with further particle size radius. This region of increasing ignition time with decreasing particle size is associated with the increase in minimum required gas temperature for ignition with decreasing particle size.

The effect of ambient temperature on predicted ignition time (radiation surroundings temperature being set equal to ambient gas temperature) is shown in Figure 15. Ignition time may be seen to be quite sensitive to gas stream temperature, ignition time decreasing with increased gas temperature. This sensitivity increases with decreasing gas stream temperature and increasing particle size. Finally, the effect of varying surroundings radiation temperature at fixed gas stream temperature is shown in Table II. As would be expected, ignition time decreases with increasing surroundings radiation temperature, all other parameters being held constant. In fact, for a gas stream temperature of 2050 °K for the conditions studied, particle ignition will not occur for a surroundings radiation temperature of 300 °K or 2050 °K, but will occur for radiation temperatures of 2500 °K or higher, ignition time decreasing markedly with further increases in radiation temperature above 2500 °K. This, of course, implies that conditions for ignition of an optically thick boron cloud or a boron-aluminum or boron-magnesium cloud should be much less stringent than for ignition of a single boron particle in a transparent gas stream looking at relatively cold radiation surroundings.

The stability analysis described in the previous section for determination of whether or not a boron particle will ignite for given boundary conditions was employed to generate the information presented in Figures 16 and 17 for a surroundings radiation temperature of 300 °K and a total pressure of one atmosphere (independent of oxygen

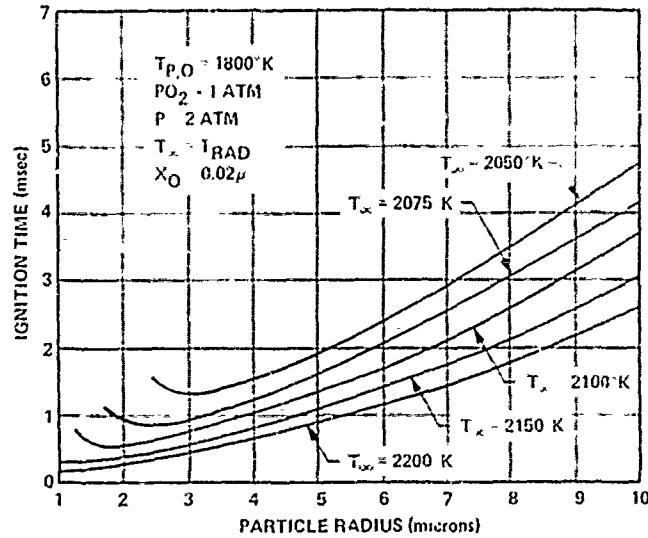


FIG. 14 Effect of particle radius on ignition time.

mole fraction). For each of several ambient gas temperatures equations (16) and (17) (with the derivatives set equal to zero) were used to generate curves of T_p (quasi-steady state temperature) versus particle radius (solid curves in Figure 16). Equation (28) was then used to determine the "stable" and "unstable" portions of these curves. For ambient gas temperatures below 1940 K, upper and lower curves were found for each gas temperature - in all such cases, the upper curve represented unstable solutions (ignition) while the lower curve represented stable solutions (no

ignition). For ambient temperatures of 1940 K and higher there were right-hand and left-hand branches. The dotted line drawn through these curves separates the ignition region (above the dotted line) from the no-ignition region (below the dotted line). It is of interest to compare these curves to similar curves generated by Williams (1972). For the larger particle sizes, they are quite similar (not surprising since for the larger sizes the diffusional resistance to B_2O_3 removal dominates, as assumed by Williams). However, at low particle sizes the curves of Figure 16 and those presented by Williams differ markedly in that Williams predicts no left-hand branches of the solid curves. This difference results from the fact that he assumed diffusion-limited B_2O_3 removal even for small particle sizes whereas the model presented herein, which treats the evaporation kinetics and diffusion process as series resistances indicates that for the smaller sizes, the evaporation kinetics dominate.

Interpretation of the results plotted in Figure 16 is as follows. At any ambient temperature below 1940 K, the particle will not ignite unless the particle temperature is initially greater than or equal to the value given on the upper curve for that ambient temperature for the given particle radius. Though this value of initial particle temperature is a necessary condition for ignition, it is not clear that it is sufficient - one can imagine a case where the initial particle temperature exceeds the necessary value, but the initial oxide thickness

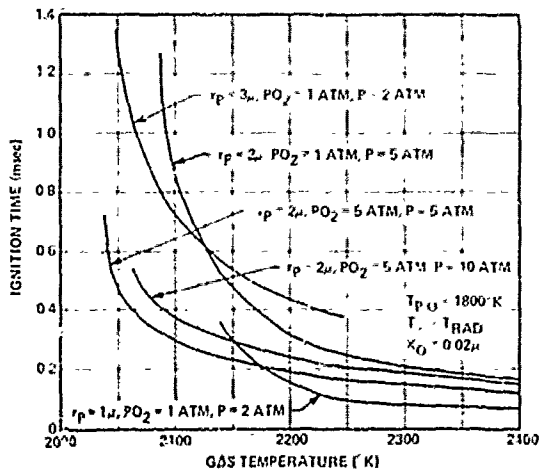


FIG. 15 Effect of gas temperature on boron particle ignition time.

TABLE II. EFFECT OF $T_{\text{RAD}} \neq T_{\infty}$ ON IGNITION TIME
 $r_p = 2\mu$, $X_O = 0.02\mu$, $PO_2 = 1 \text{ ATM}$, $P = 2 \text{ ATM}$, $T_{p,0} = 1800^\circ\text{K}$

T_{∞} ($^\circ\text{K}$)	$T_{\text{RADIATION}}$ ($^\circ\text{K}$)	IGNITION TIME (msec)
2200	300	0.288
	2200	0.268
	2500	0.260
	3000	0.232
	3500	0.201
2100	300	0.690
	2100	0.557
	2500	0.475
	3000	0.370
	3500	0.286
2075	300	1.901
	2075	0.910
	2500	0.658
	3000	0.451
	3500	0.322
2050	300	NO
	2050	NO
	2500	1.442
	3000	0.600
	3500	0.372

is so large that the particle temperature drops below the necessary value before the oxide layer thins sufficiently for thermal runaway.

For ambient gas temperatures of 1940 K and higher, there are regions where there is no particle temperature at which dT_p/dt and dX/dt can simultaneously equal zero. For instance, for an ambient gas temperature of 2000 K, this is the case for particles with radii between 3.7 and 42 microns. Thus a quasi-steady state cannot exist at 2000 K gas temperature for particles in this size region and they will ignite for any initial conditions. Outside this region (larger or smaller radius) a minimum requirement on initial particle temperature exists for ignition. This requirement is given by the portions of the 2000 K gas temperature solid curves lying above the dotted line. (Again, this is a necessary but not necessarily

sufficient condition. The numerical analysis must be performed for such cases to determine whether or not ignition will occur. However, since the heat generation terms in equations (5) and (16) are much more sensitive to particle temperature than to oxide thickness it seems likely that an initial temperature more than 25-50 K above the "necessary" value will result in ignition for virtually any initial oxide thickness.)

As indicated, for each gas temperature above 1940 K, there exists a range of particle sizes for which ignition will occur independent of initial conditions, this range being given by the right most point of the left branch of the solid curve for that gas temperature and the left most point of the right branch. Thus, the data of Figure 16 may be used to generate a curve of minimum ambient gas temperature required to guarantee ignition (for

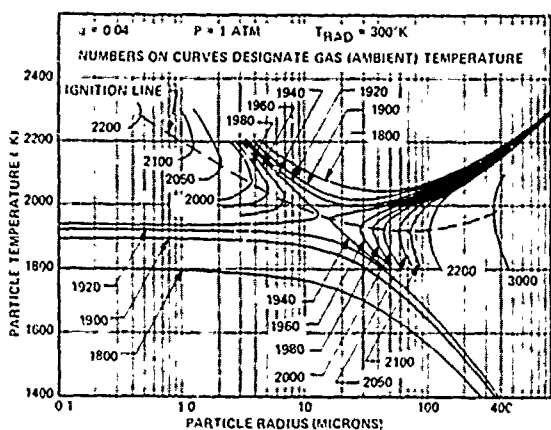


FIG. 16. Calculated particle temperature—particle radius loci of $dT_p/dt = 0$, $dx/dt = 0$ for various gas temperatures.

any initial conditions) versus particle radius. Such a curve is presented for the case of one atmosphere total pressure and 300 °K surroundings radiation temperature in Figure 17. As may be seen, there is a minimum in the curve at a particle radius of approximately 15 microns. Above this size the required ambient temperature to guarantee ignition under all initial conditions rises with particle size. This results from the fact that for large particles where diffusion controls the oxide removal rate, this rate, which strongly influences the heat generation term, is proportional to the particle radius, as is the rate of convective heat transport between particle and surroundings while the radiation loss term is proportional to the square of the radius. Accordingly, as may be shown from manipulation of equation (16) (with proper substitution for A , B , C , etc.) with the derivative set equal to zero, increasing particle radius requires a corresponding increase in gas temperature for the equality to be satisfied. Below a particle radius of approximately 15 microns however, control of oxide removal rate shifts to vaporization kinetics with the result that the heat generation term is controlled by a parameter which is proportional to the square of the particle radius. Moreover, this term is large compared to the radiation term. Manipulation of Equation 16 shows that in this regime, increasing particle radius requires a corresponding decrease in gas temperature for the derivative to be zero.

Also shown on Figure 17 are results of numerical calculations of minimum ambient temperature required for ignition for four different particle radii. (The upper end of the bar indicates the

lowest temperature tried for which ignition occurred while the lower end indicates the highest tested temperature at which ignition did not occur.) As may be seen, agreement between results of the stability analysis procedure and the numerical integration technique is excellent.

The shape of the curve in Figure 17 leads to some interesting consequences for particles above 15 μ radius. As indicated previously, the stability analysis was performed using the initial particle radius in the various equations (neglecting change in the radius during the ignition process). Accordingly, the numerical analysis results for the 50 μ radius particle shown in Figure 17 were generated with the particle radius held constant. If on the other hand, the radius is allowed to vary, the particle, after an initial transient, quickly reaches a quasi-steady state in which the temperature and oxide thickness remain nearly constant and the particle radius slowly decreases. Eventually the radius decreases far enough (say from 50 microns to 30 microns) that the minimum ambient temperature for ignition decreases correspondingly (in accordance with the curve of Figure 17, from 2030 °K to 1970 °K) that the particle may ignite even though a particle with a radius held at 50 microns would not ignite—however, the times involved are very long (thousands of milliseconds) compared to the times associated with the normal ignition process.

As part of this study, a fundamental question regarding applicability of the stability analysis approach was examined. Namely, this analysis involves solving for a quasi-steady-state temperature and oxide thickness for given boundary

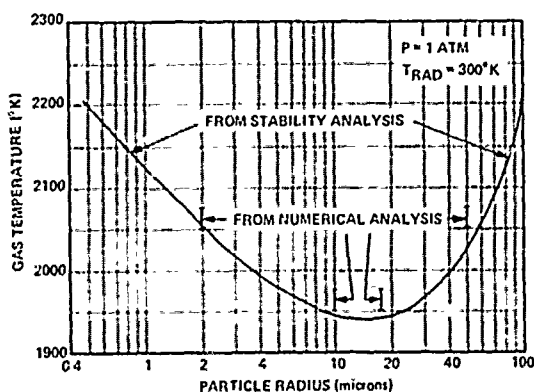


FIG. 17. Minimum gas temperature required to insure ignition for any particle initial conditions, $T_{RAD} = 300$ K.

conditions and examining this point for stability; the question arises as to whether one, starting from an arbitrary point in the particle temperature—oxide thickness plane can expect to follow a path in this plane which will take them close enough to the quasi-steady-state particle temperature—oxide thickness point associated with the given boundary conditions for the linearized stability analysis to apply. It is quite unlikely that this can be achieved for all initial conditions for a given set of boundary conditions. However, results from the numerical analysis showing essentially no dependence of minimum ambient temperature required for ignition on initial conditions and the good agreement obtained between predictions with the two analyses indicate that for a wide range of initial conditions the path followed in the particle temperature-oxide thickness plane passes close enough to the quasi-steady-state point(s) associated with the given boundary conditions to permit application of the stability analysis. The results of Figure 18 in which the paths followed by the particles in the particle temperature-oxide thickness plane are plotted for various initial conditions for one set of boundary conditions show this clearly. Over a wide range of initial conditions, the paths may be seen to pass quite close to the upper or lower "stability" points, with ignition occurring in some cases and not in others. Thus, application of a two-dimensional stability analysis to boron ignition appears quite valid.

SUMMARY

A model of the ignition of boron particles treating the removal of a boron oxide layer from the surface of the boron particle through numerical integration of difference equations describing the generation and removal rate of boric oxide has been revised to more accurately treat the various processes involved. This new model yields predicted ignition times and minimum ambient temperature requirements for particles studied by Mažek (1969) in dry gas streams which are in good agreement with his measured data. An attempt to treat the effect of water gas on boron particle ignition as being a diffusion-limited reaction of the water with the boric oxide coating to form gaseous HBO_2 was unsuccessful. Effects of various parameters on boron particle ignition were studied with this model. Oxide thickness was found to moderately affect predicted ignition times, this effect decreasing with increasing particle size. The effects of total

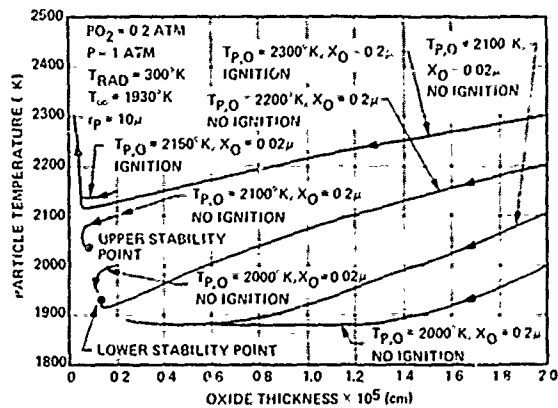


FIG. 18. Typical particle temperature-oxide thickness paths followed by boron particles in oxygen-containing gas stream.

pressure and oxygen mole fraction on minimum ambient temperature required for ignition and on ignition time were found to be fairly complex. At low oxygen mole fractions, increasing total pressure leads to more difficult ignition while at high oxygen mole fractions, the reverse is true. At low total pressure, ignition was found to be independent of oxygen mole fraction; at high pressure, increasing oxygen mole fractions lead to easier, faster ignition.

Initial particle radius effects are also somewhat complex. For the case of surrounding radiation temperature equal to the gas temperature, minimum ambient gas temperature required for ignition increases with decreasing particle size for particle radii below 10-15 microns. Ignition time generally decreases with decreasing particle size except where affected by the ignition limit dependency on particle size. Ignition time is predicted to increase strongly with decreasing gas temperature. The same type of dependency on surroundings radiation temperature is predicted in the region of ambient gas temperatures which are marginal for ignition.

The same equations used in the numerical analysis have also been used in a stability analysis to define conditions (e.g. ambient temperature) required for ignition. Excellent agreement was found between results obtained with the numerical analysis and the stability analysis.

This study was supported by AFOSR under Contract No. F44620-71-C-0124 and was monitored by Captain L. R. Lawrence.

REFERENCES

- Bird, R. B., Stewart, W. E. and Lightfoot, E. N. (1960). *Transport Phenomena*, John Wiley & Sons, NY, NY.
- Blackburn, P. E. (1965). Thermodynamics of condensed and vapor phases in the binary and ternary systems of Be-B-O, Al-B-O, Si-O, Al-Be-O, and Al-B-F, Arthur D. Little Final Report, ARPA Project Code No. 9100, ARPA Order No. 315-62.
- Gilliland, E. R. (1934). *Ind Eng. Chem.* 22, 1091.
- King, M. K. (1972). Boron ignition and combustion in air-augmented rocket afterburners. *Combustion Science and Technology* 5, 155-164.
- Maček, A. and Semple, J. (1969). Combustion of boron particles at atmospheric pressure. *Combustion Science and Technology* 1, 181-191.
- Mohan, G. and Williams, F. A. (1972). Ignition and combustion of boron in O₂/inert atmospheres. *AIAA J.* 10, 6, 776-783.
- Talley, C. P. and Henderson, U. V. (1961). Combustion of elemental boron. *Proceedings of the 4th Meeting-- JANAF-ARPA-NASA Thermochemical Panel*, p. 107.

Received April 25, 1973

VII. PREDICTIONS OF LAMINAR FLAME SPEEDS IN BORON-OXYGEN-NITROGEN DUST CLOUDS (Expanded Version of Paper Presented at the 15th International Symposium on Combustion)

Merrill K. King

Atlantic Research Corporation, Alexandria, Virginia

ABSTRACT

A detailed model of boron-oxygen-nitrogen dust cloud flames including consideration of the details of boron particle ignition and the effects of oxygen depletion has been developed and used for prediction of flame speeds as functions of numerous parameters. Reasonably good agreement between measured flame speeds and those predicted by this model has been obtained. In addition, a simplified closed-form flame speed expression has been developed and the effects of the various assumptions used in its development on predicted flame speeds have been examined. The detailed and simplified models have both been used to study the effects of initial temperature, pressure, initial oxygen mole fraction, weight fraction particles, initial particle size, initial thickness of the oxide coating on the particles, radiation feedback from the post-flame zone, and Nusselt Number. Mechanisms leading to the predicted dependencies are discussed.

INTRODUCTION AND BACKGROUND

Boron is a particularly attractive fuel for air-breathing missile engines due to its high volumetric heat of combustion. Among its possible places of application are air-augmented rockets, slurry ramjets, powder ramjets, and external burning missiles. In combustor design for these applications, information regarding laminar flame speed of boron-oxygen-diluent (e.g., boron-air) dust clouds and the dependency of this flame speed on various parameters is important for proper design of flame-holding regions.

Considerable effort has been carried out over the years on development of models for prediction of laminar flame speeds for all-gas systems: reviews of these models have been presented by Dugger, Simon, and Gerstein⁽¹⁾, Williams⁽²⁾, Von Karman⁽³⁾, and Stephenson and Taylor⁽⁴⁾, among others. The first two references contain excellent discussions of what Williams calls the "cold boundary difficulty". The problem referred to is that one cannot obtain a unique value of flame speed if he allows finite rate chemical reaction at the cold boundary of the system. This problem is avoided in practice by choosing a temperature greater than the initial temperature of the stream below which chemical heat release is set equal to zero and allowing the region between the initial temperature and the chosen temperature to be heated by feedback from downstream regions (the ignition temperature concept). A heat balance equation of the following type may then be written at the location of this chosen temperature ($X = 0$ in the coordinate system chosen for use in this paper):

$$\dot{M}_T/A \bar{C}_p (T_i - T_o) = \lambda \left. \frac{dT}{dx} \right|_{x=0} + R_A \quad (1)$$

\dot{M}_T/A	= mass flux
\bar{C}_p	= average heat capacity of stream between temperatures T_0 and T_i
T_i	= ignition temperature
T_0	= initial temperature
λ	= thermal conductivity of stream
$\left. \frac{dT}{dx} \right _{x=0}$	= temperature gradient at location where $T = T_i$
R_A	= radiation flux across $X = 0$ boundary

Various approaches to describing the temperature field for $X > 0$ and thus permitting evaluation of the terms on the right-hand side of the equation as functions of the mass flux and various independent parameters are described for gaseous systems in References 1 - 4: these permit determination of \dot{M}/A and thus the flame speed for a given set of conditions. For given conditions, only one value of mass flux will permit integration of the equations describing the flame from the known initial conditions to the known final conditions (2 - boundary eigen-value problem).

Several models have also been developed for prediction of flame speeds in liquid sprays (e.g. Williams ⁽²⁾, Sundukov and Predvoditelev ⁽⁵⁾). For the limiting case of very fine droplets which atomize before significant chemical reaction occurs, simple modification of the gas-flame models is adequate, while for very large droplets where negligible vaporization occurs before ignition, the modeling of the heat release distribution is also relatively simple. (Both of these limiting cases are described well by Williams. ⁽²⁾)

In addition, several models have been developed for prediction of flame speeds in coal dust-air clouds. Essenhigh and Csaba ⁽⁶⁾ developed a model in

which they assumed that the ignition temperature and flame temperature were essentially equal and that all heat transfer back to the pre-combustion region was accomplished by radiation from their optically thick combustion zone. Bhaduri and Bandyopadhyay ⁽⁷⁾ extended this model by including treatment of finite rate heat release in the cloud (dropping the assumption that the ignition and flame temperatures were equal), but they also neglected conductive heat feedback relative to radiative heat feedback. In addition, they made several other assumptions and approximations, including:

- (1) Temperature equilibrium between particles and gas at all positions.
- (2) No change in gas density or dust concentration through the cloud.
- (3) No ignition delay period (arbitrarily chosen ignition temperature independent of all other variables.
- (4) Heat capacities independent of composition and temperature.

For boron-air dust clouds, preliminary analysis indicates that conductive heat feedback cannot be neglected since the zone in which the boron is burning is physically and optically quite thin. (For typical cases, the ratio of the area subtended by boron particles in the combustion zone to the total geometrical area is on the order of 0.01.) The physical thinness of the combustion zone, typically less than 1 millimeter, indicated by this analysis also results in a high value of temperature gradient and thus a large conductive flux relative to the radiative flux from the combustion zone. Downstream of the combustion zone, all of the products are gaseous with a resultant low post-flame zone emissivity for reasonable effective post-flame zone thicknesses (discussed further in the model development section). In addition, studies by King ^(8,9) indicate that with boron there is an appreciable particle ignition delay time which must be included in any accurate description of boron-air dust cloud flames. Accordingly, the two models referred to above are not applicable for prediction of

boron-air dust cloud flame speeds.

Cassel, Gupta, and Guruswamy⁽¹⁰⁾ developed a closed-form expression for calculation of flame speeds in dust clouds which included radiative and conductive heat feedback through use of an equation like Equation 1 with substitution of $[(T_{\text{flame}} - T_{\text{ignition}}) / \text{Flame Zone Thickness}]$ for $dT/dx|_{x=0}$ and substitution of an expression for the radiation term which summed the radiation contribution of all of the particles in the flame zone, assuming them to all be at the final flame temperature. The flame zone thickness was estimated as a function of the flame speed by use of a d^2 - burning law to obtain the particle burning time and estimation of the ratio of densities of the burned and unburned gases to permit conversion of this time to a distance. This model is much more nearly applicable to the boron-air dust cloud flame speed calculation problem than the two previously referenced models -- however, it does have several shortcomings which are eliminated in the model developed in this study:

- (1) Particle ignition delay time is not treated analytically; instead an ignition temperature independent of other parameters is assumed.
- (2) Property (heat capacity, density, thermal conductivity) variations with temperature and composition are not treated in detail.
- (3) A linear temperature profile with respect to distance is assumed between the ignition and burnout points. It is easily shown that a continuous decrease of the temperature gradient accompanies heat release throughout the combustion zone -- thus the initial gradient must be higher than the average gradient over the zone.
- (4) The effect of oxygen depletion on burning time is not treated.

- (5) Change in gas velocity resulting from conversion of solid reactants to gaseous products is not considered.
- (6) A d^2 -law is used to describe the particle combustion. In the pressure-particle size regime of interest in this study, Macek⁽¹¹⁾ indicates that a d^1 -law (kinetics-limited combustion rather than diffusion-limited combustion) should be used for boron particle combustion.

Without development of a detailed model treating the problems listed as items 1-5, it is not clear how severely these simplifications affect flame speed predictions for boron-air dust clouds. (The effect of the last item, if large extrapolations from particle sizes for which burn-time data are available to particle sizes of interest are used is obvious.) Accordingly, a complex computer model employing a minimum of assumptions and approximations has been developed for prediction of boron-air dust cloud flame speeds. In addition a much simpler closed-form expression using the d^1 -law for particle burning but otherwise using much the same approach as that used by Cassel, Gupta, and Guruswamy⁽¹⁰⁾ has been developed for comparison.

MODEL DESCRIPTION

Prior to development of the detailed equations used in this model, a brief description of the overall model will be given. A sketch of the flame structure with division into various zones which are treated by different sets of equations is given in Figure 1. It should be noted that the model as developed is limited to fuel-lean cases, though it could be modified to also handle fuel-rich cases. Preliminary estimates indicate that Zones 1 through 3 (from $T_0 + \delta$ to T_{34} , where δ is a small number) are quite short (on the order of 1 to 5 millimeters) compared to typical flame diameters for cases of interest—accordingly one-dimensional analysis may be used for treatment of these zones.

However, as will be discussed later, the fact that the post-flame zone is all gas results in effective optical depths of tens of centimeters being required for attainment of emissivities of even 0.05 to 0.10. Thus, for typical flame diameters, multi-dimensional analysis of Zone 4 must be carried out for each given geometry to obtain an estimate of the effective emissivity of that zone as seen by the preheat region. Instead, it was decided to simply parametrically examine the effects of various assumed post-flame zone effective emissivities in this study.

Zone 1 of Figure 1 is the preheat region in which the gas-particle mixture flowing from left-to-right entering at velocity U_0 (at temperature T_0) is heated solely by conductive and radiative heat feedback from downstream from T_0 to 1600°K. (1600°K is chosen as the beginning of the ignition zone since it is safely below the temperature at which oxide-coated boron begins to react appreciably.)* In this analysis, a value of U_0 (or \dot{M}_{Total}/A , the mass flux) is guessed. An enthalpy balance over Zone 1 then permits calculation of the temperature gradient at the boundary of Zones 1 and 2 ($X = 0$). Since oxygen depletion effects are being considered and since due to nonlinearities the oxygen mole fraction and temperature profiles are not similar, either the oxygen mole fraction or its axial gradient must also be assumed at $X = 0$ (double eigenvalue problem). Assuming either one permits calculation of the other by a species mass balance across Zone 1. In this model, the gradient of oxygen mole fraction is guessed. Thus, with initial guesses of the flame speed and this gradient, all conditions at $X = 0$ are defined, permitting the beginning of integration of mass, species, and enthalpy conservation equations thru Zone 2.

In Zone 2, the boron particle ignition processes take place. The processes occurring during the ignition of a particle of boron initially coated

* Sample cases run using 1400°K rather than 1600°K as the temperature at the end of Zone 1 indicated no effect of this change on calculated flame speeds.

with an oxide layer are complex. First, there is a heatup stage during which the comparatively cold boron particle is heated solely by convective and/or radiative flux(es) from hotter surroundings. Once the particle temperature is sufficiently high (approximately 1800°K) non-negligible self-heating of the particle by exothermic oxidation begins to be superimposed on the convective and radiative fluxes. Since the boron particle is covered with a molten boric oxide layer below about 2100-2500°K, the oxygen must diffuse through the liquid oxide layer. As this oxidation occurs, of course, it makes the oxide layer thicker, increasing diffusional resistance. At the same time, as long as the particle temperature keeps rising, the viscosity of the oxide decreases and consequently the diffusivity of oxygen in the oxide increases. In addition, boron oxide simultaneously evaporates from the layer at a rate which depends on the particle temperature, tending to thin the layer. However, this evaporation is an endothermic process tending to cool the particle (or at least lower its rate of temperature rise). Once the particle temperature rises above the surroundings temperature the convective and radiative heat fluxes to the particle will turn negative, also tending to cool the particle. As long as the sum of the self-heating term and the convective/radiative term remains greater than the product of the oxide vaporization rate and the heat of vaporization, the particle temperature will continue to rise. If this situation persists to the point where the remaining oxide layer is sufficiently thin, a temperature runaway will occur, the particle will finish cleansing itself of oxide, and full-fledged combustion will occur.

In the integration of mass, species, and enthalpy conservation equations through Zone 2, an analysis of single particle boron ignition as a function of surroundings conditions developed by King ⁽⁹⁾ is coupled with

these equations to permit calculation of the removal of the oxide from the particle until thermal runaway occurs. At this point, all concentrations, temperatures, and gradients of these parameters are stored for the beginning of integration of mass, species, and enthalpy conservation equations in Zone 3. In this zone, combustion of the cleansed boron particles by a kinetics-limited (d^2 -law) process with Macek ⁽¹¹⁾ data being used for rate-constant determination is treated. The equations describing the particle combustion rate as a function of oxygen concentration and particle size are coupled with the mass, species, and enthalpy equations and the integration is carried on through Zone 3, which ends when the particle radius goes to zero (burnout).

In cases where the post-flame zone emissivity is assumed to be zero, the integration of the equations ends at $X = X_{34}$. For finite Zone 4 emissivities an energy balance is applied over Zone 4 to correct the temperature at $X = X_{34}$ to a final temperature. The final calculated temperature and oxygen mole fraction are now compared to values calculated from stoichiometric and overall enthalpy balance equations. If there is disagreement, the initial guesses on U_o and the oxygen mole fraction axial gradient at $X = 0$ are adjusted and the procedure repeated. This cycle is continued until satisfactory matching of the final boundary conditions occurs.

DETAILED MODEL DEVELOPMENT

Zone 1 - An energy balance may be written over Zone 1, in which no heat release occurs, as follows (see Nomenclature for definition of symbols):

$$\left(\frac{\dot{M}_T}{A} \right) (1600 - T_o) C_{p, \text{Avg}, 1} = \lambda_{1600} \left. \frac{dT}{dx} \right|_{x=0} + \dot{q}_{\text{RAD}, \text{IN}} - \dot{q}_{\text{RAD}, \text{OUT}} \quad (2)$$

where the total mass flux (\dot{M}_T/A) of particles plus gas is related to the flame speed (U_o) by:

$$\left(\frac{\dot{M}_T}{A}\right) = \frac{P(MW)_{gI} (1 + k_f + k_{oxf}) U_o}{R T_o} \quad (3)$$

As an early part of this study, a very simplified model (described later) was derived and used to calculate approximate flame speeds and characteristic zone dimensions for typical cases of interest. These values were then used in calculations to determine reasonable simplifications of the analysis. One such calculation indicated that the particle and gas temperatures are essentially equal at any given location within Zone 1 and thus that separate energy balances for gas and particles need not be written in this region. In addition, it was found that the burning zone is so short as to be optically thin (projected area of all particles in this region being less than 1 percent of the total area) with the result that radiation feedback from this zone to Zone 1 is negligible compared to conductive feedback (less than 5 percent) for cases of interest. Therefore, in consideration of radiation effects one is left with radiative exchange between the post-flame (all gas) Zone 4 and the preheat Zone 1. Calculation of the effective emissivity of this post-flame zone in which the only emitting species are various boron oxide gases (mostly B_2O_3) is quite geometry dependent -- accordingly it was decided to treat this emissivity, ϵ_f , parametrically in this study. However, it is instructive to estimate the post-flame zone emissivity as a function of its effective thickness. The approximate relationship* between this zone thickness and the emissivity is given by (through analogy to H_2O and CO_2 gas emissivity data presented by McAdams (12)):

$$\Delta X_4 = 2 \frac{[\exp(30 \epsilon_f) - 1]}{k_f P} \quad (4)$$

* It should be noted that this is an empirical expression fitting emissivity data for path length-partial pressure products of 5 to 150 cm-atm and should not be extrapolated outside this regime.

where P is in atmospheres and ΔX_4 in centimeters. For an initial particle-to-gas mass ratio (k_f) of 0.1 and a pressure of 1 atmosphere, this equation indicates that an effective post-flame zone thickness of approximately 400 cm is required for an emissivity of 0.1, 70 cm for an emissivity of 0.05, and 20 cm for an emissivity of 0.02. For emissivities in this range, the aforementioned simplified model indicates that radiation feedback from the post-flame zone to the preheat zone, while not negligible, does not dominate the conductive feedback. Based on the above discussion, radiative heat transfer in and out of Zone 1 was treated as exchange between Zones 1 and 4:

$$\dot{q}_{\text{RAD, IN}} - \dot{q}_{\text{RAD, OUT}} = \sigma \epsilon_f \alpha_B \left[T_f^4 - F_{10} (1600)^4 \right] \quad (5)$$

where F_{10} is a correction factor for Zone 1, ranging from approximately 0.3 for $T_o = 300^\circ\text{K}$ to 0.5 for $T_o = 1000^\circ\text{K}$, to allow for the fact that the entire zone is not at 1600°K . Equations 2, 3, and 5 may be combined to yield:

$$\left. \frac{dT}{dx} \right|_{x=0} = \frac{P(\text{MW})_{g1} (1 + k_f + k_{\text{oxf}}) U_o (1600 - T_o) C_{P, \text{Avg}, 1}}{RT_o \lambda_{1600}} - \frac{\sigma \epsilon_f \alpha_B \left[T_f^4 - F_{10} (1600)^4 \right]}{\lambda_{1600}} \quad (6)$$

The average heat capacity over Zone 1 is obtained straightforwardly by integration of the temperature -- dependent heat capacity functions for each ingredient from T_o to 1600°K . Thus, given a guessed U_o , $dT/dx \big|_{x=0}$ for the gas and particles may be obtained from Equation 6.

Due to the nonlinear nature of the equations for mass, species, and energy conservation across Zones 2 and 3, the temperature and oxygen mole

fraction profiles are not similar. Accordingly, either the oxygen mole fraction or its axial derivative at $X = 0$ must also be guessed to start the integration through the downstream zones (double eigen-value problem). In this model, the value of the gradient is guessed and the mole fraction itself is then calculated from a mass balance on O_2 across Zone 1:

$$Y_{O_2, x=0} = Y_{O_2, 1} + \frac{D_{1600}}{U_0} \frac{T_0}{1600} \left. \frac{dY_{O_2}}{dx} \right|_{x=0} \quad (7)$$

Thus, with selection of a temperature below which chemical reaction is negligible as the boundary between Zones 1 and 2 (preheat and ignition zones), and guessed values of the flame speed (U_0) and the oxygen mole fraction axial gradient at $x = 0$, we arrive at the initial conditions listed below needed to begin integration of mass, species, and enthalpy conservation equations for gas and particles through Zone 2.

$$T_{g, x=0} = T_{p, x=0}$$

(Selected as 1600°K, a temperature below which reactions are negligible)

$$\left. \frac{dT_g}{dx} \right|_{x=0} = \left. \frac{dT_p}{dx} \right|_{x=0}$$

(Obtained from Equation 6)

$$\left. \frac{dY_{O_2}}{dx} \right|_{x=0}$$

(Guessed)

$$Y_{O_2, x=0}$$

(Obtained from Equation 7)

$$r_{p, x=0}$$

(Known initial boron particle radius)

$$b_{x=0}$$

(Known initial oxide coating thickness on boron particle)

Zone 2 - In Zone 2, differential equations on gas temperature, particle

temperature, and oxygen mole fraction derived from species, mass, and enthalpy conservation equations are coupled with differential equations describing the processes taking place during the cleaning of the boron oxide coating from the surface of the boron particles (boron ignition process) and integrated from the initial conditions described in the previous paragraph to the point at which the oxide thickness approaches zero and thermal runaway occurs (end of Zone 2, the ignition zone). The equations used to describe the processes occurring during boron particle ignition were developed and described in detail in Reference 9. Application of a differential enthalpy balance to the gas (assuming that all chemical heat release occurs in the particles in this zone and is only transferred to the gas by conduction) leads to:

$$\lambda \frac{d^2 T_g}{dx^2} + \left(\frac{dT_g}{dx} \right) \left(\frac{d\lambda}{dx} \right) - \left(\frac{M_{gI}}{A} \right) C_{pg} \left(\frac{dT_g}{dx} \right) - 4\pi r_p^2 N_p h(T_g - T_p) = 0 \quad (8)$$

where the number of particles per unit volume, N_p , is given by:

$$N_p = \frac{3 P (MW)_{gI} k_f}{4\pi R T_g r_p^3 \rho_B} \quad (9)$$

In the derivation of Equation 8, variation in thermal conductivity with temperature (and thus position) was allowed for, resulting in the second term. The change in molecular weight resulting from the consumption of oxygen and production of boric oxide was neglected in this ignition zone as being second order, as were changes in the gas and particle mass fluxes accompanying these reactions. (In general, only a very small fraction of the boron is consumed during the ignition phase.)

Application of a differential oxygen mole balance, including consumption of oxygen by the boron particles, resulted in:

$$-\left(\frac{\dot{M}_{gI}}{A}\right)\left(\frac{dY_{O_2}}{dx}\right) + (MW)_{gI} d\left[\left(\frac{DP}{RT_g}\right)\left(\frac{dY_{O_2}}{dx}\right)\right]/dx - (3R_B N_p/4)(MW)_{gI} = 0 \quad (10)$$

where R_B is the molar consumption rate of boron per particle.

As with thermal conductivity in the enthalpy equation, the variation in diffusivity with temperature (and thus with axial position) was included. R_B is the molar consumption rate of boron per particle.

A differential enthalpy balance on the particles, including all heat effects associated with the reaction of oxygen which diffuses through the oxide layer to react with the boron and evaporation of the oxide, and also including radiative gains from the post-flame zone and losses to the preheat zone may be written as (for $T_p < 2450^\circ K$):

$$\begin{aligned} -\left(\frac{\dot{M}_{PI}}{A}\right) C_{PB} \left(\frac{dT_p}{dx}\right) + \sigma \epsilon_B \alpha_B N_p^2 \left(T_f^4 - T_p^4\right) - \sigma \alpha_B^2 N_p^2 \left[T_p^4 - F_{10}(1600^4)\right] \\ + N_p 4H_p^2 h(T_g - T_p) + N_p \left[R_B(Q_{RX}) - R_E(\Delta H_{VAP})\right] = 0 \end{aligned} \quad (11)$$

R_E is the molar vaporization rate of boric oxide per particle. At $2450^\circ K$, the boron particle begins to melt and $C_{PB}(dT_p/dx)$ in the first term must be replaced by $\Delta H_m(df/dx)$, where f is the mass fraction of the boron melted. When this fraction reaches one, Equation 11 is again employed, with substitution of a new heat capacity expression and a different value for Q_{RX} to allow for the heat of melting. In addition to the two second and one first order differential equations above, two additional first order differential equations describing mass balances on the boron and the condensed phase boron oxide are employed in Zone 2:

$$\frac{dr_p}{dx} = -\frac{R_B(MW_B) P (MW)_{gI}}{4H_p^2 \rho_B \left(\frac{\dot{M}_{gI}}{A}\right) RT_g} \quad (12)$$

$$\frac{db}{dx} = \frac{(R_B/2 - R_E)(MW_{B_2O_3}) P (MW)_{gI}}{4H_p^2 \rho_{B_2O_3} \left(\frac{\dot{M}_{gI}}{A}\right) RT_g} \quad (13)$$

The molar rates of consumption of boron and evaporation of boric oxide (per particle) are given by (See Reference 9):

$$R_B = \frac{64.8(10^{-8}) (r_p + b)^2 T_p e^{-22600/T_p} (P) Y_{O_2}}{b} \quad (14)$$

$$R_E = \frac{4.02 \cdot 10^8 (r_p + b)^2 e^{-44000/T_p}}{T_p^{1/2} \left[1 + \{1.8(10^6) P (r_p + b)\} / \{(T_p) (Nu)\} \right]} \quad (15)$$

The heat transfer coefficient h , appearing in Equations 8 and 9, the thermal conductivity λ , and the diffusivity D , are calculated from:

$$h = \frac{(\lambda) (Nu)}{r_p} \quad (16)$$

$$\lambda = 0.694 (10^{-6}) T_g^{0.8} \quad (17)$$

$$\frac{d\lambda}{dx} = \frac{0.555(10^{-6})}{T_g^{0.2}} \frac{dT_g}{dx} \quad (18)$$

$$D = \frac{3.6 \cdot 10^{-5} T_g^{3/2}}{P} \quad (19)$$

$$\frac{dD}{dx} = \frac{5.4 \cdot 10^{-5} T_g^{1/2}}{P} \frac{dT_g}{dx} \quad (20)$$

From the Zone 2 initial conditions, calculated as described earlier, the two second order differential equations (8, 10) and the three first order differential equations (11-13) are numerically integrated with the help of the

ancillary equations (9, 14-20) through Zone 2 until the oxide thickness approaches zero and the particle temperature begins to run away. At this point, Zone 2 calculations are terminated and values of r_p , T_g , dT_g/dx , Y_{O_2} , and dY_{O_2}/dx are saved as initial values for Zone 3.

Zone 3 - In Zone 3, the cleaned boron particles undergo full-fledged combustion, releasing heat and boric oxide gas and consuming particulate boron and oxygen. Calculations by Williams⁽¹³⁾ indicate that boron particles maintain a constant particle temperature of about 2500°K during full combustion. Since the ignition modeling studies of King^(8,9) indicated that igniting boron particles were well into thermal runaway by the time their temperature reached 2500°K, the location at which this particle temperature was achieved was chosen as the termination point of Zone 2. It was then assumed that this particle temperature remained constant throughout Zone 3, all heat release going to the gas phase. As a result differential equations required for Zone 3 are limited to equations in particle radius (r_p), oxygen mole fraction (Y_{O_2}), gas temperature (T_g), and gas mass flux (\dot{M}_g/A). (Recall, that due to the small amount of conversion of boron to oxide in Zone 2, changes in the relative amounts of gas and particle mass flux and in effective stream molecular weight were ignored in that zone -- these effects are no longer second order in Zone 3 and must be considered. A separate differential equation for particle mass flux is not required since its change is simply the negative of change in gas mass flux.) A mass balance equation on boron results in the following differential equation in gas mass flux:

$$\frac{d(\dot{M}_g/A)}{dx} = R_B^+ (MW)_B N_p \quad (21)$$

where N_p can no longer be calculated from Equation 9 due to the non-negligible changes in molar gas flux and gas molecular weight affecting the gas density, but must now be calculated as:

$$N_p = \frac{3 P (MW)_g k_f (\dot{M}_T/A)}{4 \pi R T_g^3 r_p^2 \rho_B (\dot{M}_g/A) (1 + k_f)} \quad (22)$$

Application of a species conservation equation to oxygen results in (with the approximation percentage changes in $(MW)_g$ and (\dot{M}_g/A) are equal):

$$-\frac{1}{(MW)_g} \left(\frac{\dot{M}_g}{A} \right) \left(\frac{dY_{O_2}}{dx} \right) + \frac{DP}{RT_g} \left(\frac{d^2 Y_{O_2}}{dx^2} \right) + \frac{P}{RT_g} \left(\frac{dD}{dx} \right) \left(\frac{dY_{O_2}}{dx} \right) - \frac{DP}{RT_g^2} \left(\frac{dT_g}{dx} \right) \left(\frac{dY_{O_2}}{dx} \right) - \frac{3R'_B N_p}{4} = 0 \quad (23)$$

An enthalpy balance written over a differential element of Zone 3 (assuming, as mentioned earlier, constant particle temperature in this zone) yields:

$$\frac{d^2 T_g}{dx^2} - \left(\frac{\dot{M}_g}{A} \right) C_{pg} \left(\frac{dT_g}{dx} \right) + \left(\frac{dT_g}{dx} \right) \left(\frac{d\lambda}{dx} \right) + R'_B Q'_{RX} N_p = 0 \quad (24)$$

where R'_B is the molar rate of consumption of boron per particle and Q'_{RX} is the heat release associated with the reaction of 1 mole of liquid boron at $2500^\circ K$ with $3/4$ moles of O_2 gas at T_g to yield $1/2$ mole of B_2O_3 gas at T_g .

A mass balance on boron particle mass yields:

$$\frac{dr_p}{dx} = \frac{-R'_B (MW_B) P (MW_g)}{4 \pi r_p^2 \rho_B (\dot{M}_g/A) \dot{M}_g} \quad (25)$$

Application of boron-particle burning-rate data obtained by Macek ⁽¹¹⁾ for particle radius-oxygen partial pressure products below 5 to 10 atmosphere-microns (range of interest for this study) yields the following expression for the molar consumption rate of boron per particle in full-fledged combination:

$$R_B' = \frac{2.0 \cdot \pi r_p^2 \rho_B P Y_{O_2}}{(MW_B)} \quad (26)$$

Equations 17-20 are used for the thermal conductivity (λ) and diffusivity (D), while the gas molecular weight and heat capacity are estimated as:

$$(MW_g) = \frac{1}{\left[3.22 - 3.22 \frac{(\dot{M}_{gI}/A)}{(\dot{M}_g/A)} \right] / (MW_{B_2O_3}) + \left[3.22 \frac{(\dot{M}_{gI}/A)}{(\dot{M}_g/A)} - 2.22 \right] / (MW)_I} \quad (27)$$

$$C_{pg} = \left[3.22 - 3.22 \frac{(\dot{M}_{gI}/A)}{(\dot{M}_g/A)} \right] C_{p,B_2O_3} + \left[3.22 \frac{(\dot{M}_{gI}/A)}{(\dot{M}_g/A)} - 2.22 \right] C_{pGI} \quad (28)$$

where all of the individual component specific heats are curve fit versus temperature.

Starting with the values of r_p , T_g , dT_g/dx , Y_{O_2} , and dY_{O_2}/dx stored at the end of the Zone 2 calculations and the initial value of \dot{M}_g/A , Equations 21, 23, 24, and 25 are simultaneously integrated with the use of ancillary equations 17-20, 22, 26-28 across Zone 3 until the particle radius r_p goes to zero (burnout). In cases where the post-flame zone emissivity is zero, calculation stops at this point (since it can be shown in this case that temperature is constant in Zone 4) and the final values of gas temperature (T_{g34}) and oxygen mole fraction ($Y_{O_2,34}$) are compared with those calculated from straightforward

stoichiometry and thermochemical calculations. (The thermochemical calculations are performed with no allowance for species dissociation and the same heat capacity fits as used in the above-described procedures for internal consistency.) If these do not match, adjustments are made to the guesses on flame speed (or equivalently total mass flux) and oxygen mole fraction axial gradient at $X = 0$ and the entire procedure is repeated. This loop is continued until satisfactory final boundary condition matches are achieved.

Zone 4 - For cases where a non-zero emissivity is assigned to Zone 4, calculations must be carried on through this zone to account for heat transferred out of this zone back to the preheat zone. Since earlier-mentioned estimates indicated that this zone must be quite thick to have any appreciable emissivity, and thus temperature gradients through this zone are very shallow, conductive transport is neglected in Zone 4 in this analysis. With this simplification, it is readily shown that the final temperature (which is the one to be checked against the temperature obtained from thermochemical calculations) is approximately related to the temperature of the end of Zone 3 (T_{g34}) by

$$T_{\text{final}} = T_{g34} - \frac{\sigma \epsilon_f \alpha_B [T_f^4 - (1600)^4 F_{10}]}{\left(\frac{M_T}{A}\right) C_{pg34}} \quad (29)$$

It is also easily shown that the oxygen mole fraction does not vary through Zone 4: thus, $Y_{O_2, \text{final}} = Y_{O_2, 34}$. The same type of final boundary condition checks as described above for cases where $\epsilon_f = 0$ are applied using T_{final} in place of T_{g34} .

SIMPLIFIED MODEL

As mentioned earlier, a simplified model similar to that of Cassel, Das Gupta, and Guruswamy⁽¹⁰⁾ except for use of a d^1 -law for particle combustion

and a modified radiation treatment consistent with the complex model described above was also developed for comparison purposes. The simple model begins with a combination of Equations 2, 3, and 5, with $(1 + k_f + k_{oxf})$ replaced by unity and $F_{10} (1600)^4$ replaced by T_0^4 , leading to:

$$\epsilon_f \sigma_B (T_f^4 - T_0^4) + \lambda_{T=Ti} \frac{dT}{dx} \Big|_{T=Ti} = \frac{P(MW)_g U_{O_2} \bar{C}_p (T_i - T_0)}{RT_0} \quad (30)$$

where T_i is the minimum temperature required for ignition of single boron particles under static conditions, approximately 1900°K. The temperature gradient at the ignition point is next approximated by:

$$\frac{dT}{dx} \Big|_{T=Ti} \approx \frac{T_f - T_i}{\Delta X_{flame}} \approx \frac{T_f - T_i}{T_{burn} U_{avg}} \approx \frac{T_f - T_i}{T_{burn} U_0} \left(\frac{T_i + T_f}{2T_0} \right) \quad (31)$$

The boron particle burning time is then calculated from the d'-law expression used in generation of Equation 26 (neglecting oxygen depletion) as:

$$\tau_{burn} = \frac{r_{PI}}{K_R P Y_{O_2, I}} \quad (32)$$

Combining Equations 30 - 32, one obtains the following expression for flame speed:

$$U_0 = \frac{\epsilon_f \sigma_B (T_f^4 - T_0^4) + \sqrt{\left[\epsilon_f \sigma_B (T_f^4 - T_0^4) \right]^2 + \frac{4\lambda (T_f - T_i) K_R P Y_{O_2, I} (2T_0) P(MW)_g \bar{C}_p (T_i - T_0)}{RT_0 r_{PI} (T_i + T_f)}}}{\left(\frac{2 P(MW)_g \bar{C}_p (T_i - T_0)}{RT_0} \right)} \quad (33)$$

which in the absence of radiation $\epsilon_f = 0$ reduces to:

$$U_0 = \sqrt{\frac{2 \lambda (T_f - T_i) K_R Y_{O_2,i} R T_0^2}{r_{p,i} (T_f - T_i) (MW)_g \bar{C}_p (T_i - T_0)}} \quad (34)$$

The following values were used for properties appearing in these equations:

$$\lambda = 2.54 \cdot 10^{-4} \text{ cal/cm sec } ^\circ\text{K}$$

$$\alpha_B = 0.5$$

$$\bar{C}_p = 0.2 \text{ cal/gm } ^\circ\text{K}$$

$$T_i = 1900^\circ\text{K}$$

$$(MW)_g = 30 \text{ gm/gm-mol}$$

$$K_R = 0.5 \text{ cm/atm sec}$$

For each set of conditions analyzed with the previously described detailed model, Equation 33 or 34 was used to calculate flame speed for comparison with values calculated by that model.

RESULTS AND DISCUSSION

Detailed predicted profiles of gas temperature, particle temperature, oxygen mole fraction, particle radius, and oxide thickness through the ignition and combustion zones are presented in Figure 2 for a typical boron-air dust cloud case. For this case, the initial temperature was 600°K , the pressure was 5 atmospheres, the initial mole fraction oxygen in the gas was 0.2 (air), the weight fraction of particles (1 micron radius, .02 micron oxide thickness) was 0.06, the Nusselt Number was 2 (pure conduction), and the post-flame emissivity was 0. As may be seen, the oxide coating initially thickens, due to the rate of the boron reaction with oxygen diffusing through the oxide layer exceeding the evaporation rate, until a particle temperature of approximately 2000°K is reached, at which point the evaporation rate rises above the oxide generation rate. Up to about 2100°K , both rates are sufficiently slow that the rate of heat transfer between particles and gas is sufficient to keep both at essentially the same temperature. At this point, the oxide layer has been sufficiently thinned and the rates of oxide generation and exaporation raised to the point where the particle temperature rises above the gas temperature, eventually reaching the melting point, and, soon after melting of the boron particle is complete, running away (as the oxide layer thickness goes rapidly to zero). Subsequently, the particle burns freely with the radius decreasing approximately linearly with distance until it has been consumed. Examination of the oxygen mole fraction curve reveals that diffusion from upstream of the calculation starting point (Zone 1) through Zone 2 results in the oxygen mole fraction throughout the full-fledged combustion region being nearly equal to the final stoichiometric value, indicating the importance of consideration of oxygen depletion in the modeling of boron-oxygen-nitrogen dust cloud flames.

It should be noted that the temperature of the gas at the point at which the boron particle begins full combustion is not the static single particle boron ignition temperature of approximately 1900°K (used in the simplified model), but approximately 2280°K. Moreover, examination of Table II in which results of various cases are presented reveals that this "ignition" temperature varies with the different independent variables, not being one fixed value for all cases. While in the simplified model it is assumed that full combustion begins at 1900°K, it may be seen from Figure 2 that for the case presented there, the axial distance from the 1900°K point to the end of the ignition zone is essentially equal to the length of the combustion zone itself (.012 cm versus .011cm). Finally, the non-linearity of gas temperature versus distance in the combustion zone should be noted, in comparison to the assumed linear profile in the simplified model.

It is naturally of interest that flame speeds predicted with the detailed model be compared with experimental results. An extensive search for boron-oxygen-nitrogen dust cloud flame speed data unearthed but two data points, with precise input data available for neither of them. These two data points, supplied by Dr. Irv Liebman ⁽¹⁴⁾, were obtained in tests at the Bureau of Mines in which the speed of propagation of a laminar flame through a dust cloud blown through a one-inch diameter tube was measured. The particle loadings, gas composition, initial temperature, and pressure for each test were well-defined. (See Table I for values.) However, the boron particle size was not well defined ("under ten microns"). For the calculations, the diameter was assumed to be approximately 5 microns in each case. In addition, no information was available on initial oxide thickness. In other applications of the boron ignition model employed within this model, use of an initial oxide thickness of 0.02 microns was generally found to give good agreement with data: accordingly, this value was used in the detailed model. (As will be shown later, predicted flame speed is not very sensitive to this parameter.) From the geometry of the test apparatus, the post-flame emissivity was estimated to be well

under 0.01: at this value, the effect of radiation feedback is at best second order

Measured and predicted flame speeds for these two cases are given in Table I. It should be emphasized that this is not intended as a test between the simplified and detailed models, but rather as a check to see whether these models produce reasonable flame-speed predictions. As may be seen, the results are quite encouraging, the measured flame speeds being approximately 12 cm/sec in each case compared to predictions of 11.6 and 10.4 cm/sec with the detailed model. Due to the uncertainties of some of the model input parameters, the data points do not provide as rigorous testing of the model as desired; however, they do indicate that the model is not unreasonable.

The fairly close agreement between flame speed predictions by the detailed and simplified models seen in Table I, and later in presentation of parameter effects as predicted by the two models calls for some discussion. There are three major potential error-producing assumptions associated with the simplified model (along with other lesser problems such as neglect of temperature dependence of gas properties):

1. Neglect of the effect of oxygen depletion. This should result in the simplified model underpredicting the combustion time and thus overpredicting the flame speed.
2. Neglect of ignition delay time and distance. This should also result in overpredicting of the flame speed.
3. Assumption of a linear temperature profile through the combustion zone. As is well known, heat release in a flame dominated by conductive heat feedback is accompanied by a decreasing temperature gradient (negative second derivative). Thus, the actual temperature profile in the heat release zone is curved, concave downward, and therefore, the temperature gradient at the beginning of the zone (which determines the heat feedback

to the preheat zone) is greater than the average gradient across the zone. This factor should result in the simplified model underpredicting the flame speed.

For testing of the relative effects of these errors and the degree to which the third item cancels the first two items, a third calculation was performed for Case 1, in which the third assumption was relaxed, but the first two maintained. This was done by altering the detailed model to ignore all reactions in Zone 2, start Zone 3 at $T = 1900^\circ\text{K}$, and to hold oxygen concentration equal to the initial value throughout Zone 3. Results of calculations with the detailed model, the simplified model, and this third "in-between" model are shown in Figure 3. As may be seen, elimination of the third assumption results in a considerably higher value of (dT/dx) at $x = 0$ compared to the "simple" model and thus to a much higher predicted flame speed. Further elimination of the first and second assumptions (resulting in the detailed model), however, more than compensates, yielding a value of (dT/dx) at $x = 0$ even lower than that given by the simplified model (and thus a lower flame speed). Comparison of the detailed model to the "in-between" model indicates a drastic difference in predicted flame speeds (4 to 1) as does comparison of the "simple" model to the "in-between" model (2-1/2 to 1): however, the errors are in opposite directions and largely cancel, resulting in the simplified model giving a predicted flame speed only 50% greater than that predicted by the detailed model. As may be seen from Table II, this excess varies with conditions, ranging from essentially 0% to 130% over the range of conditions studied.

As part of this study, the effects of eight independent parameters on boron-oxygen-nitrogen dust cloud flame speed were examined. These parameters were Nusselt Number, Initial Oxide Thickness, Post-Flame Emissivity, Weight Fraction of Particles, Pressure, Initial Gas Stream Oxygen Mole Fraction, Initial Boron Particle Radius, and Initial Temperature.

The effect of Nusselt Number on flame speed, as predicted by both the detailed and simplified models is shown in Figure 4. Lower flame speeds were predicted with the detailed model. In addition, while no dependency on Nusselt number was predicted with the simplified model, the detailed model indicated a decrease in flame speed with increasing Nusselt Number. Examination of detailed profile plots similar to Figure 2 indicated that this effect was caused by the higher Nusselt Number regarding the takeoff of the particle temperature (divergence away from the gas temperature) lengthening the ignition region considerably.

The predicted effect of initial oxide thickness on flame speed is shown in Figure 5. Again, considerably lower flame speeds are predicted with the detailed model than with the simplified model. With either model, flame speed is predicted to decrease with increasing oxide thickness. All of the dependency shown in the simplified model predictions and much of that shown in the detailed model predictions results from a decrease in flame temperature with increasing oxide thickness (less boron fuel for a fixed weight fraction of particles). (See Table II for flame temperatures.) Further dependence on initial oxide thickness shown by the detailed model results from the ignition zone length required for removal of the oxide layer increasing with the amount to be removed.

As shown in Figure 6, and as logically expected, increased post-flame emissivity results in increased predicted flame speeds with either model. This result basically derives from lower conductive heat feedback requirements accompanying increased radiative feedback. It should be recalled from earlier discussion, however, that for an initial particle-to-gas mass ratio of 0.1 and a pressure of 1 atmosphere, an effective post-flame thickness of approximately 80 cm is required even for an emissivity of 0.05, 400 cm for 0.10. From simple geometric view-angle analysis, the ratio of effective post-flame thickness to diameter for a circular jet flame is approximately unity--thus, very large diameter flames are required for post-flame emissivity to have appreciable effect in the absence of condensed phases.

Increasing weight fraction of particles (on the fuel-lean side of stoichiometric to which this model is currently limited) leads to predicted increases in flame speed with either model. (Again lower values are predicted with the detailed model.) This effect is due to increasing flame temperature with increased weight fraction of particles. (See Figure 7.)

Predictions of the effect of pressure on flame speed are presented in Figure 8. The simplified model predicts no dependency of flame speed on pressure since the effect of pressure on pre-heat zone heat demand rate (proportional to pressure at fixed flame speed) is just offset by the effect of pressure on burn time and thus on the temperature gradient in the combustion zone. With the detailed model, on the other hand, flame speed is predicted to decrease with increasing pressure. The reason for this is that while increased pressure lowers the particle burning time, it has little effect on the ignition time and thus the increased heat demand of the preheat zone accompanying pressure increase is not totally offset by effects on Zones 2 and 3. Since the ratio of mass flux to flame speed is proportional to pressure, it may be seen that the simplified model predicts a mass flux proportional to pressure while the detailed model predicts mass flux increasing with increasing pressure, but with a lesser dependency.

As shown in Figure 9, both models predict increased flame speed with increasing oxygen mole fraction, the detailed model again resulting in lower predicted flame speeds than the simplified model. The observed dependency results from increased oxygen mole fractions speeding up both the ignition and combustion processes (particularly the latter since it occurs mostly at or near the final oxygen mole fraction and for a given percentage increase in initial oxygen mole fraction, the percentage increase in final oxygen mole fraction is greater).

The effect of increased initial boron particle radius is to decrease predicted flame speed (with either model). This results from increased particle size causing increased combustion time and combustion zone length. This effect is shown in Figure 10.

Finally, increasing initial temperature strongly raises flame speed, as predicted by either model. (See Figure 11.) This results from two factors: (a) increased initial temperature reduces the preheat (and thus the heat feedback) requirement; and (b) increased initial temperature results in higher flame temperature, intensifying the heat feedback. It should be noted that the mass flux to flame speed ratio is inversely proportional to initial temperature. However, since as shown in Figure 11, predicted flame speed increases more rapidly percentage-wise than initial temperature, then the mass flux also increases with initial temperature.

SUMMARY

A model for prediction of boron-oxygen-nitrogen dust clouds treating the boron particle ignition and combustion processes in detail was developed. The problem was formulated as a double-eigen value problem with numerical integration of mass, species and energy difference equations in combination with difference equations describing the ignition and combustion processes through ignition and combustion zones. This model was found to yield predicted flame speeds in reasonable agreement with the limited boron-oxygen-nitrogen dust cloud flame speed data available.

In addition, a vastly simplified closed-form flame speed expression was developed. Predicted flame speeds from this model were found to exceed those predicted from the detailed model by 0 to 130% over the range of parameters examined. It was shown that two of the major error-producing approximations associated with the simplified model tend to drive predicted flame speeds down, while a third tends to drive them up, leading to a large degree of cancellation of these errors. Over the range of conditions examined, it appears that the simple closed-form model can be used with a correction factor dependent on Nusselt Number and pressure to obtain reasonable estimates of boron-oxygen-nitrogen dust cloud flame speeds.

Effects of various parameters on predicted flame speed were studied.

Predicted flame speeds were found to increase with increasing initial temperature, decreasing initial particle radius, initial oxygen mole fraction, decreasing pressure, increasing particle loading (on fuel-lean side of stoichiometric), increasing post-flame emissivity, decreasing initial oxide coating thickness, and decreasing Nusselt Number.

NOMENCLATURE

b	oxide coating thickness (cm)
C_p	heat capacity (cal/gm °K)
\bar{C}_p	average heat capacity between initial temperature and ignition temperature (cal/gm °K)
$C_{p,Avg.1}$	average heat capacity in Zone 1 in detailed model (cal/gm °K)
D	diffusivity of oxygen in oxygen-nitrogen mixture (cm ² /sec)
f	mass fraction of boron melted
F_{10}	correction factor defined in Equation 5
h	heat transfer coefficient for gas-particle transfer (cal/cm ² sec °K)
k_f	initial mass of boron per unit mass of gas
k_{oxf}	initial mass of oxide coating per unit mass of gas
K_R	constant in burning-rate expression, Equation 32 (0.5 cm/atmsec)
MW	molecular weight
\dot{M}/A	mass flux (gm/cm ² sec)
\dot{M}_T/A	Total mass flux, gas plus particles (gm/cm ² sec)
N_p	number of boron particles per unit volume (cm ⁻³)
Nu	Nusselt Number
P	Pressure (atm.)
$\dot{q}_{rad,in}$	radiation flux into preheat zone, Zone 1 (cal/cm ² sec)
$\dot{q}_{rad,out}$	radiation flux out of preheat zone, Zone 1 (cal/cm ² sec)
r_p	boron particle radius (cm)
R	gas law constant (82.057 cm ³ atm/gm-mol °K)
R_A	net radiation flux into preheat zone (cal/cm ² sec)
R_B	molar consumption rate of boron per particle in ignition zone (gm-mole/sec)

R'_B	molar consumption rate of boron per particle in combustion zone (gm-mol/sec)
R_E	molar vaporization rate of boric oxide per particle (gm-mol/sec)
Q_{RX}	heat release by reaction at $T = T_p$ of .75 moles of oxygen gas with 1.0 moles of boron solid or liquid to form 0.5 moles of B_2O_3 liquid (cal/gm-mol)
Q'_{RX}	heat release by reaction of .75 moles of oxygen at T_p with 1.0 moles of boron liquid at 2500°K to form 0.5 moles of B_2O_3 gas at T_g (cal/gm-mol)
T	temperature
T_f	flame temperature (°K)
T_{final}	final temperature at end of calculations from $X=0$ through Zone 4 (°K)
T_o	initial temperature (°K)
T_i	ignition temperature (°K)
U_{avg}	average velocity in combustion zone in simplified model (cm/sec)
U_o	flame speed [velocity at initial conditions] (cm/sec)
X_{23}	distance from end of Zone 1 to end of Zone 2 (cm)
X_{34}	distance from end of Zone 1 to end of Zone 3 (cm)
Y_{O_2}	mole of oxygen/moles gas
$Y_{O_2, final}$	oxygen mole fraction calculated at end of integration through Zones 2 and 3
α_B	boron particle absorptivity
ΔH_m	mass heat of fusion of boron (cal/gm)
ΔH_{vap}	molar heat of vaporization of boric oxide (cal/gm-mol)
ΔX_{flame}	combustion zone thickness in simplified model (cm)
ΔX_4	effective radiation depth of post-flame zone (cm)
ϵ_f	effective post-flame zone emissivity
λ	thermal conductivity (cal/cm sec °K)

ρ density (gm/cm³)
 σ Stefan-Boltzmann Constant (1.354.10⁻¹² cal/cm²sec °K⁴)
 τ_{burn} particle burn time in simplified model (sec)

COMMONLY USED SUBSCRIPTS

X = 0 conditions at end of preheat zone (Zone 1) in detailed model
I, 0 initial conditions
34 conditions at end of Zone 3 (combustion zone) in detailed model
B boron property
B₂O₃ boric oxide property
g gas property
p particle property

ACKNOWLEDGEMENT

Research sponsored by the Air Force Office of Scientific Research/AFSC, United States Air Force, under Contract F44620-71-C-0124. The United States Government is authorized to reproduce and distribute reprints for governmental purposes notwithstanding any copyright notation hereon.

REFERENCES

1. Dugger, G.L., Simon, D.M., and Gerstein, M. "Laminar Flame Propagation", Basic Considerations in the Combustion of Hydrocarbon Fuels with Air, NACA Report 1300, 1959, pp 127-162.
2. Williams, F.A., Combustion Theory, Addison-Wesley Publishing Company, Inc. Reading, Mass., 1965.
3. Von Karmon, T., "The Present Status of the Theory of Laminar Flame Propagation", 6th Int Symp on Comb, Reinhold Publishing Co., N.Y., 1957, p. 1.
4. Stephenson, P.L., and Taylor, R.G., "Laminar Flame Propagation in Hydrogen, Oxygen, Nitrogen Mixtures", Comb & Flame, 20, 1973, p. 231.
5. Sundukov, I.N., and Predvodirelev, A.S., "Flame Propagation in Two-Phase Mixtures", 7th Int. Symp. on Combustion, Butterworths Scientific Publications, London, 1959, p. 352.
6. Essenhigh, R.H., and Csaba, J. "The Thermal Radiation Theory for Plane Flame Propagation in Cool Dust Clouds", 9th Int. Symp. on Combustion, Academic Press, N.Y., 1963, p. 111.
7. Bhaduri, D. and Bandyopadhyay, S., "Combustion in Cool Dust Flames", Comb & Flame, 17, 1971 p. 15.
8. King, M.K., "Boron Ignition and Combustion in Air-Augmented Rocket Afterburners", Comb. Sci. & Technology, 5, 1972, pp 155-64.
9. King, M.K., "Burn Particle Ignition in Hot Gas Streams", Accepted for publication in Comb. Sci. & Technology, late 1973.
10. Cassel, H.M., Das Gupta, A.K., and Guruswamy, S., "Factors Affecting Flame Propagation through Dust Clouds", 3rd Symposium on Combustion, Flame and Explosion Phenomena, Williams & Wilkins Co.,
11. Macek, A., and Semple, J.M., "Composition and Combustion Characteristics of Condensed Exhaust from Boron-Containing Fuel-Rich Rocket Motors", Presented at 9th JANNAF Combustion Meeting, Sept., 1972, CPIA Publ. No. 231, Vol. I, Dec., 1972, p. 359.
12. McAdams, W.H., Heat Transmission, 3rd edition, McGraw-Hill Book Company, New York, 1954, pp 55-125.
13. Mohan, G., and Williams, F., "Ignition and Combustion of Boron in O₂/Inert Atmospheres", AIAA J., 10, 6 June, 1972, pp. 776-783.
14. Liebman, I., Bureau of Mines, Bruceton, Pa., Personal Communication, Oct., 1973.

TABLE I. Comparison of Predicted and Measured Laminar Flame Speeds in Boron-Oxygen-Nitrogen Dust Clouds

Test No.	Weight Fraction Particles(90%B)	Pressure (atm)	Mole Fraction Oxygen	Initial Temp.(°K)	Post-Flame Emissivity	Boron Particle L Diam.(microns)	FLAME SPEED (CM/SEC)		
							Measured	Detailed Model	Simplified Model
1	0.149	1.0	0.48	300	<0.01*	5	12	11.6	9.6
2	0.156	1.0	0.39	300	<0.01*	5	12	10.4	8.2

*Estimated from the experimental geometry.

**Approximate - actually probably a fairly coarse distribution of sizes

TABLE II. Effects of Various Parameters on Calculated Boron-Oxygen-Nitrogen Dust Cloud Flame Speeds - Detailed and Simplified Models.

Parameter Being Varied And Value	Flame Temp. (°K)	Final Oxygen Mole Fraction	Gas Temp. at which Ignition Step is Completed (°K)	Flame Speed (U_0), cm/sec.	
				Detailed Model	Simplified Model
Weight Fraction Particles					
.055	2225	.086	2197	4.73	10.1
.060*	2358	.074	2262	7.67	11.9
.065	2490	.061	2314	9.38	13.2
.070	2620	.048	2343	10.39	14.3
.075	2748	.035	2355	11.30	15.4
.080	2876	.021	2387	12.30	16.3
Post-Flame Emissivity					
0.00*	2358	.074	2262	7.67	11.9
0.05	2358	.074	2310	9.52	14.1
0.10	2358	.074	2339	10.99	16.5
0.15	2358	.074	2373	12.57	18.9
Initial Temperature (°K)					
500	2274	.074	2220	4.68	8.7
600*	2358	.074	2262	7.67	11.9
800	2532	.074	2335	14.43	19.6
1000	2709	.074	2392	23.19	30.1
Pressure (atm)					
1	2358	.074	2182	11.45	11.9
3	2358	.074	2234	9.09	11.9
5*	2358	.074	2262	7.67	11.9
10	2358	.074	2302	5.42	11.9
Initial Oxygen Mole Fraction					
0.16	2353	.033	2225	6.21	10.5
0.20*	2358	.074	2262	7.67	11.9
0.24	2364	.115	2285	8.10	13.0
0.30	2371	.177	2307	8.90	14.6
0.40	2384	.280	2336	9.89	17.1
Nusselt Number					
2*	2358	.074	2262	7.67	11.9
5	2358	.074	2312	6.06	11.9
Initial Oxide Thickness (microns)					
0.01	2406	.070	2285	8.57	12.3
0.02*	2358	.074	2262	7.67	11.9
0.05	2216	.084	2193	4.22	10.0
Initial Particle Radius (microns)					
1.0*	2358	.074	2262	7.67	11.9
2.0	2406	.070	2273	6.00	8.7
3.0	2421	.069	2287	4.98	7.2
5.0	2434	.068	2305	3.67	5.7

* Base Case: Weight Fraction Particles=.060, Initial Temp.=600°K, Initial Oxygen Mole Fraction 0.20, Initial Particle Radius=1 micron, Initial Oxide Thickness=0.02 micron, Pressure=5 atm., Nusselt Number=2, Post-Flame Emissivity=0.

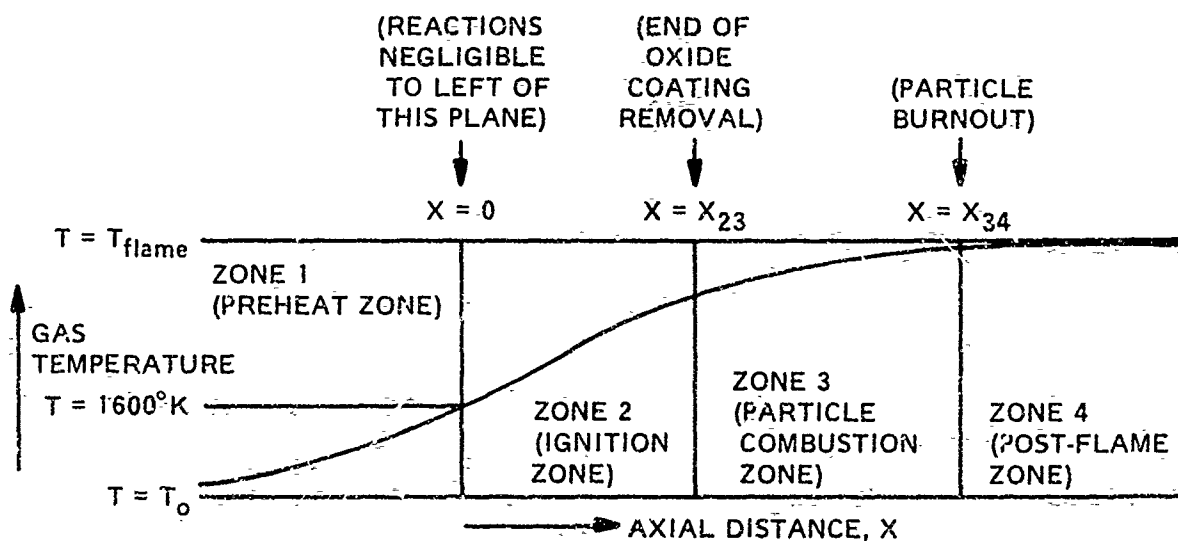


FIGURE 1. DEFINITION OF ZONES CONSIDERED IN DEVELOPMENT OF BORON-OXYGEN-NITROGEN DUST CLOUD FLAME SPEED MODEL (STATIONARY FLAME WITH DUST CLOUD ENTERING FROM LEFT AT VELOCITY U_0)

PROFILES OF IMPORTANT VARIABLES THROUGH IGNITION AND COMBUSTION ZONES AS PREDICTED BY DETAILED MODEL FOR A TYPICAL CASE

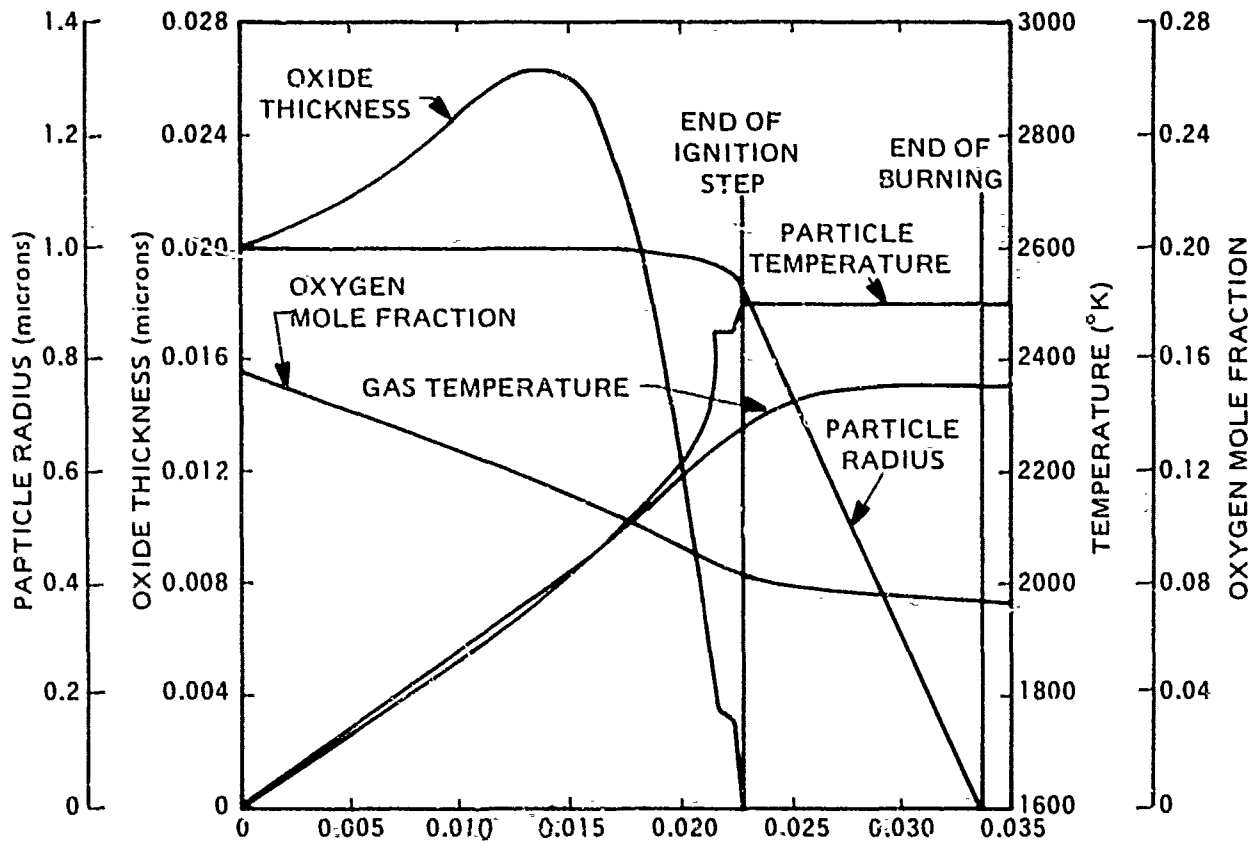


FIGURE 2. AXIAL DISTANCE FROM END OF PREHEAT ZONE (cm)

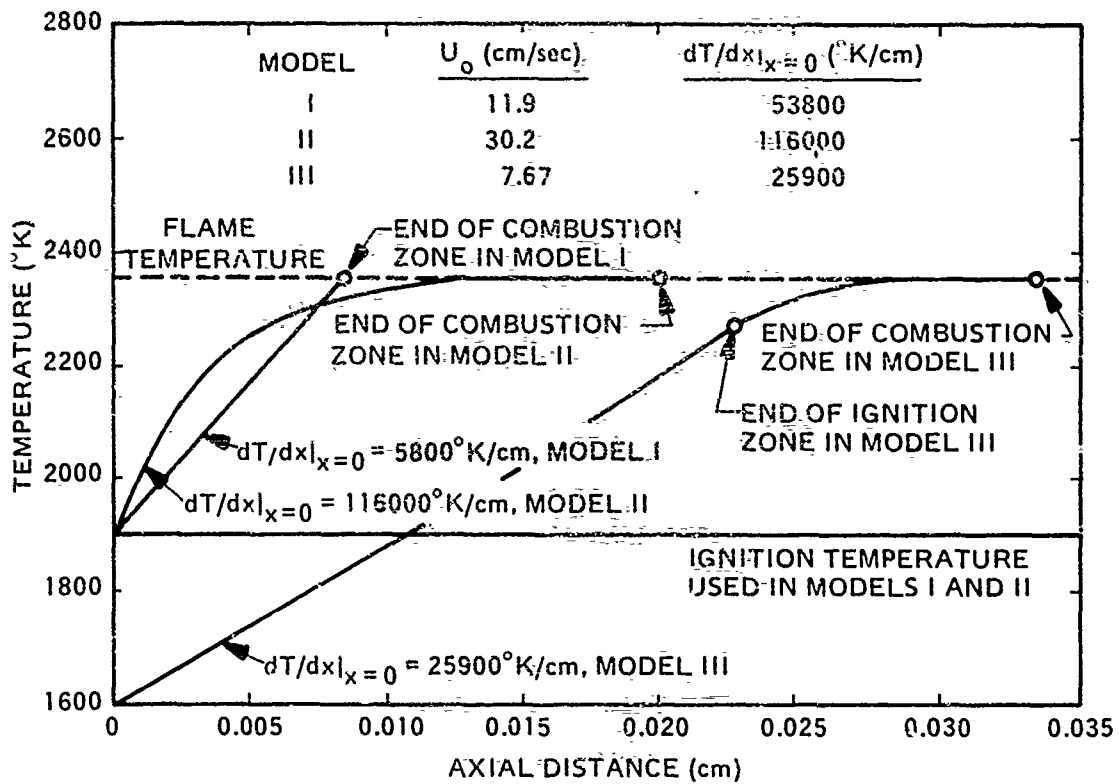


FIGURE 3. COMPARATIVE TEMPERATURE PROFILES FOR DETAILED MODEL (III), SIMPLIFIED MODEL (I) AND SIMPLIFIED MODEL WITH ALLOWANCE FOR CURVATURE IN TEMPERATURE PROFILE ACCOMPANYING HEAT RELEASE (II) - DEMONSTRATION OF PARTIAL CANCELLING OF ERRORS ASSOCIATED WITH VARIOUS ASSUMPTIONS IN SIMPLIFIED MODEL

FIGURE 4. EFFECT OF NUSSELT NUMBER ON PREDICTED FLAME SPEED

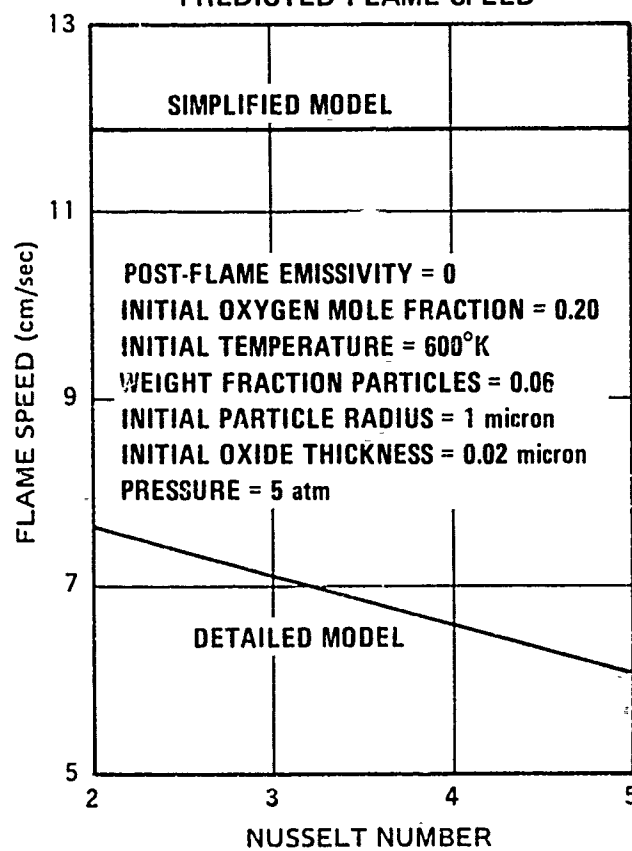


FIGURE 5. EFFECT OF OXIDE THICKNESS ON PREDICTED FLAME SPEED

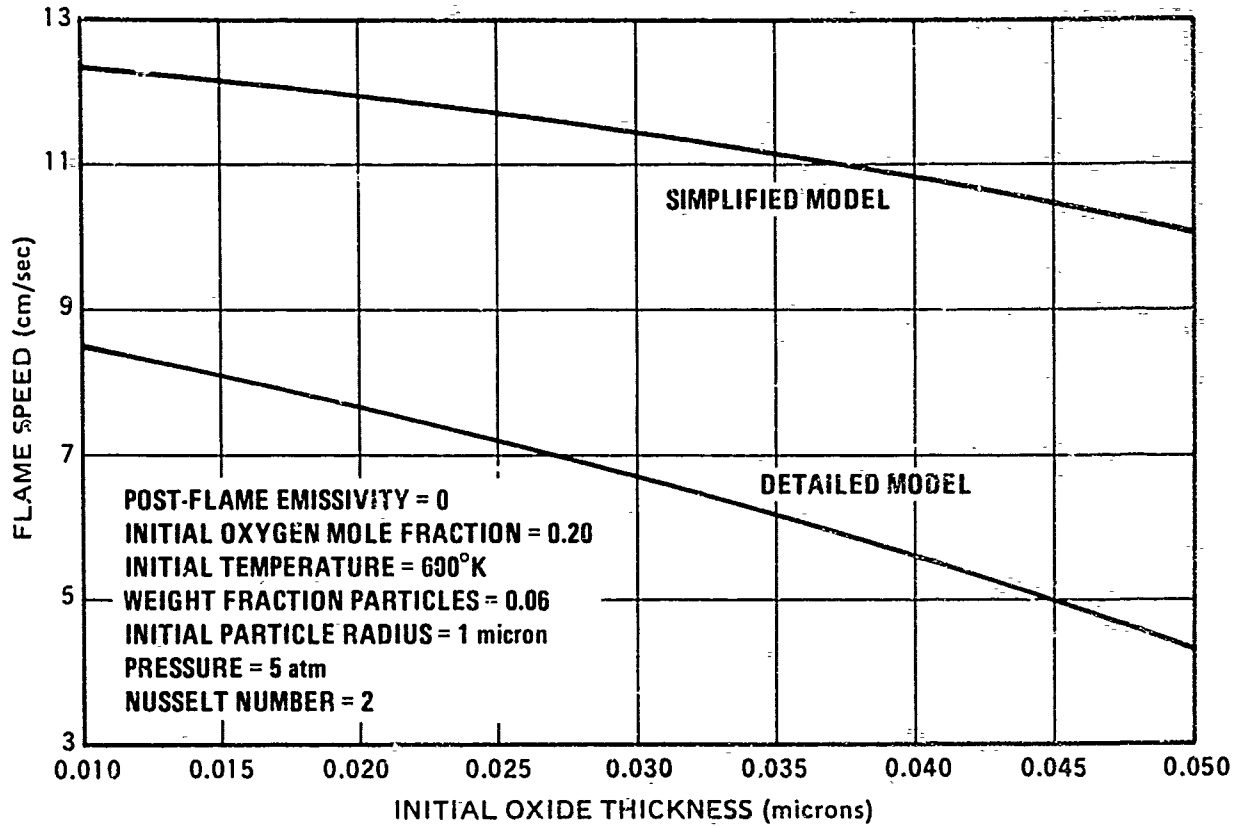


FIGURE 6. EFFECT OF POST-FLAME EMISSIVITY ON PREDICTED FLAME SPEED

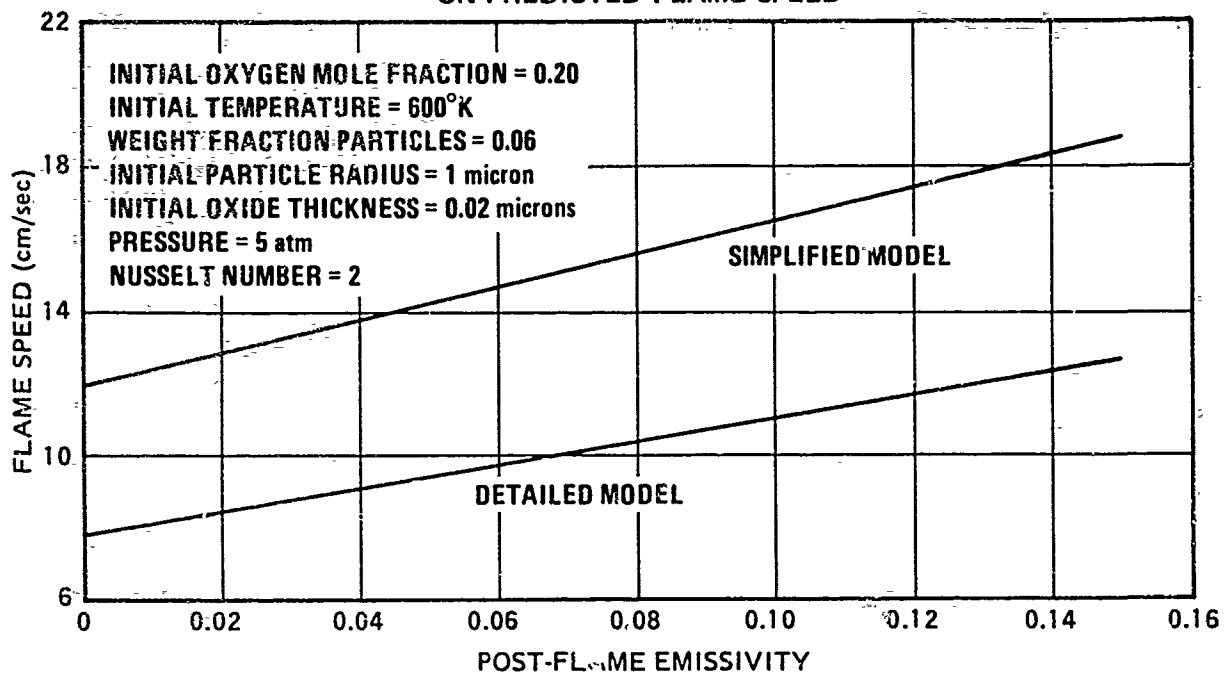


FIGURE 7. EFFECT OF PARTICLE LOADING ON PREDICTED FLAME SPEED

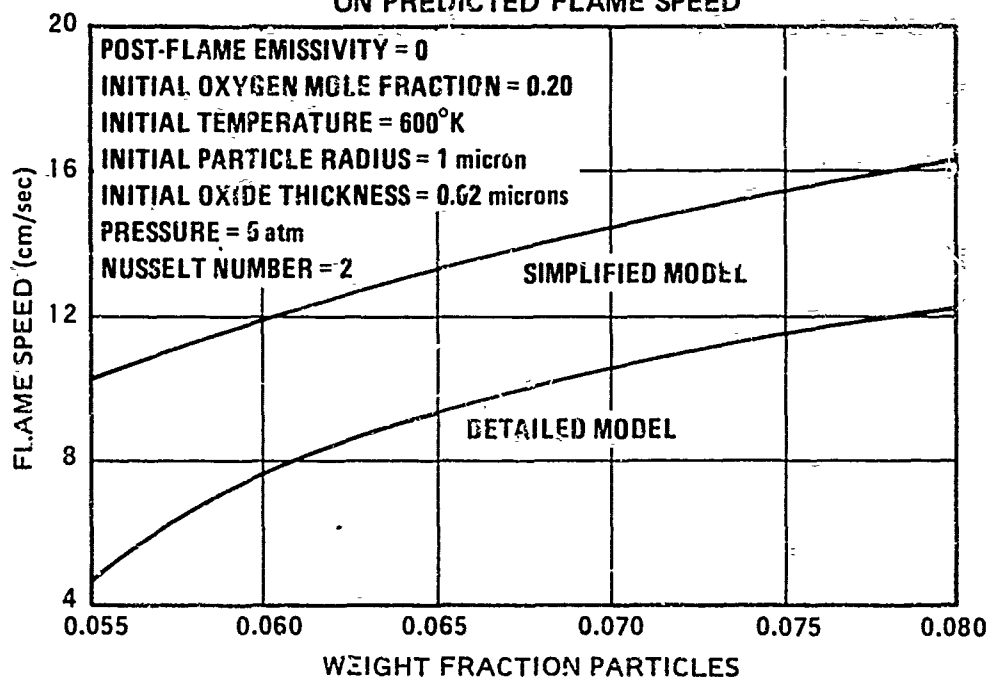


FIGURE 8. EFFECT OF PRESSURE ON PREDICTED FLAME SPEED

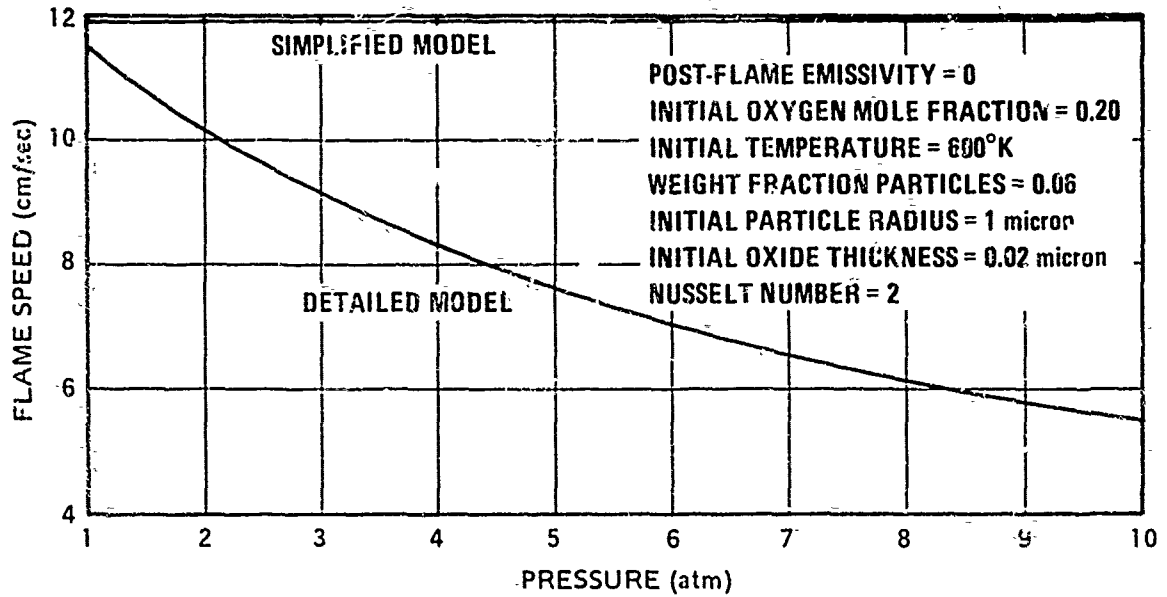


FIGURE 10. EFFECT OF BORON PARTICLE SIZE ON PREDICTED FLAME SPEED

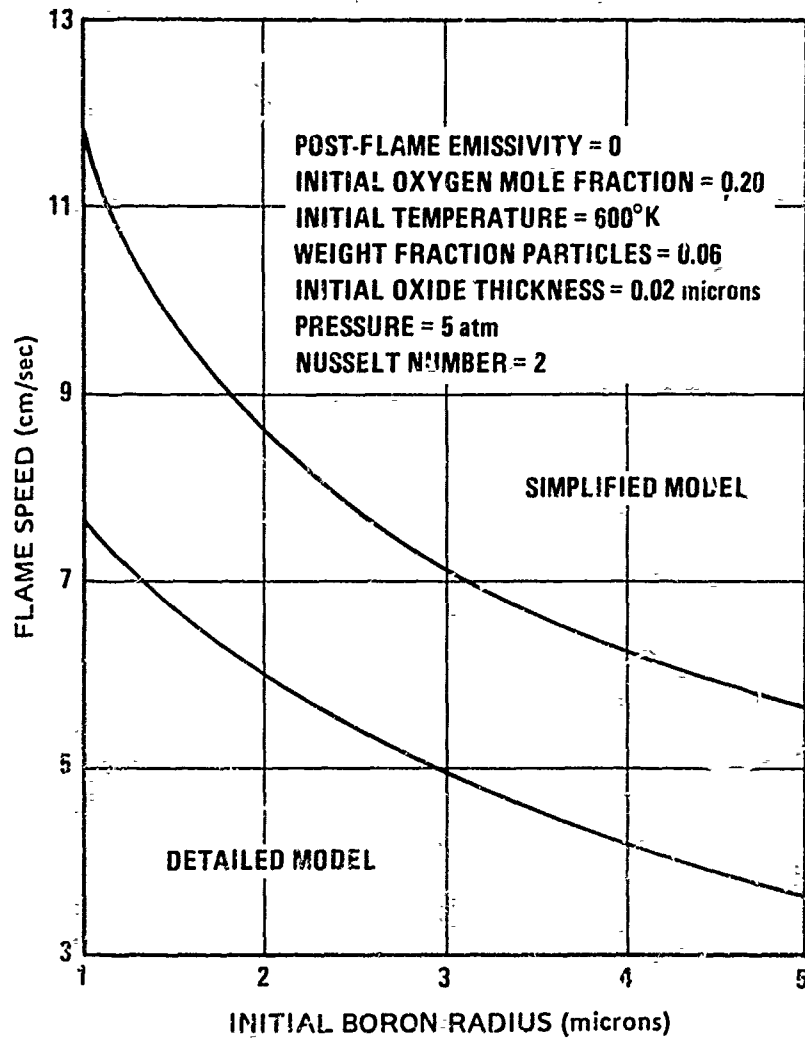


FIGURE 11. EFFECT OF INITIAL TEMPERATURE ON PREDICTED FLAME SPEED

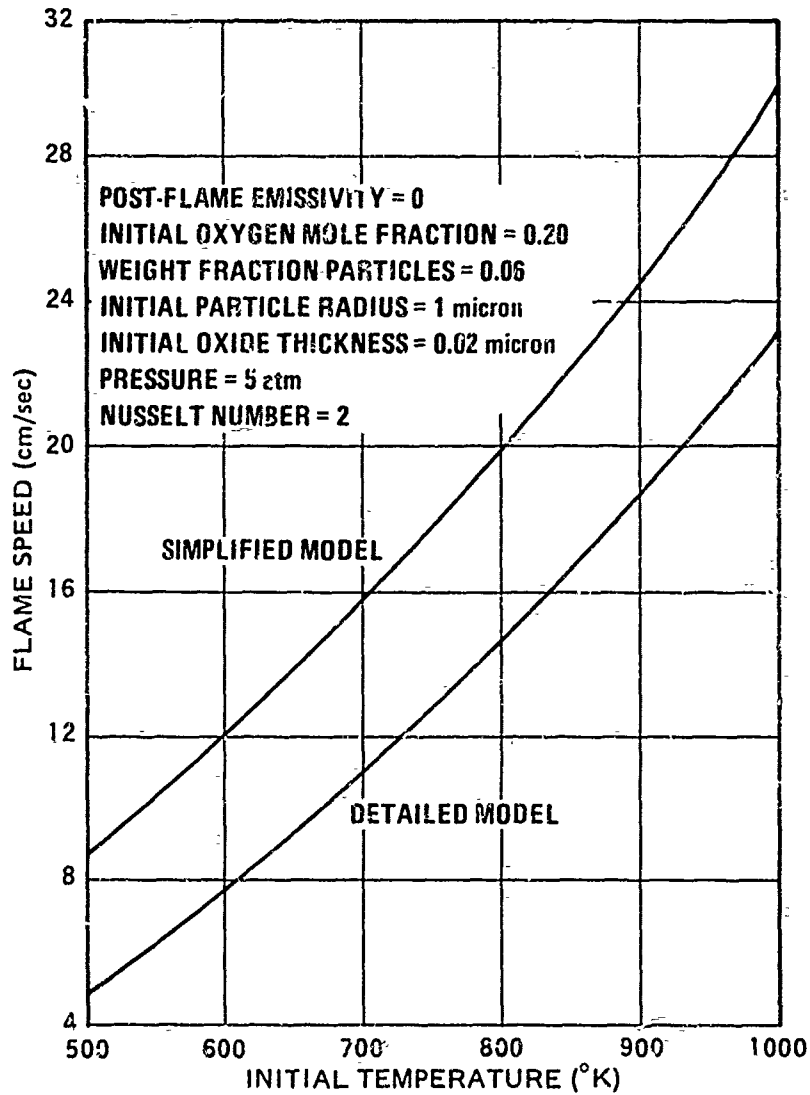


FIGURE 9. EFFECT OF OXYGEN MOLE FRACTION ON PREDICTED FLAME SPEED

